

FABRICATION AND CHARACTERIZATION OF GRAPHITE
REINFORCED POLY(LACTIC ACID) COMPOSITES

M.Phil. Thesis

SHAMSUN ALAM
Roll No. 0412143012F
Session: April 2012



BUET

Department of Physics
BANGLADESH UNIVERSITY OF ENGINEERING AND TECHNOLOGY
DHAKA-1000
JUNE, 2016


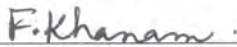


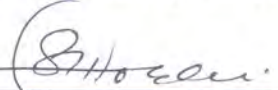
BANGLADESH UNIVERSITY OF ENGINEERING & TECHNOLOGY (BUET), DHAKA
DEPARTMENT OF PHYSICS

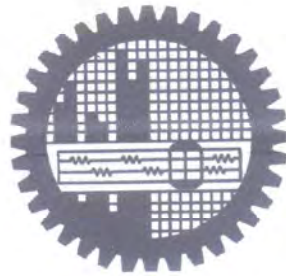


CERTIFICATION OF THESIS

The thesis titled “**FABRICATION AND CHARACTERIZATION OF GRAPHITE REINFORCED POLY (LACTIC ACID) COMPOSITES**” submitted by **Shamsun Alam**, Roll No-0412143012F, Registration No-0412143012F, Session: April-2012, has been accepted as satisfactory in partial fulfillment of the requirement for the degree of **Master of Philosophy (M. Phil.)** in Physics on 22 June, 2016.

BOARD OF EXAMINERS

1. 
Dr. Md. Forhad Mina
Professor,
Department of Physics, BUET, Dhaka. Chairman
(Supervisor)
2. 
Fahima Khanam
Professor & Head
Department of Physics, BUET, Dhaka. Member
(Ex-Officio)
3. 
Dr. Md. Abu Hashan Bhuiyan
Professor
Department of Physics, BUET, Dhaka. Member
4. 
Dr. Md. Mostak Hossain
Professor
Department of Physics, BUET, Dhaka. Member
5. 
Dr. Khandker Saadat Hossain
Professor
Department of Physics
University of Dhaka, Dhaka. Member (External)



BUET

CANDIDATE'S DECLARATION

It is hereby declared that this thesis or any part of it has not been submitted elsewhere for the award of any degree or diploma.

Shamsun Alam

Shamsun Alam

Roll No. 0412143012F

Session: April, 2012

DEDICATION

This dissertation is gratefully dedicated to my beloved
Ma

ACKNOWLEDGEMENTS

Though my name appears on the cover of this dissertation, a great many people have contributed to its production. At the very first, I express my satisfaction to praise the almighty Allah who has given me strength and opportunity to complete my thesis work.

Regarding the outcomes and completion of this thesis work, I would like to express my sincere gratitude to my supervisor Dr. Md. Forhad Mina, Professor, Department of Physics, BUET, for the continuous support of my M. Phil. research, for his patience, motivation, and immense knowledge. His guidance helped me in all the time of research and writing of this thesis.

Besides my supervisor, I shall be ever grateful, deeply indebted and extremely pleased to express my deepest thanks to Prof. Fahima Khanam, Head, Department of Physics, BUET, for allowing me to do this work. I am extremely grateful to my respected teachers Prof. Dr. Md. Abu Hashan Bhuiyan, Prof. Dr. Md. Feroz Alam Khan, Prof. Dr. Jiban Podder, Prof. Dr. A.K.M. Akther Hossain, Prof. Dr. Md. Mostak Hossain, Prof. Dr. Afia Begum, Dr. Md. Abdul Basith, Department of Physics, BUET, for their inspiration, affection and constructive suggestions for advanced research in the theoretical classes.

I would like to acknowledge the authority of BUET for giving me necessary permission and providing with the financial support for this thesis work.

My sincere thanks also goes to Dr. Md. Abdul Gafur, Principal Scientific Officer and Project Director, Pilot Plant and Process Development Center (PP & PDC) of Bangladesh Council for Scientific and Industrial Research (BCSIR), Dhaka, who gave me access to the laboratory and research facilities. Without their precious support, it would not be possible to conduct this research. I am grateful to Md. Rakibul Hasan, Engineer, PP & PDC, BCSIR, Dhaka, for his clement assistance in using the UTM machine and practical advice. I am also thankful to system staff Mr. Mainul of PP & PDC, who maintained all the machines so efficiently. I am indebted to the authority of BCSIR for their permission to conduct my research work in their laboratories.

My special thanks will go to Dr. Kazi Haniem Maria and Prof. Dr. Tetsu Mieno, Center for Instrumental Analysis, Shizuoka University, Shizuoka, 422-8259, Japan for their excellent cooperation in structural and morphological measurements.

I am also grateful to all the staff members Mr. Md. Idris Munshi, Mr. Md. Liaquat Ali, Mr. Md. Nurul Haque, Mr. Md. Lutfar Rahman Sarker, Mr. Swapan Kumar Das, Mr. Md. Mozammel Haque, Mr. Md. Abu Taher and Mr. Md. Lutfur Rahman, Department of Physics, BUET, for their help.

Last but not the least, I would like to thank my family members, especially to my parents and younger sister for supporting me spiritually through all these years during my work and my life in general.

Shamsun Alam

June 2016

ABSTRACT

Biocomposites of poly(lactic acid) (PLA) and micro-size graphite (GP) flake powder with 0 – 30 wt% GP contents have been prepared using extrusion molding followed by compression molding method. The pure PLA and PLA-GP composites (PGC) have been examined by the Fourier transform infrared (FTIR) spectroscopy, Raman spectroscopy (RS), X-ray diffraction (XRD) technique, scanning electron microscopy (SEM), transmission electron microscopy (TEM), mechanical test, micromechanical test, differential thermal analysis (DTA) and thermogravimetric analysis (TGA). Almost all the peaks of FTIR spectra for composites resemble to those of neat PLA except C-O stretching vibration at 1130cm^{-1} and another peak at 1160cm^{-1} . The shifting of these two peaks may correspond to some kind of adhesion of graphite with PLA. The Raman spectra reveals that PLA is poorly crystalline. The intensity ratio of D and G bands increases with the increase of graphite, indicating fewer defect structure in the composites. XRD shows broader peak that signifies poorly crystalline structure of PLA. Inclusion of filler affects to decrease both crystalline structure and crystallinity. SEM and TEM exhibit a clear dispersion of graphite particles in PLA matrix at lower loading and aggregates at higher loading. The tensile strength(TS) for pure PLA is 55MPa and that for composites gradually decreases to 4MPa for 30wt% graphite content. In contrast, Young Modulus(Y) for composites gradually increases and show the maximum of 2.31GPa for 30 Wt% graphite content. A theoretical model proposed by Guth-Smallwood fits well with the Y increase. The change of flexural strength and tangent modulus resemble to that of TS and Y. Microhardness is found to decrease from 220MPa for pure PLA to 143MPa for 30 wt% graphite loaded composites. The onset of thermal degradation occurs at 334°C for PLA and at 356°C for 30wt% loaded composite. On the other hand the degradation temperature for pure PLA is 363°C and that 30wt% composite is 383°C .

CONTENTS

<i>Cover page</i>	i
<i>Certification of thesis</i>	ii
<i>Declaration</i>	iii
<i>Dedication</i>	iv
<i>Acknowledgements</i>	v
<i>Abstract</i>	vii
<i>List of Figures</i>	xii
<i>List of Tables</i>	xiv
<i>Glossary</i>	xv
<i>Symbols /units</i>	xvi

Chapter	Title	Page No.
Chapter One	INTRODUCTION	1-7
	1.1 GENERAL DISCUSSION	1
	1.2 OBJECTIVES OF THIS RESEARCH	3
	1.3 STRUCTURE OF THIS THESIS	5
	REFERENCES	6
Chapter Two	LITERATURE REVIEW	8-16
	2.1 BACKGROUND	8
	2.2 REVIEW OF LITERATURE	8
	REFERENCES	15
Chapter Three	THEORETICAL BACKGROUND	17-
	77	
	3.1 POLYMER	17
	3.1.1 Classification of Polymer	17
	3.1.2 Polymerization	23
	3.1.3 Physical State of Polymer	24
	3.1.4 Glass Transition Temperature of Polymer	25
	3.2 POLY(LACTIC ACID)	26
	3.2.1 Physical and Chemical Properties of PLA	27
	3.2.1 PLA Synthesis	28
	3.3 GRAPHITE	28

3.3.1	Graphite Classification	30
3.3.2	Properties of Graphite	31
3.3.3	Application of Graphite	32
3.4	COMPOSITE MATERIALS	34
3.4.1	Classification of Composites	35
3.4.2	Application of Polymer Composites	38
3.5	THEORY OF SURFACE MORPHOLOGY	41
3.5.1	Scanning Electron Microscope	42
3.5.2	Transmission Electron Microscopy	43
3.6	THEORY OF STRUCTURAL ANALYSIS	45
3.6.1	Fourier Transform Infrared Spectrometer	45
3.6.2	Raman Spectroscopy	47
3.6.3	Theory of X-ray Analysis of Crystal	49
3.6.3.1	Long Range and Short Range Order	50
3.6.3.2	Crystallite or Particle size in Polymer	52
3.6.3.3	Wide Angle X-ray Scattering	55
3.7	DEFORMATION OF MATERIALS	55
3.7.1	Deformation	55
3.7.2	Elastic Deformation	57
3.7.3	Plastic Deformation	58
3.8	MECHANICAL PROPERTIES OF COMPOSITES	59
3.8.1	Theory of Tensile Properties	59
3.8.1.1	Engineering Strain	59
3.8.1.2	True Strain	60
3.8.1.3	Shear Strain	61
3.8.1.4	Stress	62
3.8.1.5	Engineering Stress	63
3.8.1.6	True Stress	63
3.8.1.7	Tensile Strength	64
3.8.1.8	Elongation at Break or Breaking Strain	65
3.8.1.9	Young's Modulus	65
3.8.2	Theory of Flexural Properties	66
3.8.2.1	Theory of Bending	66
3.8.2.2	Tangent Modulus	68
3.8.2.3	Flexural Stress or Strength	68
3.8.2.4	Flexural Strain	69

	3.9 THEORY OF MICROHARDNESS	69
	3.10 THEORY OF THERMAL ANALYSIS	71
	3.10.1 Thermogravimetric Analysis	72
	3.10.1 Differential Thermal Analysis	73
	REFERENCES	76
Chapter Four	MATERIALS AND METHODS	78-103
	4.1 RAW MATERIALS	78
	4.1.1 Polylactic Acid	79
	4.1.2 Graphite	79
	4.2 EQUIPMENTS FOR THE PREPARATION OF COMPOSITES SAMPLES	79
	4.2.1 Electric Balance	79
	4.2.2 Sample Die	80
	4.2.3 Extrusion machine	82
	4.2.4 Compression molding machine	85
	4.3 PREPARATION OF COMPOSITES SAMPLES	86
	4.4 SURFACE MORPHOLOGY TEST	86
	4.4.1 Surface morphology test by a SEM	87
	4.4.2 Surface morphology test by a TEM	87
	4.5 STRUCTURAL MEASUREMENTS	89
	4.5.1 Fourier Transform Infrared Spectroscopy	89
	4.5.2 Raman Spectroscopy	90
	4.5.3 X-ray Diffraction	91
	4.6 METHODS OF MEASURING MECHANICAL PROPERTIES	93
	4.6.1 Universal Testing Machine	93
	4.6.2 Measurements by Universal Testing Machine	94
	4.6.2.1 Measurements of Tensile Properties by UTM	94
	4.6.2.1 Measurements of Flexural Properties by UTM	96
	4.7 METHODS OF MEASURING MICROMECHANICAL PROPERTIES	99
	4.8 THERMAL MEASUREMENTS	100

	4.8.1	Methods of Thermal Measurement	101
	4.8.1.1	Thermogravimetric Analysis and Differential Thermal Analysis	101
		REFERENCES	103
Chapter Five		RESULTS AND DISCUSSIONS	104-127
	5.1	STRUCTURAL ANALYSES	104
	5.1.1	Fourier Transform Infrared Spectroscopy Analyses	104
	5.1.2	Raman Spectral Analyses	106
	5.1.3	XRD Analyses	108
	5.2	SURFACE MORPHOLOGY	111
	5.3	MECHANICAL PROPERTIES	114
	5.4	MICROMECHANICAL PROPERTIES	118
	5.5	THERMAL PROPERTIES	122
		REFERENCES	126
Chapter Six		CONCLUSION	128-129
	6.1	CONCLUSIONS	128
	6.2	SUGGESTIONS FOR FUTURE WORK	129

LIST OF FIGURES

Figure No.	Figure Captions	Page No.
Fig. 3.1.1	Linear Chain Polymers	20
Fig. 3.1.2	Branched Chain Polymers	20
Fig. 3.1.3	Cross Linked Polymers	20
Fig. 3.1.4	citcatA dna citcatoidnyS ,citcatosI Polymers	22
Fig 3.2.1	Synthesis of PLA	28
Fig. 3.3.1	Crystal structure of graphite.	29
Fig. 3.4.1	Systematic illustration of the structural components of composite materials. Sources: Verpoest, (1998).	36
Fig. 3.5.1	A photograph of surface morphology.	42
Fig. 3.5.2	Scanning Electron Microscope.	43
Fig. 3.5.3	Transmission electron microscope.	44
Fig.3.6.1	Fourier Transform Infrared Spectroscopy .	46
Fig.3.6.2	Raman Spectroscopy.	47
Fig.3.6.3	Raman Spectrum.	48
Fig. 3.6.4	Principle of X-ray Diffraction.	50
Fig. 3.6.5	(a) A Typical X-Ray Diffraction Pattern as Detected by a Counter and (b) A Typical X-Ray Diffraction Photograph.	51
Fig. 3.6.6	The Width of the Diffraction Peaks or Spots.	52
Fig.3.6.7	A schematic representation of x-ray diffraction from parallel planes of a crystallite of thickness t .	54
Fig. 3.7.1	Schematic Illustration of Elastic Deformation.	57
Fig. 3.7.2	Schematic Illustration of Plastic Deformation.	58
Fig. 3.8.1	Deformation of a Bar Produced by an Axial Load.	59
Fig. 3.8.2	Shear displacement on parallel planes of a solid material.	62
Fig. 3.8.3	A sample beam supported at two spans and loaded at the middle.	66
Fig. 3.9.1	(a) Schematic Sketch of an Imprint and (b) Details of Indentation Geometry.	70

Fig.3.10.1	Schematic representation of a TGA apparatus.	73
Fig. 3.10.2	Schematic Illustration of a DTA Cell.	74
Fig.4.1.1	A photograph of PLA granules	78
Fig.4.1.2	A photograph of prepared neat PLA sheet.	78
Fig. 4.2.1	A photograph of an electric balance.	79
Fig. 4.2.2 (a)	Dimensions of a dumbbell-shaped die (Top view)	80
Fig. 4.2.2 (b)	Dimensions of a dumbbell-shaped die (Side view)	80
Fig. 4.2.2(c)	Side views of the both parts of the Dumbbell-shaped dice.	81
Fig. 4.2.3 (a)	Dimensions of a bar-shaped die	81
Fig. 4.2.3 (b)	Top view of the Bar-shaped dice	82
Fig. 4.2.4	Photographs of an Extrusion machine and extrudates.	82
Fig. 4.2.5	Schematic diagram of an extrusion machine.	83
Fig. 4.2.6	Photographs of chopper machine and chopped extrudates.	84
Fig. 4.2.7	A Weber-pressen hydraulic press.	85
Fig. 4.3.1	(a) Bar shaped and (b) Dumbbell shaped sample for particle size 1.	86
Fig. 4.4.1	Scanning electron microscope.	87
Fig. 4.4.2	A Photograph of transmission electron microscopy.	88
Fig. 4.5.1	A Photograph of FTIR.	89
Fig.4.5.2	A Photograph of Raman Spectroscopy.	90
Fig. 4.5.3	A Photograph of X-ray diffractometer.	92
Fig. 4.5.4	Schematic diagram of X-ray diffractometer.	92
Fig. 4.6.1	A universal testing machine	93
Fig. 4.6.2	A typical stress versus strain curve.	95
Fig. 4.6.3	3-point (A,B,C) loading arrangement for flexural measurement.	96
Fig. 4.6.3	A typical load deflection curve.	98
Fig. 4.7.1	(a) Shimadzu microhardness tester (b) A residual impression on the surface of a polymer	99
Fig. 4.7.2	Load versus square of diagonal length plot.	100
Fig. 4.8.1	A coupled differential thermal analyzer and thermogravimetric analyzer.	101
Fig. 4.8.2	Schematic picture of a furnace and a micro balance of a TGA.	102
Fig. 4.8.3	Illustrates a scheme of the principle of TGA measurements.	102

Fig. 5.1.1	FTIR spectra of PGC.	105
Fig. 5.1.2	Raman Spectra of PGC.	107
Fig. 5.1.3	XRD spectra of PGC.	109
Fig. 5.1.4	Degree of crystallinity of PGC.	110
Fig. 5.2.1	Scanning Electron Microscope Micrograph Of PGC	112
Fig. 5.2.2	Transmission Electron Microscope Micrograph Of PGC	113
Fig. 5.3.1	Tensile Strength & Young Modulus of PGC.	114
Fig. 5.3.2	Flexural strength & Tangent Modulus Of PGC.	117
Fig. 5.4.1	Microhardness of PGC.	118
Fig. 5.4.2	Change of diagonal square length with load of PGC.	119
Fig. 5.4.3	Change of microhardness with GP content (wt%).	120
Fig. 5.5.1	DTA curves of PGC.	122
Fig. 5.5.2	TGA curves of PGC.	123
Fig. 5.5.3	DTG curves of PGC.	125

LIST OF TABLES

Table No.	Table Captions	Page No.
Table. 3.2.1	Properties of polylactic acid	27
Table. 3.3.1	Properties of commercial graphite	31
Table 5.1.2	Intensity ratio of D (I_D) to G (I_G) band of different samples	106
Table. 5.5.1	The T_o , T_f , T_{dec} and the residue content at T_{dec} °C of different samples	124

GLOSSARY

PLA	: Poly(lactic acid)	NP	: Nanoparticles
ASTM	: American Standard for Testing of Materials	PGC	: Poly (lactic acid) Graphite Composite
FTIR	: Fourier Transform Infrared Spectroscopy	PMCs	: Polymer Matrix Composites
CRT	: Cathode ray tube	RS	: Raman Spectroscopy
DTA	: Differential Thermogravimetric Analysis	SEM	: Scanning Electron Microscopy
DTG	: Derivative Thermogravimetric Analysis	SWCNT	: Single-walled Carbon nanotube
DSC	: Differential scanning calorimeter	TEM	: Transmission electron microscope.
EB	: Elongation-at-Break	TG	: Thermogravimetric
EDEX	: Energy Dispersive X-ray Analysis.	TGA	: Thermogravimetric Analysis
EDS	: Energy Dispersive Spectrometer	T _g	: Glass Transition Temperature
Eg	: Energy Gap	T _m	: Melting Temperature
FS	: Flexural Strength	TM	: Tangent Modulus
GPa	: Giga Pascal	TS	: Tensile Strength
HDPE	: High Density Polyethylene	UTM	: Universal Testing Machine
IUPAC	: International Union of Pure & Applied Chemistry	UTS	: Ultimate Tensile Strength
IR	: Infrared	UV	: Ultraviolet
JCPDS	: Joint Committee For Powder Diffraction Standard	VLDPE	: Very Low Density Polyethylene
Kgf	: Kilogram force	VMT	: Vicker's microhardness test
LED	: Light emitting diode	XRD	: X-ray Diffraction
T ₀	: Onset Temperature	YM	: Young's Modulus
T _f	: Endset Temperature		
T _{dec}	: Decomposition Temperature		
MPa	: Mega Pascal		
MMA	: Methyl Methacrylate		
NC	: Nanocomposite		

LIST OF SYMBOLS / UNITS

Å -	Angstrom unit (10^{-10}m)
λ -	Wavelength
$^{\circ}\text{C}$ -	Degree Celsius
μg -	Microgram
a, b, c -	Lattice constants
cm -	Centimetre
eV -	Electron volt
g -	Gram
GPa -	Gigapascals (or kN/mm^2)
h -	Hour
K -	Kelvin
keV -	Kilo Electron Volt
kN -	Kilo Newton
mA -	Mili Ampere
MPa -	Megapascals (or N/mm^2)
meV -	Mili Electron Volt
mL -	Mili Litre
mV -	Mili Volt
nm -	Nanometre
μm -	Micrometre
Pa -	Pascal (N/m^2)
Psi -	Pounds (force) per square inch.

INTRODUCTION

1.1 INTRODUCTION

Many well-defined structures such as metals, ceramics or polymers cannot satisfy all technological demands. Therefore, there is ongoing search for new materials with new, and especially improved properties. Such a task is met by, among others, composite materials that are defined as materials composed of at least two phases, where due to the occurring synergistic effect the material of different properties other than properties of the components is formed. A composite material is usually composed of two components, i.e. matrix and filler called also reinforcement or more broadly dispersed phase; sometimes also additional compounds are used, mostly compatibilisers. The matrix, known also as continuous phase, integrates filler particles and allows also shaping products appropriately and determines most of physical and chemical properties of material. The dispersed phase is responsible for additional enhancement of selected material properties. While, the compatibiliser is added to increase interactions between matrix and filler what has significant impact on material cohesion and homogeneity, and as a result on its processing properties and strength. High strength and low weight remain the winning combination that propels composite materials into new arenas, but other properties are equally important. Composite materials offer good vibrational damping and low coefficient of thermal expansion (CTE), characteristics that can be engineered for specialized applications. Composites are resistant to fatigue and provide design/fabrication flexibility that can significantly decrease the number of parts needed for specific applications — which translates into a finished product that requires less raw material, fewer joints and fasteners and shorter assembly time. Composites also have proven resistance to temperature extremes, corrosion and wear, especially in industrial settings, where these properties do much to reduce product lifecycle costs. These characteristics have propelled composites into wide use. The push for fuel economy in the face of rising oil prices, for example, has made light weighting a priority in almost every mode of mechanical transportation, from bicycles to large commercial aircraft.

Recently, there has been a rising demand for biodegradable polymers due to increased environmental awareness and a growing concern about the disposal of synthetic plastic waste. These ecological and disposable problems make the consumers very incurious to use the

commodity materials manufactured from synthetic plastics. As a consequence, research on biopolymers is much attracted by researchers. Many bio-polymers are derived from renewable resources, such as plant-based feedstock. Poly(lactic acid) (PLA) is such a polymer having compostable characteristics and has become a material of choice, due to its high strength and moderate barrier properties like synthetic plastics [1]. Hence, it is believed that PLA or PLA composites can meet the requirement for end-of-life disposal issues. PLA is a highly transparent and rigid material with a relatively low crystallization rate that makes it a promising candidate for the fabrication of films, containers, stretch-blown bottles, drug delivery and packaging materials [2, 3], and its composites have received potential applications in construction sectors [4–11]. With a tremendous increase in production capacity over the past years, PLA has become potentially interesting for engineering applications (electronic and electrical devices, mechanical and automotive parts, etc.), but it is required the tailoring of its properties to reach the end-user demands. For further applications, the profile of PLA properties can be tuned by combining this polyester matrix with uniformly dispersed fillers, impact modifiers, flame retardants, plasticizers, etc. [3, 5-10] However, PLA has drawbacks for some applications owing to its brittleness [12]. Therefore, increasing the crystallization speed of PLA is desirable [13]. In order to increase the crystallinity in PLA, three main routes can be considered: (i) Addition of a suitable nucleating agent, (ii) addition of a plasticizer and (iii) selection of molding conditions [14]. Several potential nucleating agents for PLA crystallization have been examined in the literatures [15-18]. However, no report as the use of expanded graphite for PLA crystallization can be found. Although graphite has been used in properties reinforcement in synthetic polymers, use of graphite in PLA reinforcement has just started [19-22]. Graphite can be used as a potential alternative reinforcement, because it contains nano-graphene layered structure with superior mechanical and thermal properties like carbon nanotubes (CNT) and is much cheaper than CNTs. It has high conductivity of electric current and heat, low thermal expansion coefficient, high thermal stability, relatively low specific gravity, high resistance to aggressive chemical compounds, and valuable tribological properties (self-lubrication).

To the best of our knowledge, although investigations on PLA-graphite composites have been conducted so far by several authors, evidences of the overall effect conferred by graphite addition in a wide range (0-30 wt%) on structural, surface morphological, mechanical, micromechanical and thermal properties of PLA in one study is relatively scarce. Generally, addition of nanofillers can provide PLA with specific properties but sometimes triggers

problems such as loss of mechanical and thermal properties, degradation of the polymer matrix, etc., aspects that need to be considered when targeting a potential application [23, 24].

Based on the above facts, addition of graphite's properties due to a wide range of graphite loading to a biodegradable polymer matrix of high interest like PLA for disclosing structure-properties relationship of the resulting composites is the aim of this paper. To obtain green products with specific end-use properties, commercially available graphite has been added to PLA by direct dosing using the melt-compounding technology and the resulting composites have been characterized in detail for highlighting their performance. It is expected that graphite based reinforced PLA composites can enable new combinations of mechanical, micromechanical and thermal properties.

1.2 OBJECTIVES OF THE RESEARCH

PLA is one of the most frequently used biodegradable polymers, especially in packaging applications due to its high strength, high modulus, good transparency, process ability and biocompatibility. However, PLA also has the drawbacks of inherent brittleness and poor toughness, which impede its wide application. Many efforts have been carried out to improve the properties of PLA so as to compete with the low cost and flexible commodity polymers. These attempts include blending PLA with other polymers, modifying PLA with plasticizers, or blending with inorganic fillers or nano-fillers. Notably, the particle size of filler can largely influence the properties of a polymer. Consequently, graphite of different ratio can be considered to tailor PLA for its improved performances. The aims of the present work are to:

Chapter 1 Introduction

- prepare composites of PLA and graphites having various loadings and sizes of tubes by extrusion followed by compression molding method.
- examine the effect of graphite size and loading on the crystalline structure and crystallinity of PLA by both the wideangle X-ray diffraction (WAXD) measurements.
- investigate the mechanical properties such as tensile strength and Young's modulus of the filler loaded PLA by mechanical test.
- observe the microhardness of PLA reinforced with various contents and sizes of graphites by microindentation method.
- study the surface morphology of PLA and composites by the scanning electron microscop (SEM).
- examine the dispersion of graphite in the PLA matrix by transmission electron microscopy (TEM).
- examine the functional group by fourier transform infrared spectroscopy (FTIR).
- examine the backbone structure by Raman spectroscopy (RS).
- study the melting temperature by differential thermal analysis (DTA).
- investigate the thermal degradation property of the samples by thermogravimetric analysis (TGA).

Chapter 1 Introduction

From structural and surface morphological observations, the effect of graphite size on the crystalline structure of PLA and dispersion graphite in PLA can be understood. These information can help explain the change in tensile strength, modulus and microhardness values of the materials. The thermal analysis by TGA will reveal information of the thermal stability in the different composites. The correlation of mechanical and thermal properties of the composites will help understand the fundamental process involved in modifying the composites by graphites of various ratio. This understanding of the mechanical and thermal behavior of the composites will be useful to find out durability and thermal of these materials for practical applications.

1.3 STRUCTURE OF THIS THESIS

This thesis contains six chapters.

- Chapter One contains Introduction, which is enclosed with general discussion, aims and objectives of this thesis.
- Chapter Two contains Literature Review that provides the literary survey relevant to the present work.
- Chapter Three consists of Theoretical Background which holds the theories and methods which are related to my work.
- Chapter Four is flourished with Materials and Methods, describing the synthesis process, preparation and measurement technique of the graphite reinforced PLA composite sample.
- Chapter Five has Results and Discussion that are thoroughly explained by the structural analysis (XRD, SEM, TEM, RAMAN, FTIR), mechanical, micromechanical and thermal (DTA, TGA) properties.
- Chapter Six includes Conclusions of this research work including suggestions for future work on these composite materials.

REFERENCES

- [1] L. Xiao, B. Wang, G. Yang and Gauthier, M, –Poly Lactic acid based biomaterials: Synthesis modification and applications; In "Biomedical Science, Engineering and Technology", Ed. : Dhanjoo, N. G., In Tech Open Access Publisher, Chapter 11, pp. 247– 271, 2012.
- [2] L-T. Lim, R. Auras M. Rubino, Processing technologies for poly(lactic acid), *Proogr. Polym. Sci.*, Vol. 33, pp. 820–852, 2008.
- [3] R. Auras, B. Harte, and S. Selke, An overview of polylactides as packaging materials, *Macromol. Biosci. J Appl Polym Sci.* Vol. 4, pp. 835-841, 2004.
- [4] J. Marikarian, Outdoor living space drives growth in wood plastic composites, *Plast. Addit. Compound*, Vol. 10(4), pp. 20–25, 2008.
- [5] V. K. Mathur, Composite materials from local materials, *Constr. Build. Mater.*, Vol. 20, pp. 470–477, 2006.
- [6] J. Marikarian, Outdoor living space drives growth in wood plastic composites, *Plast. Addit. Compound*, Vol. 10(4), pp. 20–25, 2008.
- [7] Youngquist, J.A., Unlikely partners the marriage of wood and non-wood materials, *Forest Prod. J.*, Vol. 45(10), pp. 25–30, 1995.
- [8] P. Wambua, J. Ivens, and I. Verpoest, Natural fibers: can they replace glass fiber in reinforced plastics”, *Comp. Sci. Technol.* Vol. 3, pp. 1259–1264, 2003.
- [9] V. K. Mathur, –Composite materials from local materials”, *Constr. Build. Mater.*, Vol. 20, pp. 470–477, 2006.
- [10] K. Oksman, M. Skrifvars, and J. F. Selin, Natural fibers as reinforcement in polylactic acid (PLA) composites, *Compos. Sci. Technol.* Vol., 63, pp. 1317–1324, 2003.
- [11] M. S. Islam, K. L. Pickering, and N. J. Foreman, Influence of alkali treatment on the interfacial and physico-mechanical Properties of industrial hemp fibre reinforced polylactic acid composites, *Compos. Part A Appl. Sci. Manuf.*, Vol. 41, pp. 596–603. 2010.
- [12] A. K. M. M. Alam, M. D. H. Beg, D. M. R. Prasad, M. R. Khan, and M. F. Mina, Structures and performances of simultaneous ultrasound and alkali treated oil palm empty fruit bunch fiber reinforced poly(lactic acid) composites, *Compos. Part A: Appl. Sci. Manuf.*, Vol. 43, pp. 1921-19294, 2012

- [13] D.M. Bigg, "Controlling the performance and rate of degradation of polylactide copolymers", In "Annual Technical Conference – ANTEC 2003 Conference Proceedings, Nashville, USA", Vol. 3, pp. 2816–2822, 2003.
- [14] D. Battegazzore, S. Bocchini, and A. Frache "Crystallization kinetics of poly(lactic acid)-talc composites", *eXPRESS Polym. Lett.*, Vol.5, pp. 849–858, 2011.
- [15] A. Shakoor, and N.L. Thomas, "Talc as a nucleating agent and reinforcing filler in poly(lactic acid) composites", *Polym. Eng. Sci.*, Vol. 54, pp. 64-70, 2014.
- [16] B. Nekhamanurak, P. Patanathabutr, and N. Hongsriphan, Mechanical Properties of hydrophilicity modified CaCO₃-poly (lactic acid) nanocomposite, *Int. J. Appl. Phy. Math.*, Vol. 2, pp. 98-103, 2012.
- [17] R. Kumar, M. K Yakabu, R. D Anandjiwala, Effect of montmorillonite clay on flax fabric reinforced poly lactic acid composites with amphiphilic additives, *Compos. Part A Appl. Sci. Manuf.*, Vol. 41, pp. 1620–1627, 2010.
- [18] D. Wu, Y. Cheng, S. Feng, Z. Yao, and M. Zhang, Crystallization Behavior of Polylactide/Graphene Composites, *Ind. Eng. Chem. Res.*, Vol. 52, 6731–6739, 2013,.
- [19] M. Murariu, A. L. Dechief, L. Bonnaud, Y. Paint, A. G. G. Fontaine, S. Bourbigot, P. Dubois, The Production and Properties of polylactic acid composites filled with expanded graphites, *Polymer Degradation and Stability*, Vol. 95, 889-900, 2010.
- [20] X. Li, Y. Xiao, A. Bergeret, M. Longerey, J. Che, Preparation of Polylactide/Graphene Composites From Liquid-Phase Exfoliated Graphite Sheets, *Polym. Compos.*, Vol. 35(3), 96–403, 2014.
- [21] M. Enkiewicz, J. Richert, P. Rytlewski, Agnieszkarichert, Selected electrical and thermal Properties of polylactide/graphite composites, *Polimery* 56, no.6, 2011.
- [22] P. Wei, S. Bocchini, G. Camino, Flame retardant and thermal behavior of polylactide/expandable graphite composites, *Polimery* 58, no. 5, 2013.
- [23] M. Murariu, A. D. S. Ferreira, Ph. Degée, M. Alexandre, Ph. Dubois, Polylactide compositions. Part 1: effect of filler content and size on mechanical Properties of PLA/calcium sulfate composites. *Polymer*, Vol. 48(9), 2613-2618, 2007.
- [24] N. C. Bleach, S. N. Nazhat, K. E. Tanner, M. Kellomäki, P. Törmälä, Effect of filler content on mechanical and dynamic mechanical Properties of particulate biphasic calcium phosphate polylactide composites. *Biomaterials*, Vol. 23(7), 1579-1585, 2002.

LITERATURE REVIEW

2.1 BACKGROUND

PLA is a thermoplastic and biodegradable aliphatic polyester derived from naturally occurring organic acid (lactic acid). It melts at a lower temperature (in the range of 180-220°C) with glass transition temperature 60-65°C. Further-more, PLA and its composites are biodegradable in nature; they degrade easily in physiological conditions as shown in animal model by simple hydrolysis of the ester backbone resulting in the formation of non-harmful and non-toxic compounds. Their degradation products are easily excreted through kidneys or eliminated in the form of carbon dioxide and water through metabolic processes in animals. PLA can also be recycled to its monomer by thermal depolymerization or hydrolysis. It can be processed by injection molding, extrusion, spinning film and casting, providing easy access to a wide range of materials. High molecular weight polylactides are absorbed completely and their rate of absorption depends on molecular weight, morphology, and enantiomeric purity of the polylactides. Thus, due to its biocompatibility, complete biodegradability and non-toxic nature of degradation products, PLA based polymeric materials are ideal for the preparation of various polymeric devices used for different practical applications all over the world. A remarkable number of articles based on polylactic acid composites have been published in the literature. A brief of the findings of these articles are presented below.

2.2 REVIEW OF LITERATURE

Fiore et. al. prepared first time a natural and almost inexpensive filler obtained by grinding the culms of arundo donax based PLA biocomposites. The composites were prepared by melt compounding PLA with *A. donax* filler (ADF). The influence of the content and size of ADF on the morphology and on the mechanical and thermal properties of PLA–ADF composites was evaluated [1]. Moreover, ADF was extracted from composites to evaluate the effect of processing on morphology and dimensions of the incorporated filler. Furthermore, the experimental elastic moduli of the biocomposites have been fitted, employing two theoretical models, i.e., Hill and Halpin–Tsai. The results showed that the addition of ADF significantly

influenced all the investigated properties. In particular, by increasing the ADF content, both tensile and flexural moduli greatly increased. On the contrary, both tensile and flexural strengths of the filled materials decreased if compared with the neat PLA

Im et al. studied the thermal, morphological and spectroscopy analysis of biodegradable polymer blends of poly (lactic acid) and starch composites. Blends were characterized by DSC thermal analysis, tensile test, morphological analysis and ATR IR spectroscopic analysis. To improve the toughness of blends, they used poly(ϵ -caprolactone) (PCL) up to 30wt%. The addition of starch gave little influence on thermal properties. In particular, at the starch content of 5 wt%, the crystallinity of PLA were the highest [2]. The addition of starch resulted in reducing the tensile strength and elongation ratios. PCL was found to be effective in improving toughness. ATR IR spectra showed that the C=O band of PLA shifted when starch was added, indicating that same H₂ bonding formed between the ester group of PLA & the hydroxyl group of starch. Morphological results by polarized optical microscopy showed that the size of the spherulite became smaller and less regular as the content of starch increased.

Hongwei Ma and Chang Whan Joo studied the Structure and mechanical properties of jute–polylactic acid biodegradable composites. The effect of jute fiber content, processing temperature, and alkali treatment on the structure and mechanical properties of jute–PLA composites were investigated [3]. The interfacial structure between jute fibers and PLA was analyzed by scanning electron microscope. The optimum tensile properties of jute–PLA composites were obtained at 15 wt% fiber content and a processing temperature of 210⁰C. Both the maximum flexural modulus and strength of composites were obtained at 220⁰C and 15 wt% fiber contents. X-ray diffraction profiles showed that the crystallinity of jute fibers was changed from cellulose I to cellulose II after alkali treatment. Meanwhile, the tensile modulus of single jute fiber and jute–PLA composites was increased by 29% and 76%, respectively.

Shih et. al studied biodegradable green composites reinforced by the fiber recycling from disposable chopsticks. Composites were examined by scanning electron micrpscopy, differential scanning calorimetry, thermogravimetric analysis and mechanical test [4]. They showed that the T_g of PLA was increased by the addition of fiber, which may improve the heat resistance of PLA.

The thermogravimetric analysis of the composites showed that the degradation process of fiber-filled systems started earlier than that of plain PLA, but possessed a higher char yield. Mechanical tests showed that the tensile strength of the composites markedly increased with the fiber content, reaching 115 MPa in the case of being reinforced with 40 phr fibers, which is about 3 times higher as compared to the pristine PLA. Furthermore, this type of reinforced PLA would be more environmental friendly than the artificial additive-reinforced one, and could effectively reduce and reuse the waste of disposable chopsticks.

Dimzoski et.al studied the preparation and characterization of polylactic acid rice hulls based biodegradable composites. Composites containing 20 and 30 wt.% rice hulls (RH), as well as composites where a certain amount of PLA matrix was substituted with a coupling agent, were investigated through tensile test and fracture test at low strain rate, using the concept of linear elastic fracture mechanics. Introduction of 20 wt.% rice hulls into PLA matrix resulted in increased tensile modulus and m [5]. For PLA composite with 30 wt% rice hulls, introduction of 5 wt% CA caused 33% and 40% improvement, correspondingly in the composite tensile and flexural strength, obviously as a result of improved adhesion. K_c and G_c (fracture toughness and toughness) values were determined for PLA and PLA based composites, revealing that introduction of rice hulls into PLA decreases the material toughness. Thermal stability of PLA/RH composites was lower than thermal stability of neat PLA. The examination of PLA/rice-hull-based composites revealed that rice-hull agricultural waste could be used as a biodegradable eco-friendly filler, rather to minimize environmental pollution and cost of the final product than as a reinforcement of PLA matrix.

Lee et al. investigate the thermal and mechanical properties of wood flour/talc-filled polylactic acid composites: effect of filler content and coupling treatment. They examined the effects of filler loading and silane treatment, the thermal and mechanical properties of the composites are studied [6]. Loading of WF and WF/talc mixture into neat PLA results in a small decrease in the glass transition and crystalline temperatures of the composites. The use of WF, talc and silane in the composites causes successively larger decreased in the composite crystallinity. The addition of talc and silane to PLA/WF composites improved the tensile modulus. The tensile strength of the composites decreases slightly with the addition of talc, but it considerably improves with the

use of 1wt% silane. Morphological analysis shows improved interfacial bonding with silane treatment for the composites.

Koutsomitopoulou et al. studied the characteristics of preparation and characterization of olive pit powder as filler to PLA-matrix bio-composites. In this study, a comparison of the size distribution and the densities of olive pit powders according to the grinding methods (planetary mill and centrifugal mill) were made [7]. The analyses showed that olive pits can be further studied as additive for the production of green materials. The development of an agricultural based polymer matrix compatible with olive pits and consequently a fully biodegradable composite system is the future and ultimate goal of the research undertaken. For that purpose, composite samples made out of PLA matrix, reinforced with olive pit powders were manufactured and mechanically characterized. With filler loading, an increase in the tensile modulus but a decrease of the flexural strength may be due to the poor interfacial bonding between olive pit powder and PLA.

Tewakkal et al. investigate the mechanical and physical properties of PLA-kenaf composites. They examined the effect of kenaf derived cellulose (KDC) content (0-60wt%) on the tensile elongation at the break point and during flexural and impact testing and on the water absorption and density of the composites. The elongation at the break point of the composites was 9% on average, making it less elastic than the neat PLA. The flexural strength and modulus also increased by 36% and 54% respectively [8]. The impact strength of the composites was improved at KDC contents below 40wt%, but the impact strength was reduced above 40wt%. The composites containing the highest amount of KDC (60wt%) was denser than the neat PLA and had a water uptake of approximately 12% which is notably low for a biocomposite system.

Yaacab et al. studied the thermal and thermal Properties of Paddy straw as filler in poly lactic acid biocomposites. The effects of paddy straw powder content (5-20 wt %) on mechanical and thermal properties of the biocomposites were investigated. The tensile strength of the biocomposites was above 30 MPa up to 15 wt. % of PSP whereas the elongation at break was ranged between 2-3 % with the incorporation of PSP up to 15 wt.% [9]. Modulus elasticity was increased by increasing the paddy straw powder content. DSC results have demonstrated a minor

effect of the rice straw on thermal behavior of PLA resin (TGA) demonstrated that thermal stability of PLA/PSP biocomposites is reduced by the incorporation of PSP.

Pilla et al. studied the properties of polylactide-recycled wood fiber composites. PLA recycled wood fiber (RWF) composites with a small amount of silane were compounded using a kinetic mixer and molded using an injection molding machine. The molded PLA-RWF composites were characterized using gel permeation chromatography, scanning electron microscope, XRD, DSC, tensile testing machine, and a dynamic mechanical analyzer [10]. As observed in the stress-strain plots, the amount of necking before fracture decreased with an increasing RWF content. Similarly, the strain-at-break also decreased with the RWF content. The tensile strength remained the same irrespective of the RWF content. Both the tensile modulus and the storage modulus of the PLA-RWF composites increased with the RWF content. The degree of crystallinity of the PLA increased with the addition of RWF. No reduction in the number-average molecular weight (M_n) was observed for pure PLA and PLA-10%RWF-0.5%Silane composites after injection molding; however, substantial reduction in M_n was found in PLA-20%RWF-0.5%Silane composites.

Yee et al. investigate the properties of PLA biocomposites films reinforced with oil palm empty fruit bunch (OPEFB) fiber and nanosilica. The composites were characterized via FTIR, UV-visible spectroscopy, FESEM, tensile testing and XRD. The FTIR and FESEM results showed that OPEFB fibers and nanosilica were embedded into PLA matrix. The tensile strength of the composites with addition of nanosilica increased with an increasing fiber content [11]. The XRD analysis showed that the addition of inorganic or organic silica reduced the crystallinity of the composites. The water vapour permeability test indicated the organic silica decreased the diffusion rate of water molecules through the polymer films. The OPEFB reinforced PLA blend with additional silica exhibited a higher thermal stability than the composites reinforced with inorganic silica.

Patanathabutr et al. investigate the influence of CaCO_3 and SiO_2 on mechanical properties and fracture behavior of PLA nanocomposite. Modified CaCO_3 and SiO_2 nanoparticles were prepared with different Si:Ca ratios. It is found that the Si/Ca wt% was increased with respect to

the Si:Ca mole ratio used in the reaction. Incorporating CaCO_3 and SiO_2 of 5 wt% increased elastic modulus, %elongation at break and notched impact strength of PLA nanocomposites [12]. These properties of hydrophilic-modified CaCO_3 -PLA nanocomposite was increased with respect to the increasing of SiO_2 content on the surface of CaCO_3 nanoparticles. This implies that better compatibility between PLA matrix and nano-fillers was achieved after modification surface of CaCO_3 with SiO_2 layers.

Buong et al. studied the effects of graphene nanoplatelets and reduced graphene Oxide on PLA and plasticized PLA [13]. They investigated the superlative mechanical properties of graphene-based materials make them the ideal filler materials for polymer composites reinforcement. Two types of graphene-based materials, graphene nanoplatelets (xGnP) and reduced graphene oxide (rGO), were used as nanofiller in PLA polymer matrix, as well as plasticized PLA. The addition of rGO into PLA or plasticized PLA substantially enhanced the tensile strength without deteriorating elasticity, compared to xGnP nanocomposites. In addition, the investigation of the thermal properties has found that the presence of rGO in the system is very beneficial for improving thermal stability of the PLA or plasticized PLA. SEM images of the rGO nanocomposites display homogenous and good uniformity morphology. TEM images revealed that the rGO remained intact as graphene sheet layers and were dispersed well into the polymer matrix, and it was confirmed by XRD results, which shows no graphitic peak in the XRD pattern.

Qu et al. have prepared nanocomposites of polylactic acid reinforced with cellulose nanofibrils. They used poly(ethylene glycol) (PEG 1000) as a compatibilizer to improve the interfacial interaction between the hydrophobic PLA and the hydrophilic cellulose nanofibers. Composites were characterized by tensile testing machine. AFM, SEM and FTIR [14]. The tensile test results indicated that, by adding PEG to the PLA and the cellulose nanofibrils matrix, the tensile strength and elongation rate increased by 56.7% and 60% respectively, compared with the PLA/cellulose nanofibrils composites. The FTIR analysis successfully showed that PEG improved the intermolecular interaction, which is based on the existence of intermolecular hydrogen bonding among PLA, PEG and cellulose nanofibrils.

Moshiul Alam et al. studied thermo-mechanical and morphological properties of short natural fiber reinforced PLA biocomposite. Untreated oil palm empty fruit bunch (REFB), alkali treated EFB (AEFB), ultrasound treated EFB (UEFB) and simultaneous ultrasound-alkali treated EFB (UAEFB) short fibers were incorporated in PLA for fabricating bio-composites [15]. Glass transition temperature, crystal melting temperature, decomposition temperature, melt flow index, density and mechanical properties (tensile strength, tensile modulus and impact strength) of TEPC are found to be higher than those of REPC. The observed crystallization temperature of TEPC is lower than that of REPC. Among all samples, TEPC prepared from UAEFB fiber shows better performances than other samples fabricated by REFB and AEFB fibers. SEM, FTIR and XRD analyses well support all the observed results.

R. Kumar et al. studied the effect of montmorillonite clay on flax fabric reinforced poly lactic acid composites with amphiphilic additives. Bio-composites (PF) were successfully prepared by reinforcing PLA with woven flax fibers (F) in the presence of mandelic acid, benzoic acid, dicumyl peroxide (DCP) and zein as additives [16]. To improve the mechanical properties of the bio-composites, montmorillonite clay (MMT) was also added. Characterizations of the bio-composites in presence and absence of MMT were performed by FTIR, DSC, TGA and DMTA. The interfacial adhesion between the fibers and the matrix was qualitatively assessed from SEM micrographs of fractured specimens. Intercalation of MMT with 1.4 nm basal spacing was observed in the PLA matrix leading to the increased modulus and water resistance of the bio-composites. Results indicated that mandelic acid and dicumyl peroxide acted as efficient additives for this system. This work provided us the exploratory idea of using MMT in presence of amphiphilic compounds as additives in bio-composites for possible applications.

REFERENCES:

- [1] V.Fiore, L.Botta, R. Scaffaro, A.Valenza, A.Pirrotta., “PLA based biocomposites reinforced with arundo donax fillers,” *Composites Science and Technology*, Vol. 105, pp. 110-117, 2014.
- [2] J.W Park, D.J Lee, E.S Yoo and S.S Im, “ Biodegradable polymer blends of poly (lactic acid) and starch” *Korea Polym J*”, Vol. 7(2), pp. 93-101, 1999.
- [3] H. Ma and C.W Joo, “Structural and mechanical properties of Jute poly (lactic acid) biodegradable composites”, *J. Compos Mater*, Vol. 45(14), pp. 1451-1460, 2010.
- [4] Y.F Shih, C.C Huang, P.Weichen, “Biodegradable green composites reinforced by the fiber recycling from disposable chopsticks”, *Mater. Sci Eng.* , Vol. 527(6), pp. 1516-1521, 2010.
- [5] B. Dimzoski, G. Bogoeva-Gaceva¹, G. Gentile, M. Avella, M.E. Errico, V. Srebrenkoska, “Preparation and characterization of poly (lactic acid)/ rice hulls based biodegradable composites” , *J. Polym. Eng.*, Vol. 28 (6-7), pp. 369-383, 2008.
- [6] S.Y Lee, I.A Kang, G.H Doh, H.G Yoon, B.D Park, and Q. Wu, “Thermal and Mechanical Properties of Wood Flour/Talc-filled Polylactic Acid Composites: Effect of Filler Content and Coupling Treatment”, *J. Thermoplast. Compos. Mater.*, Vol. 21, pp. 209-223, 2008.
- [7] A.F. Koutsomitopoulou , J.C. Bénézet , A. Bergeret , G.C. Papanicolaou, “Preparation and characterization of olive pit powder as a filler to PLA-matrix biocomposites”, *Powder Technology*, Vol. 255, pp. 10-16, 2014.
- [8] M.A.I Syafinaz, Tawakkal, A.R Talib, K.Abdan and C.N Ling, “Mechanical and Physical properties of Kenaf derived cellulose (KDL) filled polylactic acid composites”, *BioResources* , Vol. 7(2), pp. 1643-1655, 2012.
- [9] N.D Yaacaba, H. Ismail, S.S Ting, “Potential Use of Paddy Straw as Filler in Poly Lactic Acid/Paddy Straw Powder Biocomposite: Thermal and Thermal Properties”, *Procedia Chem* , Vol. 19 , pp. 757 – 762, 2016.
- [10] S. Pilla, S. Gong, E. O’Neill, L. Yang, R.M. Rowell, “Polylactide-Recycled Wood Fiber Composites”, *J. Appl. Polym. Sci*, Vol. 111, pp. 37–47 , 2009.
- [11] Y.Y. Yee, Y.C Ching, S. Rozali, N. A. Hashim, and R. Singh, “Preparation and characterization of poly(lactic acid)-based composites reinforced with oil palm empty fruit bunch fiber and nanosilica”, *BioResources*, Vol. 11(1), pp. 2269-2286, 2016.

- [12] B. Nekhamanurak, P. Patanathabutr, and N. Hongsriphan, “ Mechanical properties of hydrophilicity modified CaCO₃-Poly (Lactic Acid) nanocomposite”, *Int. J. Appl. Phy. Math.*, Vol. 2(2), pp. 98-103, 2012.
- [13] B.W Chieng , N. A Ibrahim , W.M.Z.W Yunus , M.Z Hussein ,Y.Y. Then and Y.Y. Loo , “ Effects of graphene nanoplatelets and reduced grapheme o xide on poly(lactic acid) and plasticized Poly(lactic acid):A Comparative Study”, *Polymers*, Vol. 6, pp. 2232-2246, 2014.
- [14] P. Qu, Y. Gao, G.F Wu & L.P. Zhang, “PLA/Cellulose nanocomposites”, *BioResources*, Vol. 5(3), pp. 1811-1823, 2010.
- [15] A. K. M. Moshiul Alam, M. F. Mina, M. D. H. Beg, A. A. Mamun, A. K. Bledzki, and Q. T. H. Shubhra, “T hermo-Mechanical and Morphological Properties of Short Natural Fiber Reinforced Poly (Lactic Acid) Biocomposite: Effect of Fiber Treatment”, *Fib. Polym*, Vol.15(6), 1303-1309, 2014.
- [16] R. Kumar, M.K. Yakabu, R.D Anandjiwala, “Effect of montmorillonite clay on flax fabric reinforced poly lactic acid composites with amphiphilic additives”, *Composites: Part A* 41, pp. 1620–1627, 2010.

THEORETICAL BACKGROUND

3.1 POLYMER

Polymers are defined as macromolecules composed of one or more chemical units (monomers) that are repeated throughout a chain. The basic part of a polymer are the monomers, the monomers are the chemical units that are repeated throughout the chain of a polymer containing ten or less atom in a row. Carbon and hydrogen are the most common atoms in monomers, but oxygen, nitrogen, chlorine, fluorine, silicon and sulfur may also be present. Think of a polymer as a chain in which the monomers are linked (polymerized) together to make a chain with at least 1000 atoms in a row. It is this feature of large size that gives polymers their special properties. Polymers are created through chemical reactions known as polymerizations, and the majority is produced through two basic reaction types. The first type of polymerization reaction is known as a condensation polymerization. The second type of reaction is known as chain-growth polymerization.

3.1.1 CLASSIFICATION OF POLYMER

The following are some of the common classifications of polymers:

<i>Basis of classification</i>	<i>Polymer type</i>	<i>Basis of Classification</i>	<i>Polymer type</i>
Origin	Natural	Tacticity	Isotactic
	Semi synthetic		Syndiotactic
	synthetic		Atactic
Thermal response	Thermoplastic	Polarity	Polar
	Thermosetting		Nonpolar
Mode of formation	Addition	Chain	Hetero
	Condensation		Homochain
Line Structure	Linear	Crystallinity	Noncrystalline
	Branched		Semicrystalline
	Crosslinked		Crystalline
Application & Physical Properties	Rubber		
	Plastic		
	Fiber		

❖ **CLASSIFICATION BASED ON ORIGIN**

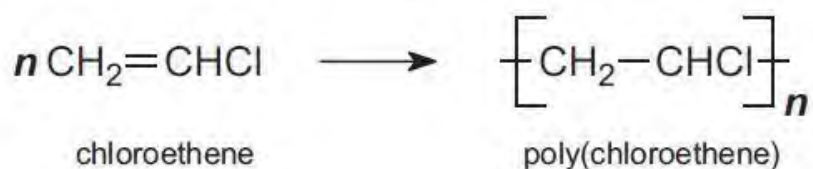
1. **Natural polymer:** - The polymers, which occur in nature are called natural polymer also known as biopolymers. Examples of such polymers are: natural rubber, natural silk, cellulose, starch, proteins, etc.
2. **Semi synthetic polymer:** - They are the chemically modified natural polymers such as hydrogenated, natural rubber, cellulosic, cellulose nitrate, methyl cellulose, etc.
3. **Synthetic polymer:** - The polymer which has been synthesized in the laboratory is known as synthetic polymer. These are also known as manmade polymers. Examples of such polymers are polyvinyl alcohol, polyethylene, polystyrene, polysulfone, etc...

❖ **CLASSIFICATION BASED ON THERMAL RESPONSE**

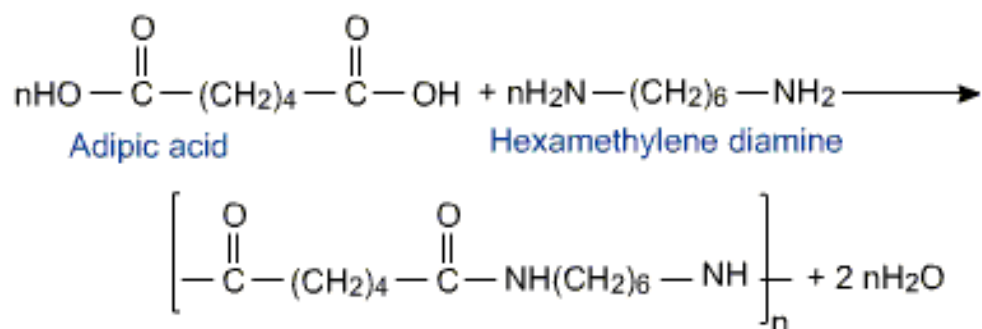
1. **Thermoplastic:** Molecules in a thermoplastic are held together by relatively weak intermolecular forces so that the material softens when exposed to heat and then returns to its original condition when cooled. Thermoplastic polymers can be repeatedly softened by heating and then solidified by cooling - a process similar to the repeated melting and cooling of metals. Most linear and slightly branched polymers are thermoplastic. All the major thermoplastics are produced by chain polymerization. Examples of such polymers are Polyolefins, nylons, linear polyesters and polyether's, PVC, sealing wax etc...Thermoplastics have a wide range of applications because they can be formed and reformed in so many shapes. Some examples are food packaging, insulation, automobile bumpers, and credit cards.
2. **Thermosets:** Thermosets cannot be reshaped by heating. Thermosets usually are three-dimensional networked polymers in which there is a high degree of cross-linking between polymer chains. The cross-linking restricts the motion of the chains and leads to a rigid material. For example Phenolic, resins, urea, epoxy resins, diene rubbers, etc.

❖ CLASSIFICATION BASED ON MODE OF FORMATION

1. **Addition polymers:** The addition polymers are formed by the repeated addition of monomer molecules possessing double or triple bonds, the polymers formed by the addition of monomers repeatedly without removal of by products are called addition polymers. e.g., the formation of polythene from ethene and polypropene from propene. However, the addition polymers formed by the polymerisation of a single monomeric species are known as homopolymers.



2. **Condensation polymers:** They are formed by the combination of two monomers by removal of small molecules like water, alcohol or NH_3 . ex... Nylon 6, 6, Nylon 6, etc. For example, nylon 6, 6 is formed by the condensation of hexamethylene diamine with adipic acid.



❖ CLASSIFICATION BASED ON STRUCTURE OF POLYMER

1. **Linear polymers on Structure :** In these polymers monomers are linked with each other and form a long straight chain. These chains has no any side chains, ex. Polyethene, PVC,

Chapter 3 Theoretical Background

Nylons, polyesters etc. Their molecules are closely packed and have high density, tensile strength. These are represented f niig.3.1.1.



Fig. 3.1.1: Linear Chain Polymers

2. **Branched chain polymers** :They have a straight long chain with different side chains. Their molecules are irregularly packed hence they have low density, tensile strength and melting point, ex... polypropylene , amylopectin and glycogen.



Fig. 3.1.2: Branched Chain Polymers

3. **Crosslinked or Network polymers:** These polymers in which two linear chains are joined together by covalent bonds and it have three dimensional. Degree of crosslinking is a number of junction point per unit volume. Polymers crosslinking are hard, rigid .and brittle due to their network structure. Polymers Cross linked do not dissolve in solvents because all the polymer chains are covalently tied together, but they can absorb solvents. Ex. Bakelite, melamine, formaldehyde resins, vulcanised rubber etc. These polymers are depicted in fig. 3.1.3.

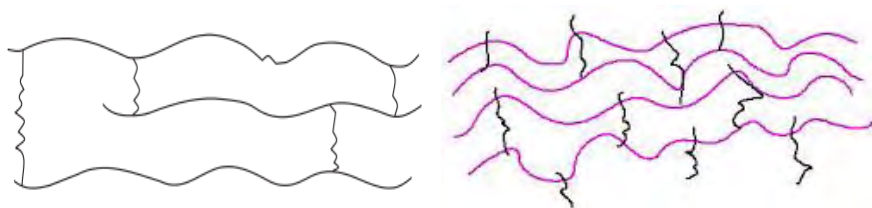


Fig. 3.1.3: Cross Linked Polymers

❖ **CLASSIFICATION BASED ON APPLICATION & PHYSICAL PROPERTIES**

- 1. Rubber (Elastomers):** Rubber is a high molecular weight polymer with long flexible chains and weak intermolecular forces. They exhibit tensile strength in the range of 300-3000 psi and elongation at break ranging between 300-1000%. Examples are natural and synthetic fiber.
- 2. Plastic:** Plastic are relatively tough substances with high molecular weight that can be molded with (or without) the application of heat. These are usually much stronger than rubbers. They exhibit tensile strength ranging between 400-15000 Psi & elongation at break ranging usually from 20 to 200% or even higher. The examples of plastic are, polyethylene, polypropylene, PVC, polystyrene etc.
- 3. Fibers:** Fibers are long chain polymers characterized by highly crystalline regions resulting mainly from secondary forces. They have a much lower elasticity than plastic and elastomers. They also have high tensile strength ranging between 20,000-150,000 Psi., are light weight & possess moisture absorption properties.

❖ **CLASSIFICATION BASED ON TACTICITY**

Tacticity: It may be defined as the geometric arrangement (orientation) of the characteristic group of monomer unit with respect to the main chain (backbone) of the polymer may be classified into three groups.

- 1. Isotactic Polymer:** It is the type of polymer in which the characteristic group are arranged on the same side of the main chain.
- 2. Syndiotactic Polymer:** A polymer is said to be syndiotactic, if the side group (characteristic group) are arranged in an alternate fashion.
- 3. Atactic Polymer:** A polymer is said to be atactic, if the side group (characteristic group) are arranged in an irregular fashion.

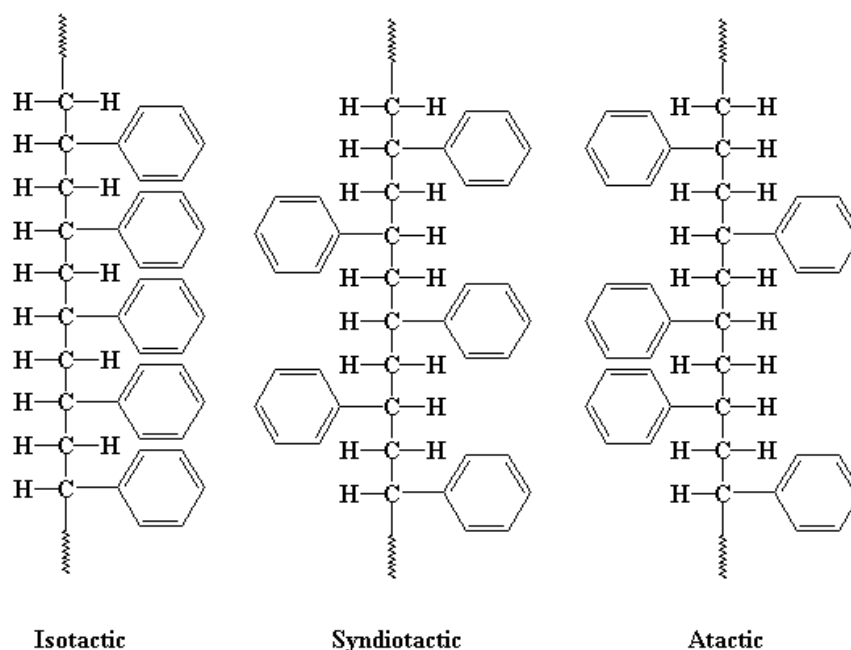


Fig. 3.1.4: Isotactic, Syndiotactic and Atactic Polymers

❖ **CLASSIFICATION BASED ON TYPES OF MONOMERS**

1. **Homopolyme:** A polymer containing a single type of repeat unit is called a homopolymers e.g., polystyrene.
2. **Hetropolymer (Copolymer):** If a polymer is made up two different monomers then it is called copolymer, e.g., butadiene –styrene rubber.

❖ **CLASSIFICATION BASED ON MORPHOLOGY**

Polymers can be classified into two classes on the basis of morphology:

1. **Crystalline polymers:** Invariably don't form perfect crystalline materials but instead are semi crystalline with both crystalline and amorphous regions. The crystalline phases of such polymers are characterized by their melting temperature (T_m).

2. Amorphous Polymers: Characterized by their glass transition temperature (T_g), the temperature at which they transform abruptly from the glass state (hard) to the rubbery state (soft). This transition corresponds to the onset of chain motion.

3.1.2 POLYMERIZATION

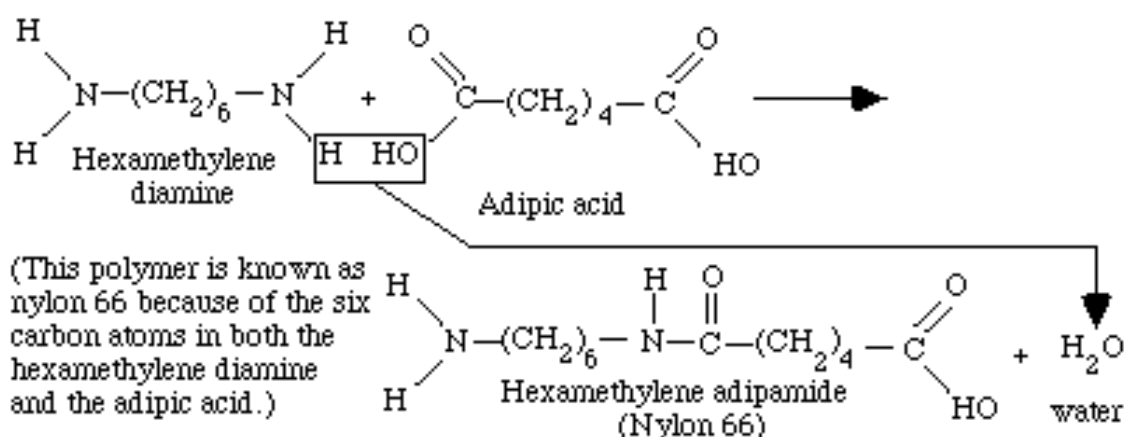
The chemical reaction in which high molecular mass are formed from monomers is known as polymerization. The processes of polymerization are divided into two groups.

1. Condensation or Step-Reaction Polymerization
2. Addition or Chain-Reaction Polymerization

1. Condensation or Step-Reaction Polymerization:

Condensation takes place between two polyfunctional molecules to produce one larger polyfunctional molecule, with the possible elimination of a small molecule such as water. The reaction continues until almost all of one of the reagents is used up; an equilibrium is established which can be shifted at will at high temperatures by controlling the amounts of the reactants and products.

Nylon 66 is an example of a common polymeric clothing material, involving one each of two monomers, hexamethylene diamine and adipic acid, reacting to form a dimer of Nylon 66.



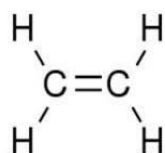
Chapter 3 Theoretical Background

There are two types of condensation polymer

1. Polymaid (Nylon)
2. Polyester

2. Addition or Chain-Reaction Polymerization

Addition polymerization involves chain reaction in which the chain carrier may be an ion or a reactive substance with one unpaired electron called a free radical. A free-radical is a chemical component that contains a free electron that forms a covalent bond with an electron on another molecule. The free radical can react to open the double bond of a Vinyl monomer and add to it, with one electron remaining unpaired. In a very short time, many more monomers add successively to the growing chain. Finally two free radicals react to end each other's growth activity and form one or more polymer molecules. Ethylene is an example of a monomer used to make a common polymer.



Ethylene

The polymerization process of addition or chain reaction polymerization consists of three steps:

1. Initiation
2. Propagation
3. Termination

3.1.3 PHYSICAL STATE OF POLYMER

The concept of three physical states of matter, gaseous, liquid and solid, is insufficient for the properties of polymers to be characterized. The concept of the phase state is not sufficient for this purpose either. So there have been introduced three physical states for polymer to exist in: The viscofluid state, the glassy state and the rubbery state.

The viscofluid state of polymers is characterized by the possibility of the intensive thermal motion of individual units, large fragments of the polymeric chain and the movement of the macromolecules as a whole, fluidity is observed in this state.

When the temperature is lowered below the flow temperature, the polymeric material goes to the rubbery state. In this state individual unit, atomic groups and segments undergo intensive thermal motion but the movement of macromolecules as a separate kinetic unit is impossible. They are capable of undergoing enormous recoverable deformations. The low temperature limit of the rubbery state is the glass transition temperature T_g , below which polymer is in the glassy state.

In glassy state polymers are no longer capable of undergoing segmental motion. The glassy state is characterized by the vibrational motion, small unit in the main chain and also atomic groups, which make up side pedant groups, can execute torsional vibration.

3.1.4: GLASS TRANSITION TEMPERATURE OF POLYMER

The glass transition (T_g) is one of the most important properties of any polymer & the temperature region is where polymer transition from a hard, glassy material to a soft, rubbery material and at which the internal energy of the chains of the polymer increases such as extends that the chains just start leaving their lattice sited. Below glass transition temperature(T_g) polymers are usually hard brittle & glass like in mechanical behavior & above glass transition (T_g), polymers are usually more soft, flexible and rubbery(elastic), like in mechanical behavior. Some polymers are used above their glass transition temperatures, and some are used below their glass transition temperature. Hard plastic like polysterene and poly (methyl methacrylate), are used below their glass transition temperature, both at around 100°C , Rubber elastomers like polyisoprene and polyisobutylene, are used above their T_g 's, that is in the rubbery state, where they are soft and flexible.

When the temperature is warm, the polymer chains can move around easily. So, when we take a piece of the polymer and bend it, the molecules, being in motion already, have no trouble moving into new position to relieve the stress that have been placed on them. But if we try to bend sample of a polymer below its T_g , the polymer chains won't be able to move into new position to relieve the stress that have been placed on them. Then one of the two things will happen. Either (A) the chains are strong enough to resist the force we apply, and the sample won't bend; or (B) the applied force will be too much for the motionless polymer chains to resist, and being unable to move around to relieve the stress, the polymer sample will break or shatter in our hands.

The change in mobility with temperature happens because the phenomenon we call “heat” is really a form of kinetic energy; that is, the energy of objects in motion. It is actually an effect of random motion of molecules, whether they are polymer molecules or small molecules. Things are “hot” when their molecules have lots of kinetic energy and move around very fast. Things are “cold” when their molecules lack kinetic energy and move around slowly, or not at all. Now the exact temperature at which the polymer chains undergo this big change in mobility depends on the structure of polymer. A small change in structure can cause a big change in T_g . For example, the small structural difference between poly (methyl acrylate) and poly (methyl methacrylate) lead to a big difference their T_g 's. There are some factors affecting the T_g (i) Chain flexibility (ii) Geometric factors (iii) Inter chain attractive forces (iv) Copolymerization (v) Chain length (vi) Cross linking and branching (vii) Crystallinity (viii) Plasticization, etc..

3.2 POLYLACTIC ACID (PLA)

Poly(lactic acid) (PLA) is highly versatile, biodegradable, aliphatic polyester derived from 100% renewable resources [1]. It has extensive applications in biomedical fields, including suture, bone fixation material, drug delivery microsphere, and tissue engineering [2]. Because of these properties the PLA has been widely studied for use in medical applications. The chemistry of PLA involves the processing and polymerization of lactic acid monomer. Since, lactic acid is a chiral molecule, PLA has stereoisomers, such as poly (L-lactide) (PLLA), poly (D-lactide) (PDLA), and poly(DL-lactide) (PDLLA). Isotactic and optically active PLLA and PDLA are crystalline, whereas relatively a tactic and optically inactive PDLLA is amorphous [3]. The L-isomer is a biological metabolite and constitutes the main fraction of PLA derived from renewable sources since the majority of lactic acid from biological sources exists in this form (α , β , and γ) (Lim et al., 2008). PLLA has gained great attention because of its excellent biocompatibility and mechanical properties. However, its long degradation times coupled with the high crystallinity of its fragments can cause inflammatory reactions in the body. In order to overcome this, PLLA can be used as a material combination of L-lactic and D, L-lactic acid monomers, being the latter rapidly degraded without formation of crystalline fragments during this process [4].

3.2.1 PHYSICAL AND CHEMICAL PROPERTIES OF PLA

L-lactic acid and D-lactic acid, the two isomers of lactic acid, are shown in Fig. (3.2.1). Pure L lactic acid or D-lactic acid, or mixtures of both components are needed for the synthesis of PLA. The homopolymer of LA is a white powder at room temperature with T_g and T_m values of about 55°C and 175°C, respectively. High molecular weight PLA is a colorless, glossy, rigid thermoplastic material with properties similar to polystyrene. The two isomers of LA can produce four distinct materials: Poly (*D*-lactic acid) (PDLA), a crystalline material with a regular chain structure; poly (*L*-lactic acid) (PLLA), which is hemicrystalline, and likewise with a regular chain structure; poly(*D,L*-lactic acid) (PDLLA) which is amorphous; and *meso*-PLA, obtained by the polymerization of *meso*-lactide. PDLA, PLLA and PDLLA are soluble in common solvents including benzene, chloroform, dioxane, etc. and degrade by simple hydrolysis of the ester bond even in the absence of a hydrolase. PLA has a degradation half-life in the environment ranging from 6 months to 2 years, depending on the size and shape of the article, its isomer ratio, and the temperature. The tensile properties of PLA can vary widely depending on whether it is annealed or oriented, or its degree of crystallinity [5]. Some of the physical and chemical properties of PLA are summarized in table 3.2.1.

Table 3.2.1: Properties of polylactic acid

Properties	PLA
Density	125 g/cm ³
Elongation at break	6%
Elastic (Young's Tensile)Modulus	3.5 GPa
Flexurul Modulus	4 GPa
Flexural Strength	80 MPa
Glass Transition Temperature	60 ⁰ C
Heat deflection temperature at 455 KPa	65 ⁰ C
Melting onset (solidus)	160 ⁰ C
Shear Modulus	24 GPa
Specific heat capacity	1800 J/kg
Strength to weight ratio	40 KN-m/kg
Tensile strength (ultimate)	50 MPa
Thermal Conductivity	0.13 w/m-K

3.2.2 PLA SYNTHESIS

There are two important methods for PLA synthesis: direct polycondensation of lactic acid and ring opening polymerization of lactic acid cyclic dimer, known as lactide. Figure 3.2.1 shows the reaction mechanism for both of them. In direct condensation, solvent is used and higher reaction times are required. The resulting polymer is a material of low to intermediate molecular weight.

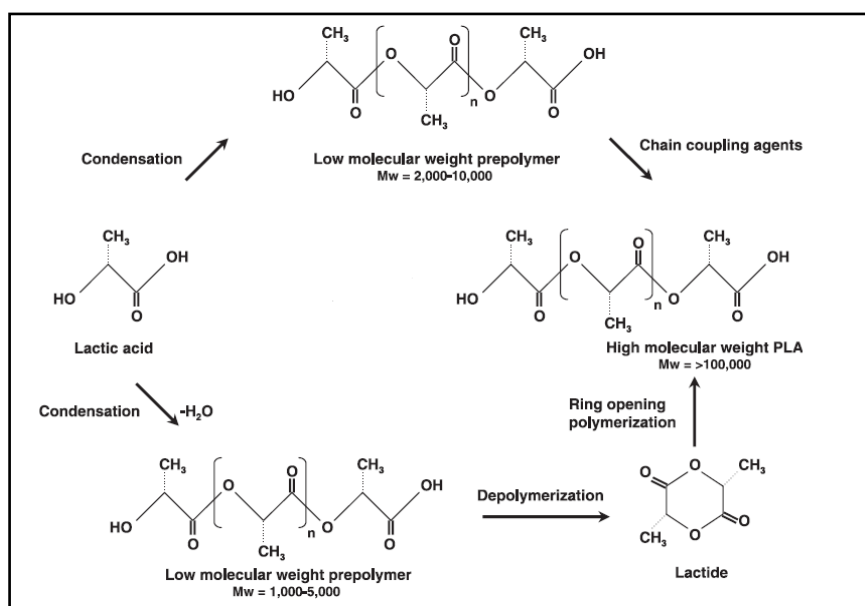


Fig 3.2.1: Synthesis of PLA

Ring-opening polymerization (ROP) of the lactide needs catalyst but results in PLA with controlled molecular weight [6]. Depending on monomer used and controlling reactions conditions, it is possible to control the ratio and sequence of D and L-lactic acid units in the final polymer. This polymerization route was selected for this study.

3.3 GRAPHITE

Carbon has two natural crystalline allotropic forms: graphite and diamond. Each has its own distinct crystal structure and properties. Graphite derives its name from the Greek word "graphein", to write. The material is generally greyish-black, opaque and has a lustrous black sheen. It is unique in that it has properties of both a metal and a non-metal. It is flexible but

not elastic, has a high thermal and electrical conductivity, and is highly refractory and chemically inert. Graphite has a low adsorption of X-rays and neutrons making it a particularly useful material in nuclear applications. The unusual combination of properties is due its crystal structure (Fig. 3.3.1). The carbon atoms are arranged hexagonally in a planar condensed ring system. The layers are stacked parallel to each other. The atoms within the rings are bonded covalently, whilst the layers are loosely bonded together by Vander Waals forces. The high degree of anisotropy in graphite results from the two types of bonding acting in different crystallographic directions. For example, graphite's ability to form a solid film lubricant comes from these two contrasting chemical bonds. The fact that weak Vander Waals forces govern the bonding between individual layers permits the layers to slide over one another making it an ideal lubricant. World production of graphite was estimated to be about 602,000 tons in 2000, with China being the biggest producer followed by India, Brazil, Mexico and then the Czech Republic.

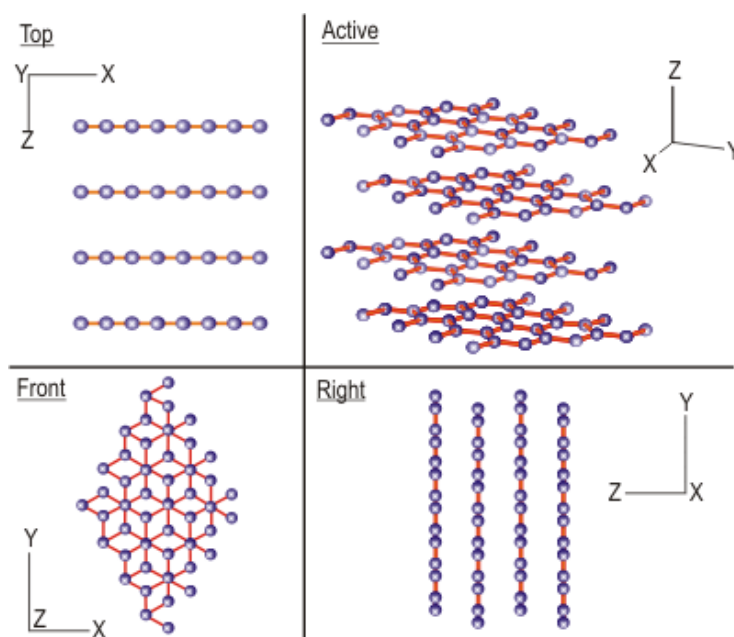


Fig. 3.3.1: Crystal structure of graphite.

3.3.1 GRAPHITE CLASSIFICATIONS

There are two main classifications of graphite, natural and synthetic.

Natural Graphite: Natural Graphite is a mineral consisting of graphitic carbon. It varies considerably in crystallinity. Most commercial (natural) graphite's are mined and often contain other minerals. Subsequent to mining the graphite often requires a considerable amount of mineral processing such as froth flotation to concentrate the graphite. Natural graphite is an excellent conductor of heat and electricity. It is stable over a wide range of temperatures. Graphite is a highly refractory material with a high melting point (365⁰C.)

Natural graphite is subdivided into three types of material:

- Amorphous
- Flake
- High Crystalline

Amorphous Graphite: Amorphous graphite is the least graphitic of the natural graphite's. However, the term "amorphous" is a misnomer since the material is still crystalline. Amorphous graphite is found as minute particles in beds of mesomorphic rocks such as coal, slate or shale deposits. The graphite content ranges from 25% to 85% dependent on the geological conditions. Amorphous graphite is extracted using conventional mining techniques and occurs primarily in Mexico, North Korea, South Korea and Austria.

Flake Graphite: Flake graphite is found in metamorphic rocks uniformly distributed through the body of the ore or in concentrated lens shaped pockets. Carbon concentrations vary between 5% and 40%. Graphite flake occurs as a scaly or lamella form in certain metamorphic rocks such as limestone, gneisses and schist's. Flake graphite is removed by froth flotation. "As floated" graphite contains between 80% and 90% graphite. Flake graphite is produced with >98% through chemical beneficiation processes. Flake graphite occurs in most parts of the world.

Crystalline Graphite: Crystalline vein graphite is believed to originate from crude oil

deposits that through time, temperature and pressure have converted to graphite. Vein graphite fissures are typically between 1cm and 1 m thick, and are typically > 90% pure. Although this form of graphite is found all over the world, it is only commercially mined in Sri Lanka by conventional shaft or surface mining techniques.

Synthetic Graphite: Synthetic graphite can be produced from coke and pitch. It tends to be of higher purity though not as crystalline as natural graphite. There are essentially two types of synthetic graphite. The first is electro graphite, which is pure carbon produced from calcined petroleum coke and coal tar pitch in an electric furnace. The second type of synthetic graphite is produced by heating calcined petroleum pitch to 2800°C. On the whole synthetic graphite tends to be of a lower density, higher porosity and higher electrical resistance. Its increased porosity makes it unsuitable for refractory applications. Synthetic Graphite consists mainly of graphitic carbon that has been obtained by graphitization, heat treatment of non-graphitic carbon, or by chemical vapour deposition from hydrocarbons at temperatures above 2100K.

3.3.2 PROPERTIES OF GRAPHITE : Some properties of commercial graphite are summarized in table 3.2.1.

Table 3.3.1: Properties of commercial graphite

Property	Commercial graphite
Bulk Density (g/cm ³)	1.3-1.95
Porosity (%)	0.7-53
Modulus of Elasticity (GPa)	8-15
Compressive strength (MPa)	20-200
Flexural strength (MPa)	6.9-100
Coefficient of Thermal Expansion (x10 ⁻⁶ /°C)	1.2-8.2
Thermal conductivity (W/m.K)	25-470
Specific heat capacity (J/kg.K)	710-830
Electrical resistivity (Ω.m)	5x10 ⁻⁶ -30x10 ⁻⁶

3.3.3 APPLICATIONS OF GRAPHITE

➤ Refractory Materials

Due to its high temperature stability and chemical inertness graphite is a good candidate for a refractory material. It is used in the production of refractory bricks and in the production of “Mag-carbon” refractory bricks (Mg-C.) Graphite is also used to manufacture crucibles, ladles and moulds for containing molten metals. Additionally graphite is one of the most common materials used in the production of functional refractories for the continuous casting of steel. In this application graphite flake is mixed with alumina and zirconia and then isostatically pressed to form components such as stopper rods, subentry nozzles and ladle shrouds used in both regulating flow of molten steel and protecting against oxidation. This type of material may also be used as shielding for pyrometers. In the production of iron, graphite blocks are used to form part of the lining of the blast furnace. Its structural strength at temperature, thermal shock resistance, high thermal conductivity, low thermal expansion and good chemical resistance are of paramount importance in this application. The electrodes used in many electrical metallurgical furnaces are manufactured from graphite such as the electric arc furnaces used for processing steel.

➤ Chemical Industry

There are many high temperature uses for graphite in the chemical industry such as in the production of phosphorus and calcium carbide in arc furnaces. Graphite is used as anodes in some aqueous electrolytic processes such as in the production of halogens (chlorine and fluorine.)

➤ Nuclear Industry

High purity electrographite is used in large amounts for the production of moderator rods and reflector components in nuclear reactors. Their suitability arises from their low absorption of neutrons, high thermal conductivity and their high strength at temperature.

➤ Electrical Applications

The main application for graphite as an electrical material is in the manufacture of carbon

brushes in electric motors. In this application the performance and lifetime of the component is very dependent on grade and structure.

➤ **Mechanical Applications**

Graphite is used widely as an engineering material over a variety of applications. Applications include piston rings, thrust bearings, journal bearings and vanes. Carbon based seals are used in the shafts and fuel pumps of many aircraft jet engines.

Other Applications

Amorphous graphite has applications in:

- Metallurgy
- Pencil production
- Refractories
- Coatings
- Lubricants
- Paint production

Crystalline graphite is used in:

- Batteries
- Lubricants
- Grinding wheels
- Powder metallurgy.

Flake graphite is used predominantly in refractory applications mainly in secondary steel making; in addition to this it may also be used in lubricants, powder metallurgy, pencils and coatings.

Most sources of natural graphite are also used in the fabrication of graphite foil.

Synthetic graphites are used in:

- Aerospace applications

Chapter 3 Theoretical Background

- Batteries
- Carbon brushes
- Graphite electrodes for electric arc furnaces for metallurgical processing
- Moderator rods in nuclear power plant.

Due to its increased porosity synthetic graphite tends not be used in refractory applications.

3.4 COMPOSITE MATERIALS

Composites can be defined as materials that consist of two or more chemically and physically different phases separated by a distinct interface. The different systems are combined judiciously to achieve a system with more useful structural or functional properties nonattainable by any of the constituent alone. Composites, the wonder materials are becoming an essential part of today's materials due to the advantages such as low weight, corrosion resistance, high fatigue strength, and faster assembly. They are extensively used as materials in making aircraft structures, electronic packaging to medical equipment, and space vehicle to home building [7]. The basic difference between blends and composites is that the two main constituents in the composites remain recognizable while these may not be recognizable in blends. The predominant useful materials used in our day-to-day life are wood, concrete, ceramics, and so on. Surprisingly, the most important polymeric composites are found in nature and these are known as natural composites. The connective tissues in mammals belong to the most advanced polymer composites known to mankind where the fibrous protein, collagen is the reinforcement. It functions both as soft and hard connective tissue. Composites are combinations of materials differing in composition, where the individual constituents retain their separate identities. These separate constituents act together to give the necessary mechanical strength or stiffness to the composite part. Composite material is a material composed of two or more distinct phases (matrix phase and dispersed phase) and having bulk properties significantly different from those of any of the constituents. Matrix phase is the primary phase having a continuous character. Matrix is usually more ductile and less hard phase. It holds the dispersed phase and shares a load with it. Dispersed (reinforcing) phase is embedded in the matrix in a discontinuous form. This secondary phase is called the dispersed phase. Dispersed phase is usually stronger than the

matrix, therefore, it is sometimes called reinforcing phase. Composites in structural applications have the following characteristics:

1. They generally consist of two or more physically distinct and mechanically separable materials.
2. They are made by mixing the separate materials in such a way as to achieve controlled and uniform dispersion of the constituents.
3. They have superior mechanical properties and in some cases uniquely different from the properties of their constituents [8].

Wood is a natural composite of cellulose fibers in a matrix of lignin. Most primitive man-made composite materials were straw and mud combined to form bricks for building construction. Most visible applications pave our roadways in the form of either steel and aggregate reinforced Portland cement or asphalt concrete. Reinforced concrete is another example of composite material. The steel and concrete retain their individual identities in the finished structure. However, because they work together, the steel carries the tension loads and concrete carries the compression loads. Most advanced examples perform routinely on spacecraft in demanding environments. Advanced composites have high-performance fiber reinforcements in a

polymer matrix material such as epoxy. Examples are graphite/epoxy, Kevlar/epoxy, and boron/epoxy composites. Advanced composites are traditionally used in the aerospace industries, but these materials have now found applications in commercial industries as well.

3.4.1 CLASSIFICATION OF COMPOSITES

On the basis of matrix phase, composites can be classified into *metal matrix composites (MMCs)*, *ceramic matrix composites (CMCs)*, and *polymer matrix composites (PMCs)* (Fig.3.4.1) [9]. The classifications according to types of reinforcement are particulate composites (composed of particles), fibrous composites (composed of fibers), and laminate composites (composed of laminates). Fibrous composites can be further subdivided on the basis of natural/biofiber or synthetic fiber. Biofiber encompassing composites are referred to as biofiber composites. They can be again divided on the basis of matrix, that is,

nonbiodegradable matrix and biodegradable matrix [10]. Bio-based composites made from natural/biofiber and biodegradable polymers are referred to as green composites. These can be further subdivided as hybrid composites and textile composites. Hybrid composites comprise of a combination of two or more types of fibers.

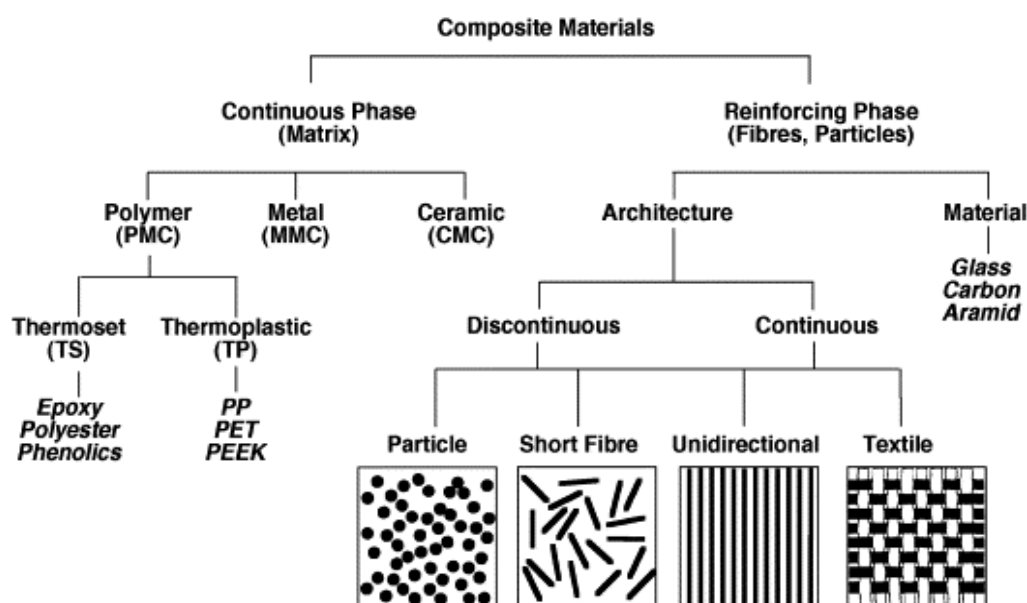


Fig. 3.4.1: Systematic illustration of the structural components of composite materials. Sources: Verpoest, (1998).

❖ Polymer Matrix Composites

Most commercially produced composites use a polymer matrix material often called a resin solution. There are many different polymers available depending upon the starting raw ingredients. There are several broad categories, each with numerous variations. The most common are known as polyester, vinyl ester, epoxy, phenolic, polyimide, polyamide, polypropylene, polyether ether ketone (PEEK), and others. The reinforcement materials are often fibers but can also be common ground minerals [11]. The various methods described below have been developed to reduce the resin content of the final product. As a rule of thumb, hand layup results in a product containing 60% resin and 40% fiber, whereas vacuum infusion gives a final product with 40% resin and 60% fiber content. The strength of the

product is greatly dependent on this ratio. PMCs are very popular due to their low cost and simple fabrication methods. Use of non-reinforced polymers as structure materials is limited by low level of their mechanical properties, namely strength, modulus, and impact resistance. Reinforcement of polymers by strong fibrous network permits fabrication of PMCs, which is characterized by the following:

- a) High specific strength
- b) High specific stiffness
- c) High fracture resistance
- d) Good abrasion resistance
- e) Good impact resistance
- f) Good corrosion resistance
- g) Good fatigue resistance
- h) Low cost

The main disadvantages of PMCs are

- a) Low thermal resistance and
- b) High coefficient of thermal expansion

❖ Metal Matrix Composites

Metal-matrix composites are energetic composites which when combined with metal oxides and nanoscale aluminium powder, can form superthermite materials. Metal matrices offer higher strength, fracture toughness and stiffness than those offered by their polymer counterparts. They can withstand elevated temperature in corrosive environment than polymers. Most metal alloys could be used as matrices and they require reinforcement materials, which are stable at elevated temperature and non-reactive too. Light metals form the matrix for low temperature applications and their low density is also an advantage.

Titanium, aluminium and magnesium are popular metal matrix materials.

❖ Ceramic Matrix Composites

In this group of composites the main part of the volume is occupied by a ceramic, i.e. a chemical compound from the group of oxides, nitrides, borides, silicates etc.. In most cases, ceramic-matrix composites encompass a metal as the second component. Ideally both

components, Ideally both components, the metallic one and the ceramic one, are finely dispersed in each other in order to elicit the particular nanoscopic properties. Nanocomposites from these combinations were demonstrated in improving their optical, electrical and magnetic properties as well as tribiological, corrosion-resistance and other protective properties. The binary phase diagram of the mixture should be considered in designing ceramic metal composites and measure have to be taken to avoid a chemical reaction between both components. The metallic component may easily react with the ceramic and thereby loosing its metallic character. So it is essential to carefully choose immiscible metal and ceramic phases. A good example for such a combination is represented by the ceramic-metal composite of TiO_2 and Cu. The preparation of the ceramic component generally requires high process temperatures.

3.4.2 APPLICATION OF POLYMER COMPOSITE

Improved mechanical, thermal and electrical properties have resulted in major interest in composites materials in numerous automotive, household and general/ industrial applications [12]. Some of major applications are discussed below:

❖ Food Packaging

The gaseous barrier property improvement that can result from incorporation of relatively small quantities of nanoclay materials is shown to be substantial. Data provided from various sources indicates oxygen transmission rates for polyamide-organoclay composites which are usually less than half that of the unmodified polymer. Further data reveals the extent to which both the amount of clay incorporated in the polymer, and the aspect ratio of the filler contributes to overall barrier performance. In particular, aspect ratio is shown to have a major effect, with high ratios (and hence tendencies towards filler incorporation at the nano level) quite dramatically enhancing gaseous barrier properties. Such excellent barrier characteristics have resulted in considerable interest in nanoclay composites in food packaging applications, both flexible and rigid. Specific examples include packaging for processed meats, cheese, confectionery, cereals and boil-in-the-bag foods, paperboard for fruit juice and dairy products, beer and carbonated drinks bottles. The use of nanocomposites formulations would be expected to enhance considerably the shelf life of many types of food. Triton systems and the US Army are conducting further work on barrier performance in a joint investigation. The

requirement here is for a non-refrigerated packaging system capable of maintaining food freshness for three years. Nanoclay polymer composites are currently showing considerable promise for this applications. It is likely that excellent gaseous barrier properties exhibited by nanocomposite polymer system will result in their substantial use as packaging materials in future years.

❖ **Automobiles and Aerospace**

In automobiles and aerospace there are huge demand and possibilities of polymeric nanocomposites. They are used in different components of the automobiles such as timing belt covers, hood applications, engine covers, tires, step resistant components, structural seat backs, fuel lines and fuel system components etc. The first commercial example of polymeric nanocomposites in automotive applications was clay-nylon-6 nanocomposites used for making timing belt covers (the Toyota Motor Company, 1991). More Significantly, these composites have been in use in under the hood applications in the Toyota Camry. Unitika, Japan introduced nylon-6 for engine covers on Mitsubishi's GDI engines. Chevrolet Impalas developed doors with thermoplastic polyolefin nanocompsite. After that General Motors and Basell published the application of clay/polyolefin nanocomposites as a step assistant component for GMC Safari and Chevrolet Astro vans in 2001, Honda Acura developed clay-PP nanocomposites for structural seat backs and with clay-nylon-12 nanocomposites Ube developed fuel lines and fuel system components for automotives. Organic polymer with uniformly dispersed nanoscale fillers in organic precursors may enable polymeric materials to withstand the harsh space environment and be used as critical weight reduction materials. Selfrigidizing and self-passivating nanocomposite materials could be used to construct space vehicle components that are both highly resistant to space-borne particles and resistant to degradation from electromagnetic radiation, while reducing the overall weight of the spacecraft. Researchers at NASa Langely Center developed transperant nanocomposites with chemically modified clay, which is lightweight, durable and microcracking resistant and suitable for a variety of aerospace applications.

❖ **Film and membranes**

The presence of filler incorporation at nano-levels has also been shown to have significant effects on the transparency and haze charateristics of films. In comparison to conventionally filled polymers, nanoclay incorporation has been shown to significantly enhance transparency and reduce haze. With polyamide based composites, this effect has been shown to be due to

modifications in the crystallization behaviour brought about by the nanoclay particles; spherulitic domain dimensions being considerably smaller. Similarly, nano-modified polymers have been shown, when employed to coat polymeric transparency materials, to enhance both toughness and hardness of these materials without interfering with light transmission characteristics. An ability to resist high velocity impact combined with substantially improved abrasion resistance was demonstrated by Haghghat of Triton system .

❖ **Flammability resistance Materials**

The ability of nanoclay incorporation to reduce the flammability of polymeric materials was a major theme of the paper presented by Gilman of the National Institute of Standards and Technology in the US. In his work Gilman demonstrated the extent to which flammability behavior could be restricted in polymers such as polypropylene with as little as 2% nanoclay loading. In particular heat release rates, as obtained from cone calorimetry experiments, were found to diminish substantially by nanoclay incorporation. Although conventional microparticle filler incorporation, together with the use of flame retardant and intumescent agents would also minimize flammability behavior, this is usually accompanied by reductions in various other important properties. With the nanoclay approach, this is usually achieved whilst maintaining or enhancing other properties and characteristics.

❖ **Electrical, Electronic and Optoelectronic devices**

Nanotechnology is deeply embedded in the design of advanced devices for electrical, electronic and optoelectronic applications. The dimensional scale for electronic devices has now entered the nanorange. The utility of polymer based nanocomposites in these areas is quite diverse involving many potential applications. One specific nanocomposite type receiving considerable interest involves conjugated polymers and carbon nanotubes. A recent review of this area notes a litany of potential applications including photovoltaic (PV) cells and photodiodes, supercapacitors, sensors, transparent conductive coating, printable conductors, light emitting diodes (LED) and field effect transistors. The electrical conductivity of carbon nanotubes in insulating polymers has also been a topic of considerable interest. The potential applications include electromagnetic interference shielding, transparent conductive coatings, electrostatics dissipations, supercapacitors, electromechanical actuators and various electrode applications. The percolation threshold for electrical conductivity of

epoxy composites containing multi-wall carbon nanotubes was found to be 0.0025 wt% MWCNT's, considerably lower than nanoscale dispersed carbon black particles. Polymer based nanocomposites are most relevant for the anode, hole injection layer, light emitting layer and light harvesting layer. In the case where flexible transparent substrates are desired, nanocomposites or nanolayered combinations of polymer and barrier nanomaterials can be employed to provide barrier properties to oxygen and water permeation. Silicon-based PV devices offer high efficiency, excellent stability and proven commercial utility.

❖ Biomedical Applications

The applicability of polymer nanotechnology and nanocomposites to emerging area of development. One area of intense research involves electrospinning for producing bioresorbable nanofiber scaffolds for tissue engineering applications. Another area also involving nanofibers is the utilization of electrically conducting nanofibers based on conjugated polymers for regeneration of nerve growth in a biological living system. Nanoparticle silver, silver oxide and silver salts have been incorporated into polymer matrices to provide antimicrobial activity. Silver is also introduced in natural rubber for the application in antimicrobial latex gloves. Polymer nanocomposites based on hydroxyapatite [$\text{Ca}_{10}(\text{PO}_4)_6(\text{OH})_2$] have been investigated for bone repair and implantation.

❖ Sports items

One of the initial uses for exfoliated clay is in polyisobutylene for permeability barrier applications involved a 20 μm coating on the interior of tennis and soccer balls to prevent depressurization. The product was developed by InMat LLC and introduced in 2001. Sports equipments was one of the initial areas where carbon fiber composites were commercialized. CNT (at low levels) reinforced epoxy matrix is used in tennis rackets and hockey sticks to increase their strength and stiffness. In such applications, performance overrides the economic disadvantages of the expensive carbon nanotube inclusion.

3.5 THEORY OF SURFACE MORPHOLOGY

Morphology is a qualitative evaluation of the three dimensional shape of a surface, i.e., "what a sample looks like," and also evaluate the size of a line, an area, or a volume; the texture or

topography of a surface; the habit of a crystal; the distribution of phases in a system (material). is best evaluated using imaging techniques, such as optical microscopy or Scanning Electron Microscopy (SEM). These methods can also provide layer thickness and other quantitative information.

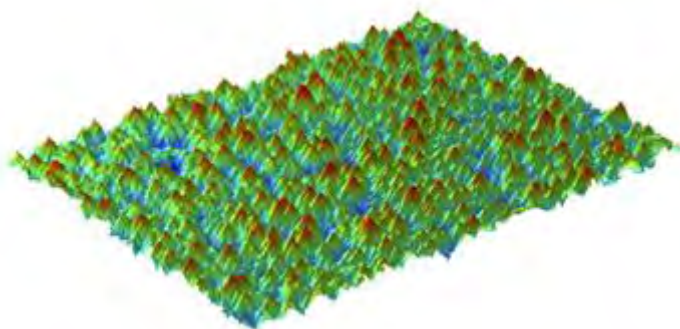


Fig. 3.5.1: A photograph of surface morphology.

3.5.1 SCANNING ELECTRON MICROSCOPE

SEM scans a focused electron beam over a surface to create an image. The electrons in the beam interact with the sample, producing various signals that can be used to obtain information about the surface topography and composition.

Electrons are generated at the top of the microscope by metallic filament. This region is referred to as the electron gun. The filament is very similar to what we see inside a light bulb. The emitted electrons are then formed into a beam and accelerated down the column toward the specimen. The beam is further focused and directed by electromagnetic lenses as it moves down the column. When the beam reaches the specimen, electrons are knocked loose from the surface of the specimen. These electrons are referred to as secondary electrons. These electrons are “seen” by a detector that amplifies the signal and sends it to a monitor. The electron beam scans back and forth across the sample building up an image from the number of electrons emitted from each spot on the sample.

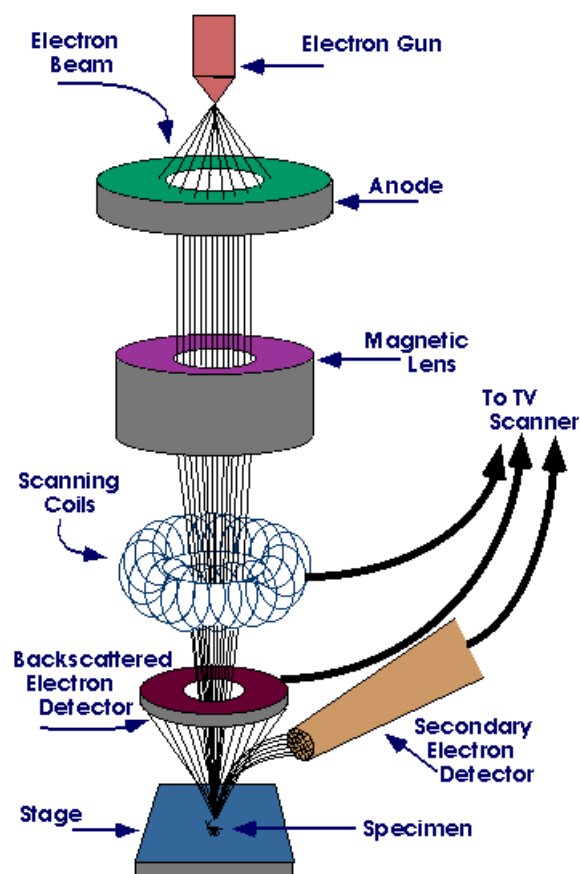


Fig. 3.5.2: Scanning Electron Microscope.

3.5.2 TRANSMISSION ELECTRON MICROSCOPY

TEM is an imaging technique whereby a beam of electrons is focused onto a specimen causing an enlarged version to appear on a fluorescent screen or on a photographic film or to be detected by a CCD camera. Electrons are generated by a process known as thermionic discharge in the same manner as in a cathode ray tube, or by field emission; they are then accelerated by an electric field and focused by electrical and magnetic fields onto the sample. The electrons can be focused onto the sample providing a resolution far better than that possible with light microscopes, with improved depth of vision. Details of a sample can be enhanced in light microscopy by the use of stains. Similarly with electron microscopy, compounds of heavy metals such as osmium, lead or uranium can be used to selective deposit on the sample to enhance structural details. The electrons that remain in the beam can be detected using a photographic film, or fluorescent screen. So areas where electrons are

scattered appear dark on the screen, as on a positive image. TEM is a straight forward technique to determine the size and shape of the nanostructure materials as well as to obtain structural information. In TEM, electrons accelerated to 100 keV or higher, are projected on to a thin specimen by means of a condenser lens system and they penetrate into the sample [13].

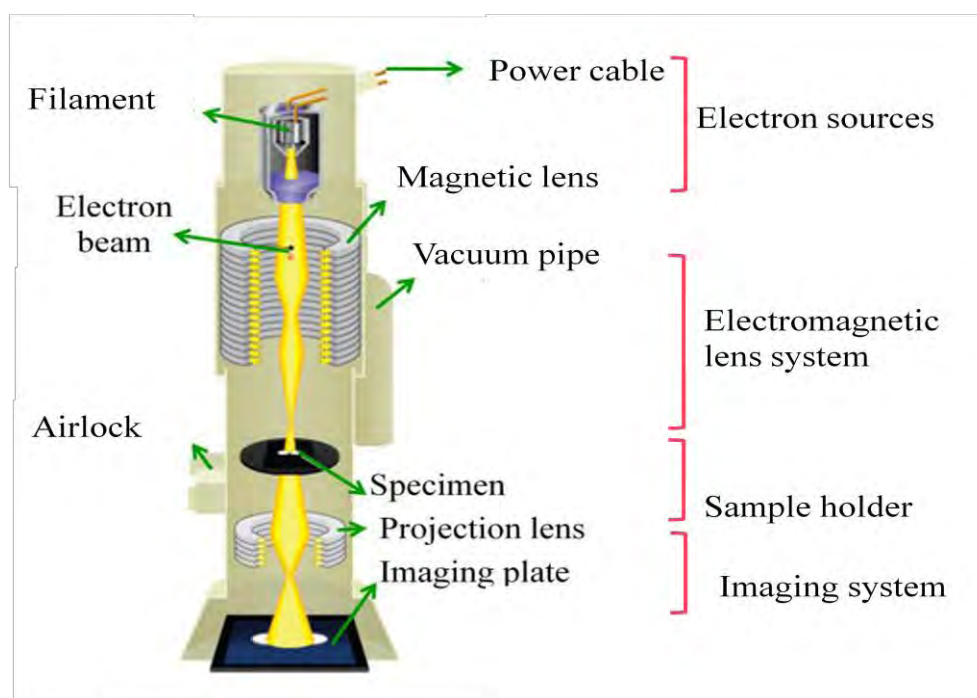


Fig. 3.5.3: Transmission electron microscope.

TEM uses transmitted and diffracted electrons which generate a two dimensional projection of the sample. The principal contrast in this projection or image is provided by diffracted electrons. In bright field images, the transmitted electrons generate bright regions while the diffracted electrons produce dark regions. In dark field image, the diffracted electrons preferentially form the image. In TEM, one can switch between imaging the sample and viewing its diffraction pattern by changing the strength of the intermediate lens. The great advantages that TEM offers are the high magnification ranging from 50 to 106 and its ability to provide both image and diffraction information of the same sample. The schematic of a TEM is shown in Fig. 3.5.3.

3.6 THEORY OF STRUCTURAL ANALYSIS

Many of the analytical techniques used to determine the molecular structure of unknown organic compounds are also used in polymer characterization. Spectroscopic techniques such as ultraviolet-visible spectroscopy, infrared spectroscopy, Raman spectroscopy, nuclear magnetic resonance spectroscopy, electron spin resonance spectroscopy, X-ray diffraction, and mass spectrometry are used to identify common functional groups.

3.6.1 FOURIER TRANSFORM INFRARED SPECTROSCOPY

Infrared spectroscopy is a non-destructive technique for materials analysis and is used in the laboratory for over seventy years. Infrared absorption spectroscopy is the study of the interaction of infrared radiation with matter as a function of photon frequency. Fourier Transform Infrared Spectroscopy (FTIR) provides specific information about the vibration and rotation of chemical bonds and molecular structures, making it useful for analyzing organic materials and certain inorganic materials. An infrared spectrum represents a fingerprint of a sample with absorption peaks that correspond to the frequencies of vibrations between the bonds of the atoms making up the material. Because each different material is a unique combination of atoms, no two compounds produce the exact same infrared spectrum. Therefore, infrared spectroscopy can result in a positive identification (qualitative analysis) of every different kind of material. In addition, the size of the peaks in the spectrum is a direct indication of the amount of material present. With modern software algorithms, infrared is an excellent tool for quantitative analysis.

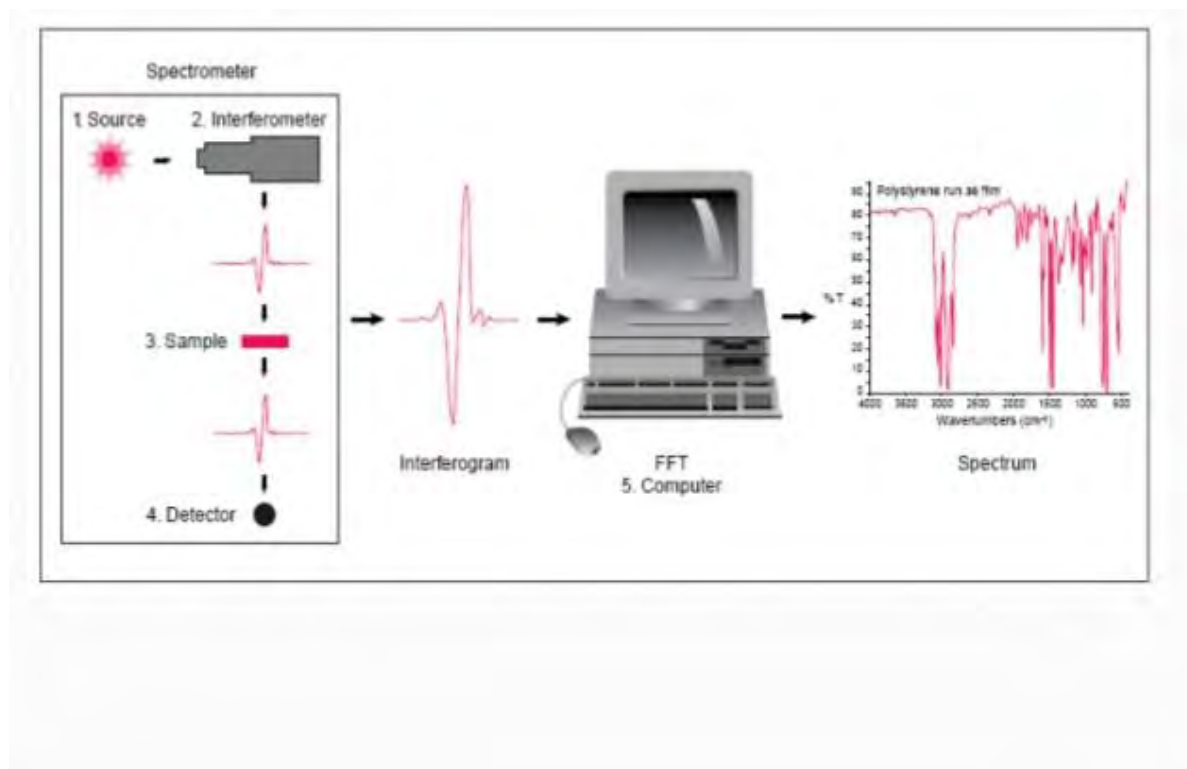


Fig.3.6.1: Fourier Transform Infrared Spectroscopy.

The IR region is commonly divided into three smaller areas: near - IR ($400 - 10 \text{ cm}^{-1}$), mid - IR ($4000 - 400 \text{ cm}^{-1}$), and far - IR ($14000 - 4000 \text{ cm}^{-1}$). Infrared photons have enough energy to cause groups of atoms to vibrate with respect to the bonds that connect them. Like electronic transitions, these vibrational transitions correspond to distinct energies, and molecules absorb infrared radiation only at certain wavelengths and frequencies. Chemical bonds vibrate at characteristic frequencies, and when exposed to infrared radiation, they absorb the radiation at frequencies that match their vibration modes. Measuring the radiation absorption frequency produces a spectrum that can be used to identify functional groups and compounds. Some impurities produce their own characteristic bands in infrared region. Spectral measurements of these bands are used to determine the impurities and their bonding with the host materials. Identification, the measured interferogram signal cannot be interpreted directly. A means of “decoding” the individual frequencies is required. This can be accomplished via a well-known mathematical technique called the transformation is performed by the computer which then presents the user with the desired spectral information for analysis.

3.6.2 RAMAN SPECTROSCOPY

Raman spectroscopy provides information about molecular vibrations that can be used for sample identification and quantitation. The technique involves shining a monochromatic light source (i.e. laser) on a sample and detecting the scattered light. The majority of the scattered light is of the same frequency as the excitation source; this is known as Rayleigh or elastic scattering. A very small amount of the scattered light (ca. $10^{-5}\%$ of the incident light intensity) is shifted in energy from the laser frequency due to interactions between the incident electromagnetic waves and the vibrational energy levels of the molecules in the sample. Plotting the intensity of this "shifted" light versus frequency results in a Raman spectrum of the sample. Generally, Raman spectra are plotted with respect to the laser frequency such that the Rayleigh band lies at 0 cm^{-1} . On this scale, the band positions will lie at frequencies that correspond to the energy levels of different functional group vibrations. The Raman spectrum can thus be interpreted similar to the infrared absorption spectrum.

When a sample is irradiated with an intense monochromatic light source (usually a laser), most of the radiation is scattered by the sample at the same wavelength as that of the incoming laser radiation in a process known as Rayleigh scattering. However, a small proportion of the incoming light – approximately one photon out of a million – is scattered at a wavelength that is shifted from the original laser wavelength.

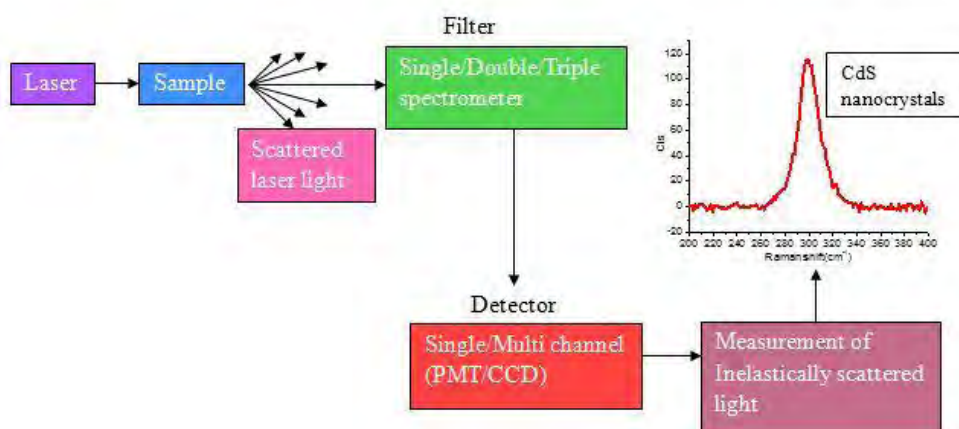
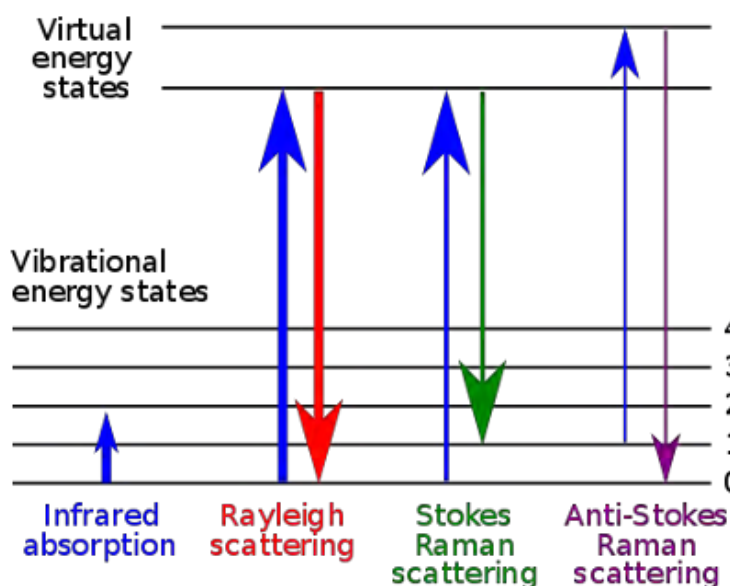


Fig.3.6.2: Raman Spectroscopy.

As illustrated in the simplified energy level diagram, a molecule at rest resides in the ground vibrational and electronic states. The electric field of the laser beam raises the energy of the system for an instant by inducing a polarization in the chemical species. The polarized condition is not a true energy state and is referred to as a “virtual state”. Relaxation from the virtual state occurs almost instantaneously and is predominantly to the initial ground state. This process results in Rayleigh scatter, which is scattered light of the same wavelength as the excitation laser. Relaxation to the first excited vibrational level results in a Stokes-Raman shift. Stokes-Raman shift scattered light is of lower energy (longer wavelength) than that of the laser light. In addition, most systems have at least a small population of molecules that are initially in an excited vibrational state. When the Raman process initiates from the excited vibrational level, relaxation to the ground state is possible, producing scatter of higher energy (shorter wavelength) than that of the laser light. This type of scatter is called anti-Stokes Raman scatter and is not illustrated.

**Fig.3.6.3:** Raman Spectrum.

The vibrational states probed by Raman spectroscopy are similar to those involved in infrared spectroscopy. However, the two vibrational spectroscopy techniques are complementary, in that vibrations that are strong in an infrared spectrum (those involving strong dipole

moments) are typically weak in a Raman spectrum. Likewise, non-polar functional group vibrations that give very strong Raman bands usually result in weak infrared signals. As an example, hydroxyl- or amine-stretching vibrations and the vibrations of carbonyl groups are usually very strong in an FT-IR spectrum and are weak in a Raman spectrum. The stretching vibrations of carbon double and triple bonds and the symmetric vibrations of aromatic groups give a very strong Raman signal. Raman spectroscopy provides key information about the structure of molecules. The position and intensity of features in the spectrum reflect the molecular structure and can be used to determine the chemical identity of the sample. Spectra may also show subtle changes depending on the crystalline form. With the extensive spectral libraries that are now available, it is very straightforward to identify compounds by spectral library searching.

3.6.3 THEORY OF X-RAY ANALYSIS OF CRYSTALS

Atoms scatter X-ray waves, primarily through their electrons. X-ray striking an electron produces secondary spherical waves emanating from the electron. This phenomenon is known as elastic scattering and the electron is known as the scatterer. A regular array of scatterers produces a regular array of spherical waves. Although these waves cancel one another out in most directions through destructive interference, they add constructively in a few specific directions, determined by Bragg's law [14]:

$$2d \sin\theta = n\lambda \quad (3.6.1)$$

where d is the spacing between diffracting planes, θ is the incident angle, n is any integer and λ is the wavelength of the beam. These specific directions appear as spots on the diffraction pattern called reflections. Thus, XRD results from an electromagnetic wave (the X-ray) impinging on a regular array of scatterers (the repeating arrangement of atoms within the crystal). As seen in the Fig. 3.6.4, the incoming beam (coming from upper left) causes each scatterer to re-radiate a small portion of its intensity as a spherical wave. If scatterers are arranged symmetrically with a separation d , these spherical waves will superimpose constructively only in directions where their path-length difference $2d \sin \theta$ equals an integral

multiple of the wavelength λ . In that case, part of the incoming beam is deflected by an angle 2θ , producing a reflection spot in the diffraction pattern.

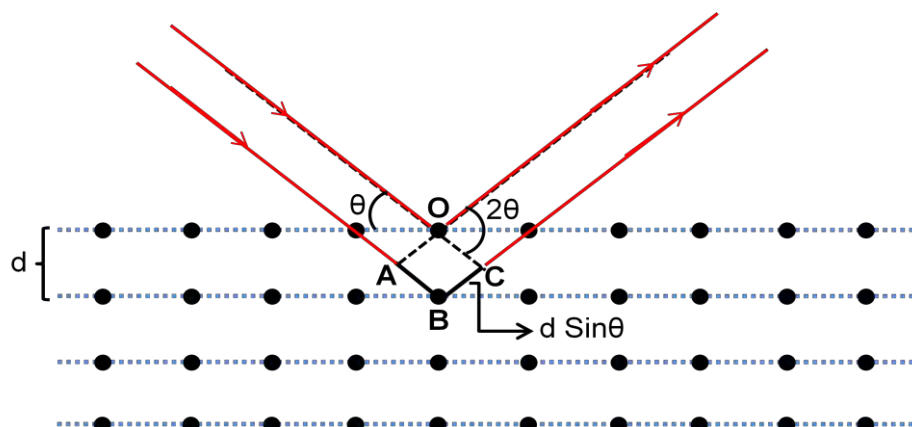


Fig. 3.6.4: Principle of X-ray Diffraction.

3.6.3.1 LONG-RANGE AND SHORT-RANGE ORDER

Polymers exhibit both crystalline and amorphous structures. These two structures co-exist in the polymeric material. In most cases, crystalline polymers show lamellar structure or layer structure. The order of crystalline structure is of a few angstroms, whereas the lamellar structure is of several hundred angstroms. In order to understand the arrangement of molecules in crystalline polymers, we follow two different techniques: small angle X-ray scattering and wide angle X-ray scattering. Parts of some polymers are crystalline so they have a regular and ordered structure. The spacing between these ordered arrays of molecules is typically a few ten thousand millionths of a meter. This is too small to be observed by an ordinary microscope, but we can use XRD to study these long-ordered arrangements.

Fig. 3.6.5 (a) shows a typical XRD pattern produced by a crystalline polymer as recorded by a detector [15]. The sharp peaks are caused by reflections from the various lattice planes in the sample. They are observed at different angles according to the Bragg's law described earlier. In case of polycrystalline polymers, crystallites are randomly oriented with respect to each other. The scattering is the same in all directions and in this case we use a solid-state point detector or position sensitive proportional counter that shows peaks as that shown in

Fig. 3.6.5 (a). To detect the orientational information, counter is not viable. In this case, X-ray photograph is used that gives two-dimensional pattern [Fig. 3.6.5 (b)] from which we can analyze the orientational effect in the polymer or macromolecular crystal.

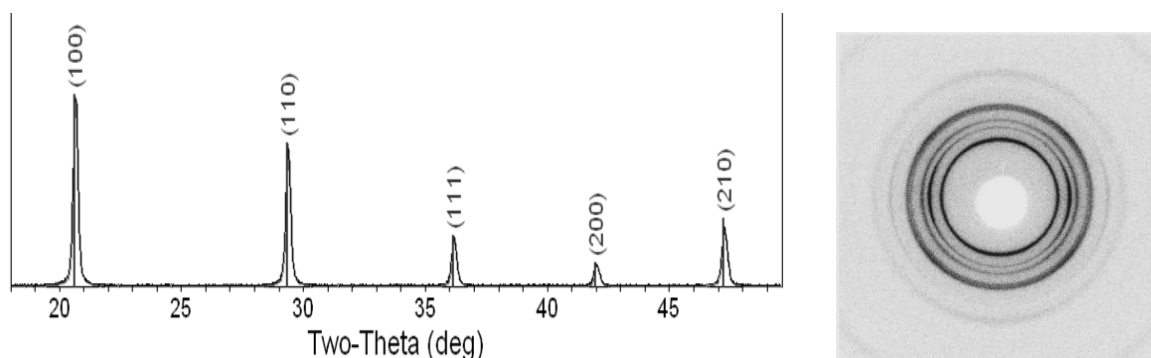


Fig. 3.6.5: (a) A Typical X-Ray Diffraction Pattern as Detected by a Counter and
(b) A Typical X-Ray Diffraction Photograph.

Usually a large numbers of polycrystalline areas grouped together in a polymer form lamellae. The thicknesses of these lamellae differ depending on the types of polymers and the processing conditions for crystallization. For example, the thickness of polyethylene lamella is about 250Å [15]. This large periodicity presents a problem of detection as can be seen from Bragg's law. If $d = 250\text{Å}$, then for a fixed wavelength of 1.54Å , the angle 2θ at which we observe the scattering, would be 0.17° . This is an order of magnitude smaller than the angles at which the crystalline peaks are observed. Besides, crystalline polymers also consist of large number of crystallites which may be arranged in the polymer sample either orderly or isotropic ally. The size of the crystallites could have a range of several nanometers to microns. The scattering angle, 2θ , in this case will be very small, even less than 0.01° . This suggests to detect the diffraction pattern at small-angle. On the other hand, apart from lamellar structure the polymer shows crystalline order of a few angstroms. For this range of values and for wavelength of 1.54Å , the scattering angle could be greater than 5° . This suggests to detect the diffraction pattern at wide-angle. Hence the structure of the lamellae or the size of crystallite is determined by small angle X-ray scattering and the crystalline part is studied by wide angle X-ray scattering [15, 16].

3.6.3.2 CRYSTALLITE OR PARTICLE SIZE IN POLYMERS

Fig. 3.6.7 shows parallel planes of a crystallite from which X-ray beams are reflected. Here the plane distance is assumed to be d_{hkl} and the crystallite consists of n number of planes. Therefore, the thickness t of the crystallite will be nd_{hkl} .

Let us consider that a diffraction peak as shown on the right side is obtained, which is similar to those peaks of Fig. 3.6.5 (a). The peak has a maximum value at $2\theta_B$ and minimum values at $2\theta_1$ and $2\theta_2$ in Fig. 3.6.6. We know that the diffraction maximum occurs when Bragg law is satisfied. Thus for $2\theta_B$, λ and d_{hkl} , we can write for $22'$ and nn' :

$$2t \sin \theta_B = n\lambda \quad (3.6.2)$$

This means all $22'$, $55'$, -----, nn' will constructively interfere for which diffraction at $2\theta_B$ occurs. On the other hand, let rays $1A$, $4B$, -----, mC be incident with slightly larger angle than θ_B . Let these beams be incident on the planes by an angle θ_1 . Then, the path difference between $11'$ and $44'$ will be somewhat larger than the path difference between $22'$ and $55'$. Thus the path difference between $11'$ and mm' will be larger than $n\lambda$. Let us consider that the path difference between $11'$ and mm' is $(n+1)\lambda$. Then there is a plane inside the crystallite

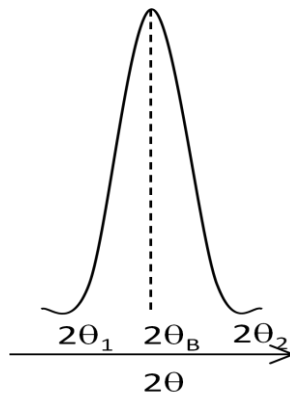


Fig. 3.6.6: The Width of the Diffraction Peaks or Spots.

having light, say pp' , of path difference $(n+1)\lambda/2$. This light ray (pp') will interfere destructively, with mm' due to out of phase. The parallel rays just above mm' and pp' will

Chapter 3 Theoretical Background

also produce destructive interference due to the same reason. In this way, all parallel rays to $11'$ will produce destructive interference and we get minimum intensity at $2\theta_1$. Similarly, explanation can be given to $2\theta_2$ and in this case the path difference will be smaller. Therefore, we can write,

$$2t \sin\theta_1 = (n+1)\lambda \quad (3.6.3)$$

$$2t \sin\theta_2 = (n-1)\lambda \quad (3.6.4)$$

Subtracting eqn. (3.6.4) from eqn.(3.6.3),

$$\text{Or, } 2t (\sin\theta_1 - \sin\theta_2) = 2\lambda$$

$$\text{Or, } t (\sin\theta_1 - \sin\theta_2) = \lambda$$

$$\text{or, } t \cdot 2 \cos \frac{\theta_1 + \theta_2}{2} \sin \frac{\theta_1 - \theta_2}{2} = \lambda \quad (3.6.5)$$

Since θ_1 and θ_2 are close to θ_B , therefore,

$$\theta_1 \approx \theta_2 = \theta_B \quad \text{and}$$

$$\sin \frac{\theta_1 - \theta_2}{2} \approx \frac{\theta_1 - \theta_2}{2}$$

Using this relation in eqn. (3.6.5):

$$2t \cos \theta_B \left(\frac{\theta_1 - \theta_2}{2} \right) = \lambda$$

$$\text{or, } t \cos \theta_B (\theta_1 - \theta_2) = \lambda \quad (3.6.6)$$

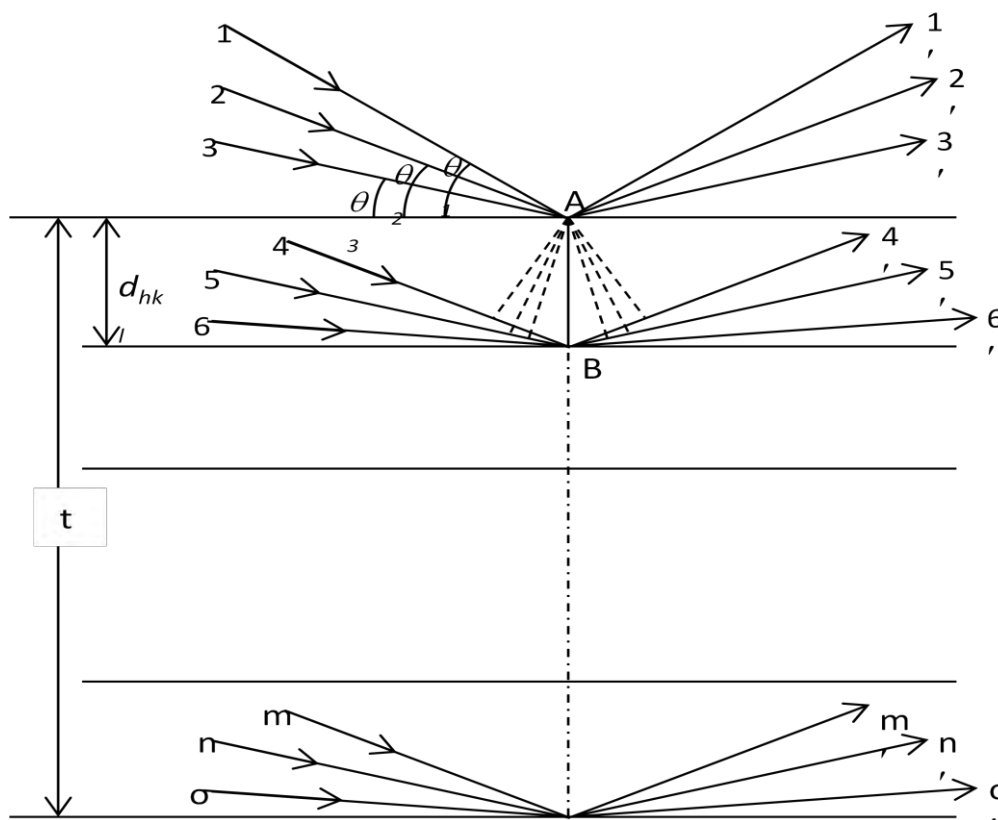


Fig. 3.6.7: A schematic representation of x-ray diffraction from parallel planes of a crystallite of thickness t .

The width of the diffraction peak is taken at half of the maximum intensity. If we consider the peak as an equilateral triangle, then the width of the peak at half of the maximum intensity is

$$B = \frac{l}{2}(2\theta_1 - 2\theta_2) = \theta_1 - \theta_2$$

Thus eqn. (3.6.6) becomes: $tB \cos \theta_B = \lambda$

$$\text{or, } t = \frac{\lambda}{B \cos \theta_B} \quad (3.6.7)$$

However, using detailed mathematical treatment Scherrer derived t as:

$$t = \frac{K\lambda}{B \cos \theta_B} \quad (3.6.8)$$

In case of PLA, $K = 0.98$ [17].

B can be obtained from the width of the diffraction peaks or spots of Fig. 3.6.6. θ_B is the midpoint of the peaks or spots, K and λ are known. Thus the crystallite size or particle size in polymer can be obtained from XRD pattern.

3.6.3.3 WIDE ANGLE X-RAY SCATTERING

If the X-ray diffraction measurement is performed in a range of $2\theta > 5^\circ$, then the measurement technique is called wide angle X-ray scattering (WAXS) [15]. WAXS is performed to detect the lattice parameters of the order of a few angstroms. In WAXS measurement, the film or detector is placed close to the sample. WAXS is performed in order to investigate crystalline level of a few angstroms of a polymer. Usually single or polycrystals of inorganic origins show crystalline order of a few angstroms. So, WAXS is very useful for this type of material. In case of polymer, WAXS is used to measure the crystalline order. This order exists among the neighboring molecules of the polymer crystal, parallel to the lamellar surface.

3.7 DEFORMATION OF MATERIALS

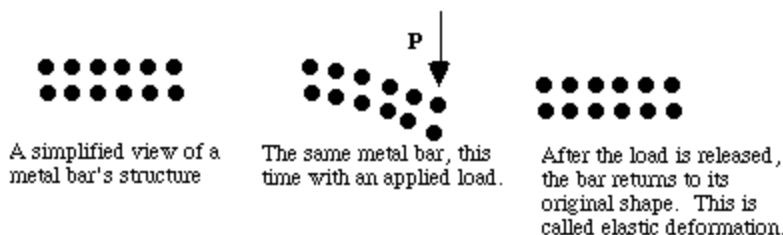
3.7.1 DEFORMATION

Any time a stress is placed on a metal, the metal undergoes a deformation where the material's shape changes either temporarily or permanently. The amount of change the material experiences is due to the amount of stress being placed on the object and the yield strength of the material. A material's yield strength is a measure of how much stress the object can undergo before it begins plastic deformation and is also an excellent representative of a material's load-bearing capabilities.

There are two types of deformations that a material can experience. These are elastic and plastic deformation. When the stress placed on the metal is small, meaning that the stress is less than the yield strength of the material, the metal experiences elastic deformation. In elastic deformation, the material is distorted temporarily, thus when the stress is removed the

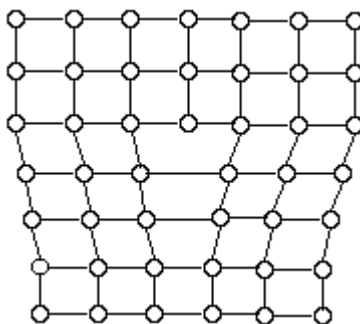
Chapter 3 Theoretical Background

material returns to its original shape with no permanent rearrangement of atoms. However, when the stress placed on the metal exceeds the yield strength of that material, it experiences plastic deformation. Once the metal experiences plastic deformation its atomic structure and overall shape are permanently rearranged and changed. Once plastic deformation has occurred, the material does not return to its original shape when the stress is removed.

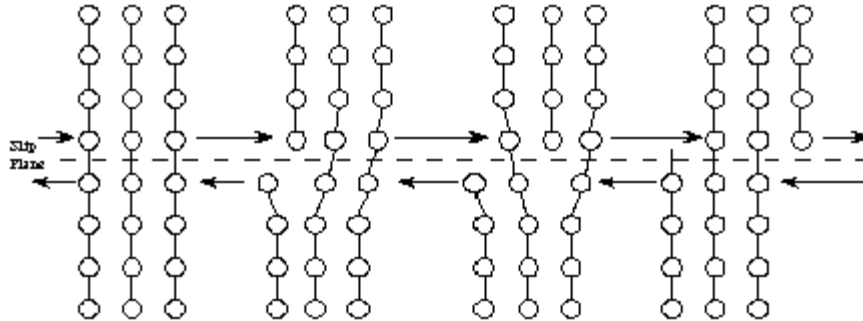


In order to discover why plastic deformation occurs, we must look at the atomic makeup of metals. Most metals are crystalline solids which contain orderly arrangement of atoms. These atoms exist in a lattice form which varies from material to material. Within the lattice structure exist smooth surfaces between layers of atoms. Slipping, which is the most common reason for plastic deformation, occurs when the sheets of atoms slide across each other causing bonds to break. Once the original bonds have been broken, the atoms lose track of their original positions and form new bonds forever changing the shape of the material.

Slipping is due to a couple of reasons. First, whenever a metallic bond relies on the relatively non-directional sharing of electrons, the atoms have a tendency to slip under little stress because relative position is not a major factor in keeping the bonds together. Consequently, metallic crystals are not perfect; therefore sometimes atoms are missing causing lines of defective bonding, known as dislocations, as seen in the following illustration.



Dislocations have a tendency to move easily in metals due to the de-localized bonding, thus the sheet slips gradually resulting in plastic deformation. The following image illustrates how a deformation can move through a metal.



3.7.2 ELASTIC DEFORMATION

The displacement of atoms from their equilibrium positions constitutes deformation. Such deformation is termed elastic if the atoms can resume their equilibrium positions when the imposed forces are released. Elastic deformation then is recoverable and indicates the relative resilience of a material. For example, a rubber band can be stretched quite far yet snap back to its original dimensions upon being released. A slightly different manner of stating this concept of elasticity is that it is the property of a material to return to its initial form and dimension after the deforming force is removed.

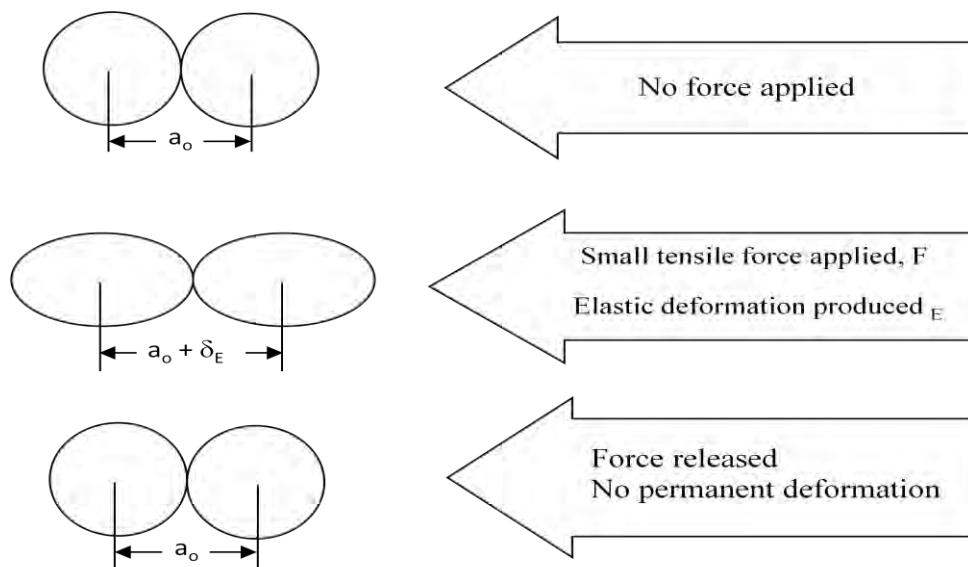


Fig. 3.7.1: Schematic Illustration of Elastic Deformation.

The process of elastic deformation is presented schematically in the Fig. 3.7.1. Here the atoms are represented as hard spheres on a lattice, when no forces are applied. Let us assume the equilibrium separation is a_0 . A relatively small tensile force tends to pull the atoms apart producing elastic deformation (δ_E). Their separation is now slightly larger by a_0 . However, when the force is released, the atoms resume their equilibrium positions and no deformation or displacement remains. The material is restored to its initial condition.

3.7.3 PLASTIC DEFORMATION

If the engineering material undergoes deformation, which exceeds the elastic capability (elastic limit) to restore the atoms to their equilibrium positions, the deformation is permanent and termed plastic. Plastic deformation is non-recoverable and leaves the atoms permanently displaced from their original positions where the forces are released. Deformation of materials may be entirely elastic, or elastic plus plastic. The total deformation may then consist of the combined elastic and plastic portion. In this case, removal of the load or forces producing the deformation results in recovery of the elastic portion, while the plastic portion remains. This process is illustrated in the Fig. 3.7.1 and Fig 3.7.2.

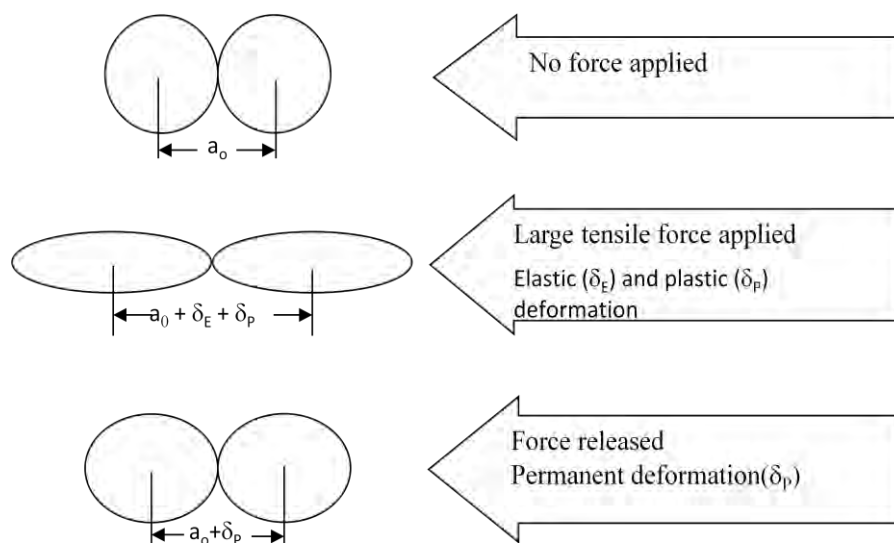


Fig. 3.7.2: Schematic Illustration of Plastic Deformation.

Plastic deformation of engineering materials is permanent in that work or energy must be supplied to restore the atoms to their original equilibrium positions. For instance, the effect of this type of deformation can be alleviated by thermal treatments, when necessary [18, 19].

3.8 MECHANICAL PROPERTIES OF COMPOSITES

3.8.1 THEORY OF TENSILE PROPERTIES

3.8.1.1 ENGINEERING STRAIN

We have just briefly described the response of atoms to deformation by mechanical forces. If this concept of atomic displacement is extended to bulk engineering materials, we can define the deformation in terms of original dimensions of the material under consideration in other words, the ratio of dimensional change to original dimension.

Engineering strain is the amount that a material deforms per unit length in a tensile test. (also known as normal strain).

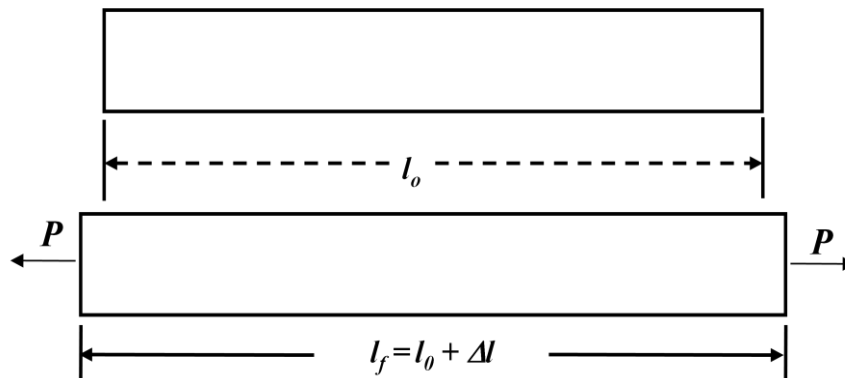


Fig. 3.8.1: Deformation of a Bar Produced by an Axial Load.

For example, consider a bar of length l_0 as shown in figure. Under the action of an applied load P this bar experiences deformation and elongates to a new length l_f . The ratio of this change in length to the original length l_0 is the “average linear strain” (ϵ) and can be expressed as follows [18].

$$\epsilon = \frac{\Delta l}{l_0} = \frac{l_f - l_0}{l_0} \quad (3.8.1)$$

This quantity is referred to as the average linear strain because only the dimensional change in the axial direction is considered and it is considered over the entire length of the sample. In reality, because its volume remain constant, the bar diameter does decrease slightly, resulting in a decrease in the cross-sectional area, but for small strains this response is usually insignificant. Average strain ϵ is commonly referred to as the engineering strain and expressed in units of in/in or mm/mm. However, strain may also be treated as a dimensionless quantity because these units cancel. From eqn.(3.8.1), it is clear that strain is unitless.

3.8.1.2 TRUE STRAIN

Engineering strain is used in stress-strain graph and other numericals becoz it is easy since we only need to know change in length. But in true strain we need to know the current length which is bit difficult to calculate every time.

Since a material undergoing deformation is continuously changing its dimension (i.e. length and width or diameter), a more precise definition of strain is given by the ratio of the change in dimension to the instantaneous dimension. In the case of round bar, this may be viewed as the change in length (dl) with respect to the instantaneous length (l) at any point in the process. This ratio is actually the true strain (E) and is expressed as follows [18, 19]:

$$E = \frac{dl}{l}$$

A more specific expression for E is obtained by placing some limits on the above equation. For example, if the initial length is l_0 and the final length is l_f , we can integrate this equation as follows:

$$\begin{aligned} E &= \int_{l_0}^{l_f} \frac{dl}{l} = [\ln l]_{l_0}^{l_f} \\ &= (\ln l_f) - (\ln l_0) \end{aligned}$$

$$\therefore E = \ln \frac{l_f}{l_0} \quad (3.8.2)$$

Chapter 3 Theoretical Background

The engineering strain ε is related to the true strain and this relationship can be demonstrated as follows,

$$\varepsilon = \frac{l_f - l_0}{l_0}$$

$$\text{or, } \varepsilon = \frac{l_f}{l_0} - 1$$

$$\text{or, } \frac{l_f}{l_0} - \varepsilon = 1$$

Then substituting these results in eqⁿ (3.8.2) we obtain,

$$E = \ln(\varepsilon + 1) \quad (3.8.3)$$

So, True strain equals the natural log of the quotient of current length over the original length.

3.8.1.3 SHEAR STRAIN

Shear strain is the strain resulting from the application of opposing forces in a direction parallel to a surface or to a planar cross section of a body. It is an angular change at some point in a shape. In addition to linear strain, an engineering material can experience shear strain γ , this type of strain is due to the applying force, the displacement of parallel planes through a certain angle θ as shown in Fig 3.8.2. The shear strain is therefore defined as the ratio of the displacement x to the distance h between the planes, expressed as follows [18, 19]:

$$\gamma = \frac{x}{h} \quad (3.8.4)$$

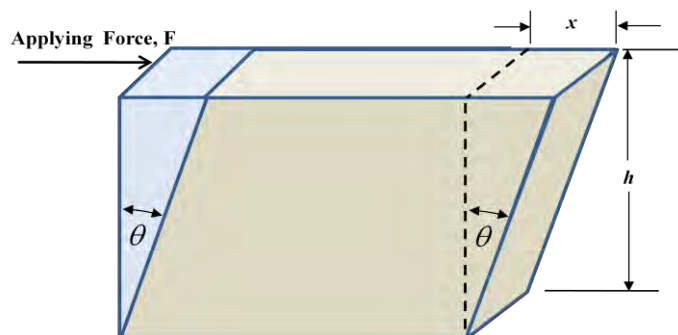


Fig. 3.8.2: Shear displacement on parallel planes of a solid material.

3.8.1.4 STRESS

The response of an engineering material to impose forces on it has been discussed in terms of deformation and strain. Now let us analyze the resistance of a material for deformation. We know that, the net force on an atom is zero only for the equilibrium position. Displacement in either direction produces an increase in the forces (tensile or compressive) that oppose the deformation. This resistance is due to the inter-atomic attraction and repulsive forces that operate in a particular material. Stress σ is the result of the internal response that a material exhibits when forces are imposed on it. To simplify matters at this point, we will assume that the forces acts uniformly over a certain area, Then we can state that the stress is a force per unit area. Consider the load P is applied to a cylindrical bar. The bar remains intact, indicator that the external force is balanced internally by a response of the material. If we section this bar at any particular location (normal to the axis of the applied load) P must be opposed by the stress produced in each elemental area dA . Since it is previously assumed that the force uniformly applied over the cross section, the summation of stress over the entire area may be expressed as follows [18]:

$$P = \sigma \int_0^A dA$$

$$\text{or, } P = \sigma A$$

Therefore, the stress can be expressed as,

$$\sigma = \frac{P}{A} \quad (3.8.5)$$

Chapter 3 Theoretical Background

Where, P = load or force

A = cross sectional area over which the force act.

Stress is commonly denoted in unit's lb/in^2 (psi) or in international unit (SI) of Pascal (Pa). Since the Pascal is a rather small value of stress, it is customary to express stress values in megapascals (MPa).

3.8.1.5 ENGINEERING STRESS

Engineering stress is the applied load divided by the original cross-sectional area of a material, also known as nominal stress.

$$\sigma = \frac{P}{A_0} \quad (3.8.6)$$

The only modification to our basic stress equation is A_0 , which represents the original area; therefore, engineering stress treats cross sectional area is constant. Although this is not completely accurate, for elastic striations in the loading direction the corresponding changes in cross sectional area are generally small. Furthermore, most design and structure are based on service condition in the structures and the elastic range, thus the engineering stress is very useful parameter.

3.8.1.6 TRUE STRESS

The concept of engineering stress treats the area under consideration as a constant (A_0). In reality, however, the area does not remain constant and in the case of an axially loaded tensile bar, gradually decreases as the stress and corresponding manifestation of Poisson's ratio effect. The true stress therefore can be expressed as follows [18, 19]:

$$\sigma_{\text{tr}} = \frac{P}{A_i} \quad (3.8.7)$$

Where A_i is the actual instantaneous area over which the force is acting. Ordinarily, the true stress is larger than the engineering stress. However, in the elastic region, change in area is

Chapter 3 Theoretical Background

usually inconsequential and the engineering stress is sufficiently accurate. When the elastic limit is exceeded and plastic strain comes into play the discrepancy between engineering strain and true strain becomes more significant. The true stress σ_{tr} is related to the engineering stress in the following manner:

$$\sigma_{tr} = \frac{P}{A_i} \frac{A_0}{A_0}$$
$$\text{or, } \sigma_{tr} = \frac{P}{A_0} \frac{A_0}{A_i} = \sigma \frac{A_0}{A_i} \quad (3.8.8)$$

In this type of analysis, the volume of material is constant (even though the dimensions may change). Therefore the following relationships also apply.

Initial volume (V_0) = instantaneous volume (V_i)

$$V_0 = V_i$$

$$\text{or, } A_0 l_0 = A_i l_i$$

$$\text{or, } \frac{A_0}{A_i} = \frac{l_i}{l_0}$$

Substituting above in eqn. (3.8.8), we get,

$$\sigma_{tr} = \sigma \frac{l_i}{l_0}$$

But from the section on strain,

$$\frac{l_i}{l_0} = \epsilon + 1$$

so we can substitute for l_i/l_0 as follows:

$$\sigma_{tr} = \sigma (\epsilon + 1) \quad (3.8.9)$$

Thus, the true stress equals the engineering stress times the quantity engineering strain plus 1.

3.8.1.7 TENSILE STRENGTH

The maximum load (or force) to which a material is subjected during stretching divided by its original cross-sectional area is called the tensile strength.

Let the maximum load or force = F_{max} and original cross-sectional area = A

$$\therefore \text{Tensile strength, } TS = \frac{F_{max}}{A} \quad (3.8.10)$$

3.8.1.8 ELONGATION-AT-BREAK OR BREAKING STRAIN

Elongation-at-break or breaking strain is defined as the strain at which the material under study breaks. If length of the original material is l_0 and its length after stretching is l , then

$$\text{strain} = \frac{l-l_0}{l}$$

Elongation-at-break(%) is defined as

$$EB(\%) = \frac{l-l_0}{l} \times 100\% \quad (3.8.11)$$

EB(%) correspond to the strain at breaking point.

3.8.1.9 YOUNG'S MODULUS

The elastic limit of an engineering material is the highest stress that can be produced without experiencing any plastic (Permanent) deformation. In most materials for values of stress below the elastic limit, stress is proportional to strain as follows.

$$\sigma = Y\varepsilon \quad (3.8.11)$$

This relationship is known as Hooke's law, and the proportionality constant Y is the modulus of elasticity or Young's modulus. Young's modulus is a measure of the stiffness of an isotropic elastic material. It is defined as the ratio of the uniaxial stress over the uniaxial strain in the range of stress in which Hooke's Law holds. This can be experimentally determined from the slope of a stress-strain curve created during tensile tests conducted on a sample of the material. Young's modulus is the ratio of stress, which has units of pressure, to strain, which is dimensionless; therefore Young's modulus itself has units of pressure. The SI

unit of Young's modulus is the pascal (Pa or N/m²); the practical units are megapascals (MPa or N/mm²) or gigapascals (GPa or kN/mm²). In United States customary units, it is expressed as pounds (force) per square inch (psi).

3.8.2 THEORY OF FLEXURAL PROPERTIES

3.8.2.1 THEORY OF BENDING

Consider that beam of polymer sample is supported on the two knife edges A and B (Fig 3.8.3). The length of the beam between the two points A and B is L. The width and thickness of the beam are b and d, respectively. A load W is applied at the middle of the beam. The reaction at each support is W/2 along vertically upward direction. After loading the sample is deflected at a distance y from its initial horizontal position. Let the position of loading be at a distance x from either A or B. In equilibrium position, the bending couple is equal to the restoring couple. For mechanical equilibrium of the bending beam [20].

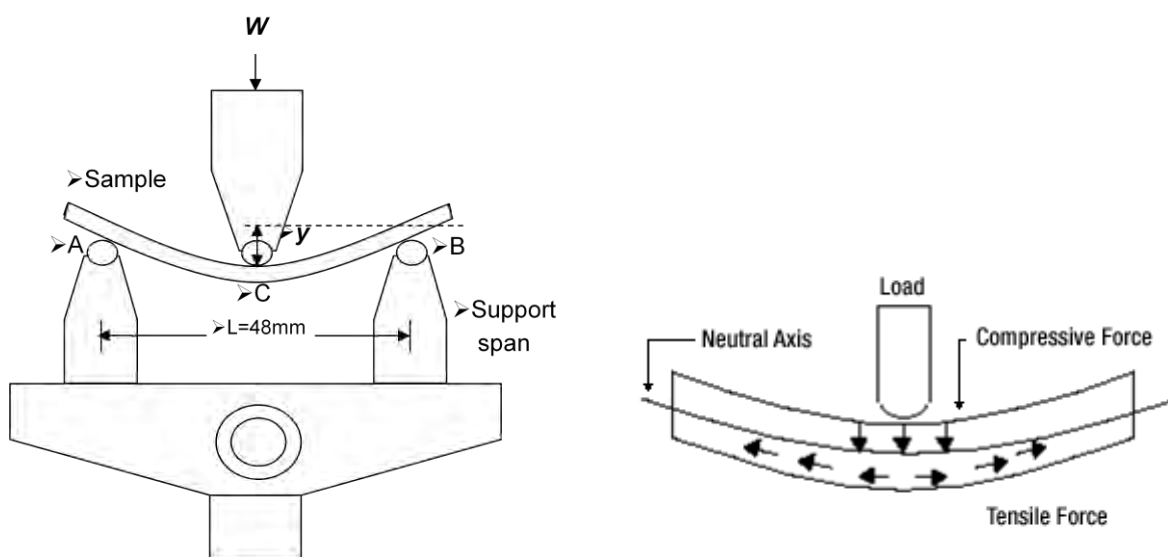


Fig. 3.8.3: A sample beam supported at two spans and loaded at the middle.

$$\frac{GI_g}{R} = W \left[\frac{1}{2} - x \right] - \frac{W}{2} (1 - x)$$

Chapter 3 Theoretical Background

Where, G = tangent Modulus, I_g = geometrical moment for the rectangular beam and R = radius of curvature of the bending beam.

$$\begin{aligned} \text{or, } \frac{GI_g}{R} &= -\frac{W}{2}x \\ \text{or, } \frac{1}{R} &= -\frac{Wx}{2GI_g} \end{aligned} \quad (3.8.12)$$

From the theory of bending, we know [19]

$$\frac{1}{R} = \frac{d^2y}{dx^2} \quad (3.8.13)$$

From eqns. (3.8.12) and (3.8.13), we get,

$$\begin{aligned} \therefore \frac{d^2y}{dx^2} &= -\frac{Wx}{2GI_g} \\ \frac{dy}{dx} &= -\frac{Wx^2}{4GI_g} + C_1 \\ \text{or, } 0 &= -\frac{Wl^2}{16GI_g} + C_1 \end{aligned}$$

Since at $x = \frac{l}{2}$ (where the bending is maximum), $\frac{dy}{dx} = 0$

$$\begin{aligned} \therefore C_1 &= \frac{Wl^2}{16GI_g} \\ \therefore \frac{dy}{dx} &= -\frac{Wx^2}{4GI_g} + \frac{Wl^2}{16GI_g} \end{aligned}$$

Again integrating w.r.t.x,

$$\begin{aligned} y &= -\frac{Wx^3}{12GI_g} + \frac{Wl^2}{16GI_g}x + C_2 \\ y &= -\frac{Wx^3}{12GI_g} + \frac{Wl^2}{16GI_g}x \quad \text{Since at, } x = 0, y = 0; C_2 = 0 \end{aligned}$$

Again at C, $x = \frac{l}{2}$, So,

$$\begin{aligned} y &= -\frac{Wl^3}{96GI_g} + \frac{Wl^3}{32GI_g} \\ \therefore y &= \frac{Wl^3}{48GI_g} \end{aligned} \quad (3.8.14)$$

This is the relation of deflection y with load W .

3.8.2.2 TANGENT MODULUS

Tangent Modulus is defined as the ratio between shearing stress and shearing strain. For a rectangular bar , geometrical moment,

$$I_g = \frac{bd^3}{12}$$

Putting in equation (3.8.14)

$$y = \frac{Wl^3}{4Gb d^3}$$

$$G = \frac{Wl^3}{4yb d^3}$$

$$\therefore \text{Tangent Modulus, } G = \frac{Kl^3}{4bd^3} \quad (3.8.15)$$

Where, $K' = \frac{W}{y}$ = Slope of load deflection curve.

3.8.2.3 FLEXURAL STRESS OR STRENGTH

Flexural means bending. Likewise, the tensile strength, flexural strength is the maximum bending required to make fracture of the material [21]

We know that,

$$\text{Tensile stress, } \sigma = \frac{\text{Force}}{\text{Cross-sectional area}} = \frac{W}{A}$$

$$\text{Tensile strain, } \varepsilon = \frac{\text{deformation}}{\text{original length}} = \frac{y}{L_0}$$

$$\text{and Young's Modulus, } Y = \frac{\sigma}{\varepsilon} = \frac{WL_0}{Ay} \quad (3.8.16)$$

In flexural situation, the above relations cannot be applied. From three points loading (Fig.3.8.3), the relevant equation for flexural stress, FS is [16]:

$$FS = \frac{MY}{I_g}$$

Where, M=bending moment at loading point = $\frac{W}{2} \times \frac{l}{2} = \frac{Wl}{4}$

$$y = \text{half depth of the beam} = \frac{d}{2}$$

$$I_g = \text{geometrical moment of a rectangular sample} = \frac{bd^3}{12}$$

$$\text{Thus, FS} = \frac{\frac{Wl}{4} \times \frac{d}{2}}{\frac{bd^3}{12}}$$

$$\therefore \text{FS} = \frac{3Wl}{2bd^3} \quad (3.8.17)$$

3.8.2.4 FLEXURAL STRAIN

This is the strain at which flexure occurs. Flexural strain is deduced as follows [21]. From equation (3.8.17) we get,

$$\begin{aligned} y &= \frac{Wl^3}{48GI_g} = \frac{Wl^3}{4Gb d^3} \\ &= \frac{3Wl}{2bd^3} \times \frac{l^2}{6Gd} \\ &= \text{FS} \times \frac{l^2}{6Gd} \\ \therefore \text{FS} &= \frac{6Gyd}{l^2} \end{aligned}$$

Now, we know that, Tangent Modulus, $G = \frac{\text{Flexural Stress, FS}}{\text{Flexural strain, FB}}$

$$\text{or, FB} = \frac{\text{FS}}{G} = \frac{6Gyd}{G l^2}$$

$$\therefore \text{FB} = \frac{6yd}{l^2} \quad (3.8.18)$$

3.9 THEORY OF MICROHARDNESS

One of the simplest methods of determining the microhardness of a material is microindentation test, which involves local deformation of the test material on a very small scale. This technique has been used in the study of hardness, particularly of metals and ceramics for a long time and has proved it to be sensitive to the chemical composition and microscopic structure of the materials [22, 23]. Microindentation test uses a square-based pyramid indenter of diamond, which penetrates the surface of a sample upon the application of a given load at constant rate. Thus we see an indentation pattern or an area of impression

Chapter 3 Theoretical Background

on the sample surface. Depending on the sample category, whether it is amorphous or crystalline, upper view of indentation (imprint) will, in general, show either a square or a rhombus [Fig.3.9.1 (a)] like pattern. It is reasonably assumed that indented surface will have the similar geometrical configuration as that of the pyramid-like indenter. Consequently, the area of pyramid faces will denote the projected area of impression. In general, hardness implies resistance to local surface deformation against indentation. Microhardness (H) is conveniently measured from the following mathematical relation:

$$H = \frac{P}{A} \quad (3.9.1)$$

Fig.3.9.1 (b) represents the details of indentation geometry from which A can be derived. Considering the square pattern of an imprint, the length of all sides AB, BC, CD and AD is equal. Let us assume that this length is l and y is a length from O to the midpoint of AB. In case of square, $\angle ACB$ or $\angle ACD$ is 45° and hence, $l = d \cos 45^\circ$,

$$\text{i.e. } l = d / \sqrt{2} \quad (3.9.2)$$

If S is supposed to be the area of the triangle $\triangle AOB$ i.e. one of the faces of the pyramid, then, $S = \frac{l}{2} \times y$. Substituting the value of l in the relation of S, one obtains,

$$S = \frac{y}{2} \times \frac{d}{\sqrt{2}}$$

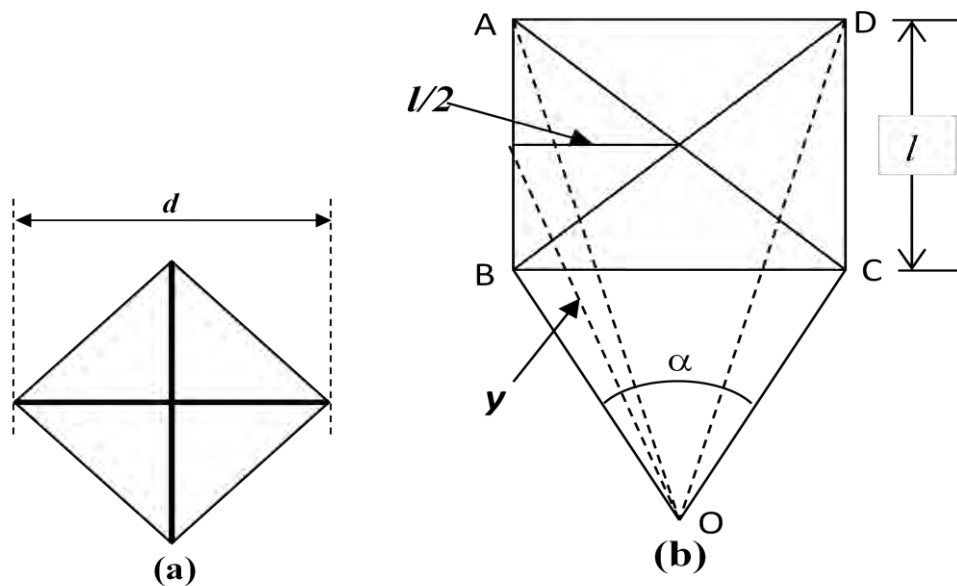


Fig. 3.9.1: (a) Schematic Sketch of an Imprint and (b) Details of Indentation Geometry.

Thus, the total area of pyramid faces will be

$$A = 4 \times S = \sqrt{2}d \times y \quad (3.9.3)$$

Since, according to Fig.3.9.1 (b), $\frac{l}{2} = y \sin \frac{\alpha}{2}$, then $y = \frac{\frac{l}{2}}{\sin \frac{\alpha}{2}}$.

$$\text{or, } y = \frac{\frac{d}{2}}{\sqrt{2} \sin \frac{\alpha}{2}} \quad [\text{Using eqn. (3.9.2)}]$$

Using this formula of y in eqn. (3.9.3), we get

$$A = \frac{d^2}{2 \sin \frac{\alpha}{2}}$$

Introducing A in eqn.(3.9.1), one can easily deduce: $H = K \frac{P}{d^2}$ (3.9.4)

Where, $K = 2 \sin \frac{\alpha}{2}$ is called a geometrical factor equal to 1.854. The unit of H is measured in megapascals, if P is in Newton's and d is measured in meters.

3.10 THEORY OF THERMAL ANALYSIS

The term thermal analysis (TA) is frequently used to describe analytical experimental techniques which investigate the behaviour of a sample as a function of temperature. This definition is too broad to be of practical use. TA techniques such as DSC, DTA, TG, TMA and DMA.

3.10.1 THERMOGRAVIMETRIC ANALYSIS (TGA)

Thermo gravimetric analysis (TGA) is one of the members of the family of thermal analysis techniques used to characterize a wide variety of materials. TGA provides complimentary and supplementary characterization information to the most commonly used thermal technique, DSC. TGA measures the amount and rate (velocity) of change in the mass of a sample as a function of temperature or time in a controlled atmosphere. The measurements are used primarily to determine the thermal and/or oxidative stabilities of materials as well as their compositional properties. The technique can analyze materials that exhibit either mass loss or gain due to decomposition, oxidation or loss of volatiles (such as moisture). It is especially useful for the study of polymeric materials, including thermoplastics, thermosets, elastomers, composites, films, fibers, coatings and paints. TGA measurements provide valuable information that can be used to select materials for certain end-use applications predict product performance and improve product quality. The technique is particularly useful for the following types of measurements:

- Compositional analysis of multi-component materials or blends
- Thermal stabilities

Chapter 3 Theoretical Background

- Oxidative stabilities
- Estimation of product lifetimes
- Decomposition kinetics
- Effects of reactive atmospheres on materials
- Filler content of materials
- Moisture and volatiles content

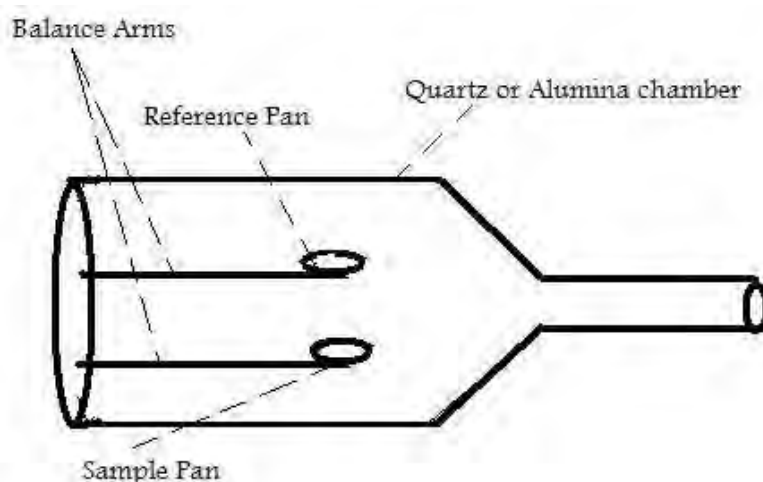


Fig.3.10.1:Schematic representation of a TGA apparatus.

Fig.3.10.1 shows a sample-balance-beam and a reference-balance-beam that are independently supported by a driving coil/pivot. Inside the TGA, there are two pans, a reference pan and a sample pan. The pan material can be either aluminium or platinum. The type of pan used depends on the maximum temperature of a given run. As platinum melts at 1760 °C and aluminum melts at 660 °C, platinum pans are chosen when the maximum temperature exceeds 660 °C. Under each pan there is a thermocouple which reads the temperature of the pan. Before the start of each run, each pan is balanced on a balance arm. The balance arms should be calibrated to compensate for the differential thermal expansion between the arms. If the arms are not calibrated, the instrument will only record the temperature at which an event occurred and not the change in mass at a certain time. To calibrate the system, the empty pans are placed on the balance arms and the pans are weighed and zeroed.

3.10.2 DIFFERENTIAL THERMAL ANALYSIS DTA

DTA is an important tool of studying structural and phase changes occurring in solid and liquid materials during heat treatment. Thus changes may be due to dehydration, transition from one crystalline to another, destruction of crystalline structure, melting, oxidation, decomposition, degradation temperatures etc. DTA is a process of accurate measurement of difference of temperature in between a thermocouple embedded to a sample and a thermocouple in a standard inert material such as aluminum oxide while both are being heated at a uniform rate [24]. Any physical or chemical change in the test sample at a specific temperature, which is a characteristic feature of the material under study, is usually associated with a thermal transition leading to an enhanced difference of temperature ΔT , between the test and reference sample. ΔT is recorded as a function of temperature T . For no transition in the shape, ΔT remains nearly constant. In DTA, the correlation between ΔT and energy change ΔE for a transition is unknown, thereby making an uncertain conversion of endothermic or exothermic peak areas of energies. DTA measures the temperatures and temperature differences (between sample and reference) associated with transitions in materials as a function of time and temperature in a controlled atmosphere.

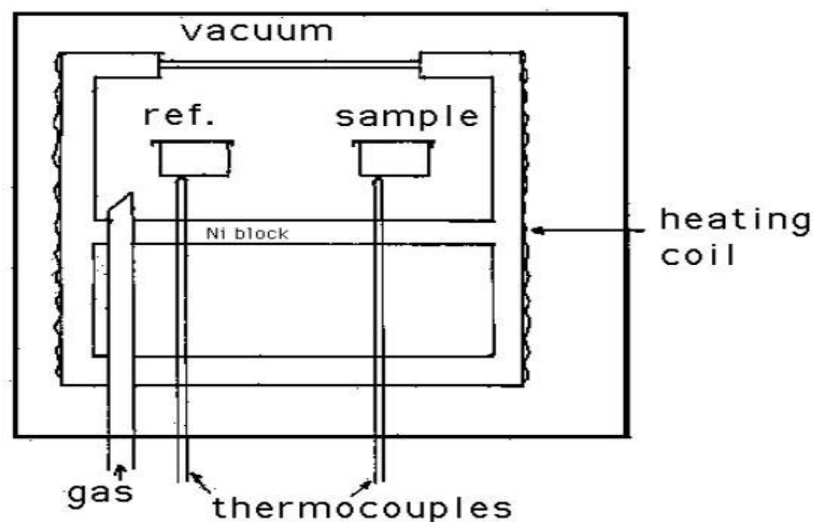


Fig. 3.10.2: Schematic Illustration of a DTA Cell.

The principal of DTA consists of measuring heat changes associated with the physical or chemical changes occurring when any substance is gradually heated. The thermocouple (platinum-platinum rhodium 13%) for DTA is incorporated at the end of each of the balance

Chapter 3 Theoretical Background

beam ceramic tubes, and the temperature difference between the holder on the sample side and the holder on the reference side is detected. This signal is amplified and becomes the temperature difference signal used to measure the thermal change of the sample. Fig.3.10.2 shows a schematic illustration of a DTA cell. It contains two holders attached with thermocouples. Sample is inserted in one holder and a reference sample is placed in the other. The difference in temperature is measured from the difference in e.m.f between the thermocouples. These differences of temperatures appear because of the phase transitions or chemical reactions in the sample involving the evolution of heat and are known as exothermic reaction or absorption of heat known as endothermic reaction. The exothermic and endothermic reactions are generally shown in the DTA traces as positive and negative deviations respectively from a base line. So DTA offers a continuous thermal record of reactions in a sample. The areas under the bands or peaks of DTA spectra are proportional to the amount of heat absorbed or evolved from the sample under investigation, where temperature and sample dependent thermal resistance are the proportionality factors. Thus DTA is needed primarily for the measurement of transition temperature. It can be used to study thermal properties and phase changes which do not lead to a change in enthalpy. The baseline of the DTA curve exhibits discontinuities at the transition temperatures and the slope of the curve at any point will depend on the microstructural constitution at that temperature.

REFERENCES

- [1] R.E. Drumright, P.R. Gruber, D.E. Henton, “Polylactic acid technology”, *Ad. Mater.* Vol. 12, pp. 1841–1846, 2000.
- [2] K.M. Nampoothiri, R.N. Nair, P.R. John, “ An overview of the recent developments in polylactide (PLA) research”, *Bioresour. Technol.* Vol. 101, pp. 8493–8501, 2010.
- [3] L. Bouapao, H. Tsuji, K. Tashiro, J. Zhang, M. Hanesaka, “Crystallization, spherulite growth, and structure of blends of crystalline and amorphous poly(lactide)s”, *Polymer.* Vol. 50, pp. 4007–4017, 2007.
- [4] K. Fukushima, Y. Kimura, “An efficient solid-state polycondensation method for synthesizing stereocomplexed poly(lactic acid)s with high molecular weight”, *J. Polym. Sci. Part A: Polym. Chem.* Vol. 46, pp.3714–3722, 2008.
- [5] D. Garlotta, “A literature review of poly(lactic acid)”, *J. Polym. Env.*, Vol.9(2), pp. 63-84, 2001.
- [6] B. Gupta, N. Revagade, J. Hilborn, “Poly(lactic acid) fiber”, *Prog. Polym. Sci.* Vol. 34, pp. 455–482, 2007.
- [7] A. Shaw, S. Sriramula, P.D. Gosling, and M.K. Chryssanthopoulo, “ Introduction to polymer composites” *Composites Part B*, Vol. 41, pp. 446–453, 2010.
- [8] C. Mayer, X. Wang, M. Neitzel, “Polymer composites, macro-and microcomposites”, *Composites Part A: App. Sci. Manu.*, Vol.29, pp. 783–793, 1998.
- [9] A.F Avila, C.M. Paulo, D.B. Santos, and C.A Fari, “Materials Characterization”, *Composites Part A: App. Sci. Manu.*, Vol. 50, pp. 281–291, 2003.
- [10] I. Nicoleta, and H.Hickel, “Macro-,micro-and nano-mechanical investigations on silorane and methacrylate-based composites”, *Dental Materials*, Vol. 25, pp. 810-819, 2009.
- [11] A. Mkaddem, I. Demirci, and M.E. Mansori, “A micro-macro combined approach using FEM for modelling of machining: Cutting forces analysis”, *Compost. Sci. and Tech.*, Vol. 68, pp. 3123–3127, 2008.
- [12] D.R. Paul, L.M. Robeson, “Polymer nanotechnology: Nanocomposites”, *Polymer*, Vol. 49, pp. 3187-3204, 2008.
- [13] Amelinckx S. (Ed:), “Electron microscopy: principles and fundamentals”, VCH, 1997.
- [14] Egami T., Billinge S. J. L., “Underneath the Bragg Peaks Structural Analysis of Complex Materials”, Vol. 7, Elsevier: Oxford, 2003.
- [15] Asano T., Mina M.F., Fujiwara Y., “A Survey of Polymer Crystallization by X-ray Diffraction”, Chapter 5, SKP Inc. Shizuoka, Japan, 2006.

Chapter 3 Theoretical Background

- [16] Mina M.F., Alam M.M., Akhtar F., Imaizumi K., Yoshida S., Toyana N., Asano T., “Centrifuging effect on the structure and property of natural rubber latex films”, *Polym. Plast. Technol. Eng.*, 42, 503-514, 2003.
- [17] Wunderlich B., “Crystal Structure, Morphology and Defects”, *Macromolecular Physics: Vol. 1*, Academic Press: New York and London, 1973.
- [18] William D., Callister, J.R., “Materials Science: An Engineering Introduction”, John Wiley & Sons Inc, New York, USA, 2000.
- [19] Donald R.A., “The Science and Engineering of Materials”, Alternate Edition, PWS-KENT Publication, Massachusetts, USA, ISBN 0-534-05034-4, 1985.
- [20] B.E. Conway, *Electrochemical supercapacitors- scientific fundamentals and technological applications*, Kluwer Academic, Dordrecht, 1999.
- [21] E. Frackowiak, and F. Beguin, *Carbon*, Vol. 40, pp. 1775, 2002.
- [22] Calleja F.J., Fakirov S., “Microhardness of Polymers” Cambridge University Press, 2000.
- [23] Mina M.F., Akbar S. “Versatile applications of microindentation test in the characterization of polymers and their blends”, *Bangladesh J. Phys.*, 1(1), 84-94, 2004.
- [24] Keatch, C.J. and Dollimore, D., *An introduction to thermogravimetry*, Heyden and Son Ltd, New York, 1969.

MATERIALS AND METHODS

4.1 RAW MATERIALS

In the recent year application of the composites are worldwide, in this research work composites were prepared from a mixture of Polylactic acid (PLA) and graphite. PLA is a granular-shaped plastic and graphite is black in color. The composites have particular ratios of graphite at different particle sizes in PLA. Brief descriptions of PLA and graphite, which are used in this study, are given below.

4.1.1 POLYLACTIC ACID

PLA is a biodegradable thermoplastic aliphatic polyester. PLA thermoplastic used in this study was a product of Nature Works PLA, 2002D, Germany with melt index of 5-7 g/10 min at a temperature 210°C and specific gravity of 1.24, derived from renewable resources.



Fig.4.1.1: A photograph of PLA granules



Fig.4.1.2: A photograph of prepared neat PLA sheet.

4.1.2 GRAPHITE

The graphite flake was purchased from of Zhengzhou Sino Chemical Co, Ltd., China was collected from the local market. It looks shiny ash color with particle size of $10\text{--}50\ \mu\text{m}$ and density of $\approx 2.2\ \text{g/cm}^3$. The graphite powder (GP) was the prepared by grinding the flakes using a mortar and pastel.

4.2 EQUIPMENT FOR THE PREPARATION OF COMPOSITES SAMPLES

Several equipments were used in the fabrication of composites. The main equipments are as follows:

- (a) Electric balance
- (b) Sample die: (i) *Dumbbell-shaped* and (ii) *Bar-Shaped*
- (c) Extrusion machine
- (d) Compression molding machine: Weber-Pression hydraulic press

Brief description of these equipments used for the sample preparation are given below-

4.2.1 ELECTRIC BALANCE

In Fig. 4.2.1 is shown an electric balance (HP 200) used for measurement of weight of the sample. The balance is sensitive and has a measuring capacity of 0.001 gm.



Fig. 4.2.1: A photograph of an electric balance.

4.2.2 SAMPLE DIE

To cast the ultimate fabricated composites, two types of dice were used. One is dumbbell-shaped and the other is bar-shaped. Both types of dice have a male and a female part. These two shapes of the dice were prepared according to the ASTM standard [1, 2].

(i) Dumbbell- Shaped Die

In case of dumbbell-shaped die, when male is attached with female part, the hollow space inside the die has the dimensions shown in Fig. 4.2.2(a) and 4.2.2(b). Melt is usually injected inside hollow space of the die through an orifice located at the middle of the die.

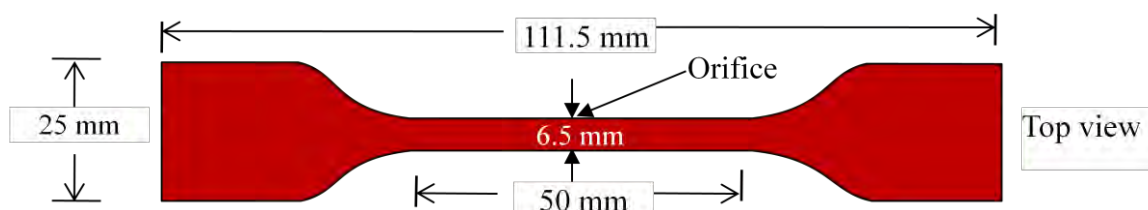


Fig. 4.2.2(a): Dimensions of a dumbbell-shaped die



Fig. 4.2.2(b): Dimensions of a dumbbell-shaped die.

In dumbbell-shaped die, the hollow space is in the female part and the dumbbell shape is in the male part. The male is to be attached with female part, the sample inserted into the hollow space; the schematic diagram is shown in Fig. 4.2.2(c). Shape of the sample is the same as that of the die.

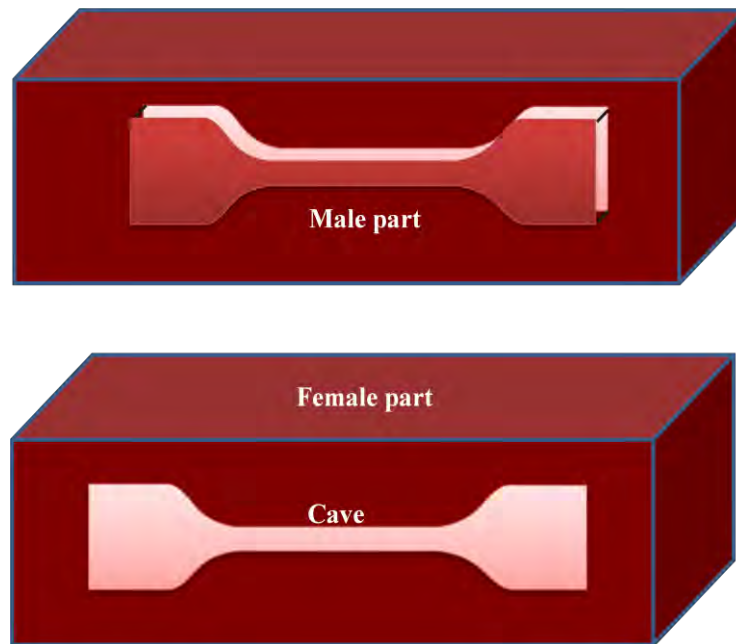


Fig. 4.2.2(c): Side views of the both parts of the Dumbbell-shaped dice.

(ii) *Bar-Shaped Die*

For bar-shaped die, when male part is attached with female part, the hollow space inside the die has the dimensions shown in Fig. 4.2.3(a).

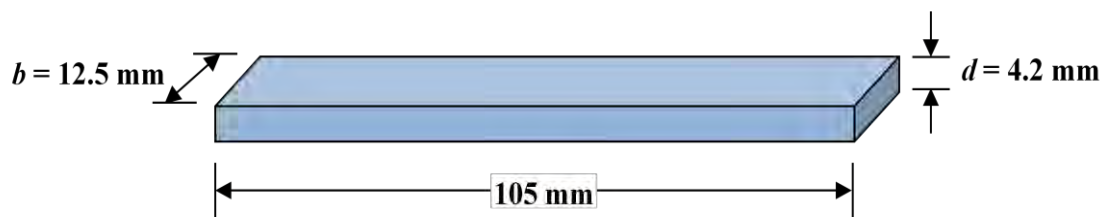


Fig. 4.2.3(a): Dimensions of a bar-shaped die.

Similarly for bar-shaped die, the hollow space is in the female part and the bar shape is in the male part. The male is to be attached with female part, the sample inserted into the hollow space; the schematic diagram is shown in Fig. 4.2.3 (b). Also in this case, the shape of the sample is the same as that of the die.

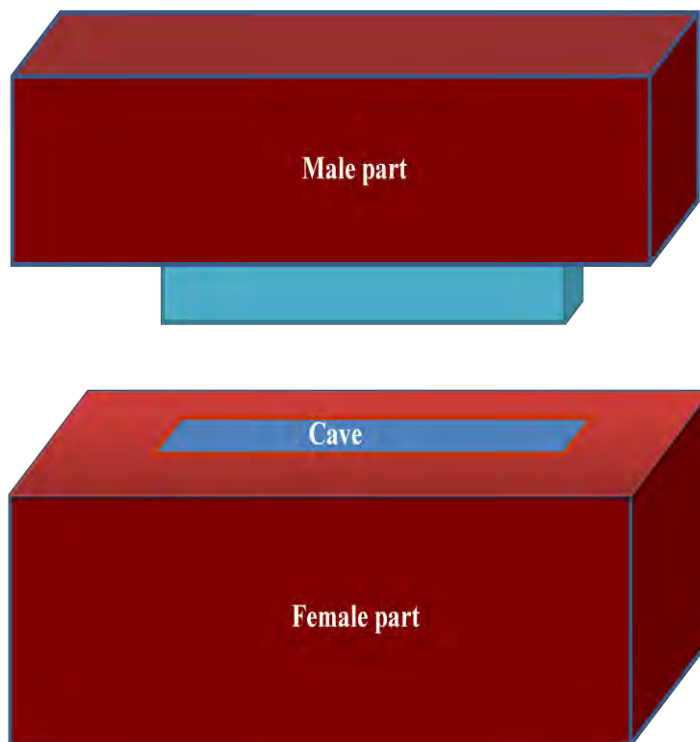


Fig. 4.2.3(b): Top view of the Bar-shaped dice.

4.2.3 EXTRUSION MACHINE

Extrusion is the process of pushing the heated billet or slug of polymers, composites etc. through an orifice or outlet. An extrusion machine, model Axon AB, Sweden is used to give a definite shape of granular or powder polymeric materials as that of a die. It is also used to make melt mixing of the components of a polymeric composite. The melt is ejected through the orifice or outlet. This ejected melt is called extrudates.



Fig. 4.2.4: Photographs of an Extrusion machine and extrudates.

The shape of the extrudates is similar to that of a die placed at the orifice. The extrudates can have good tolerance and surface finish. Complex shapes of the extrudates can be given according to the shape of the die. The extrusion machine used in this investigation to mix PLA and graphite is shown in Fig. 4.2.4 along with the extrudates. The schematic diagram of the apparatus is shown in Fig. 4.2.5. Various parts of the extrusion machine are described below [3] :

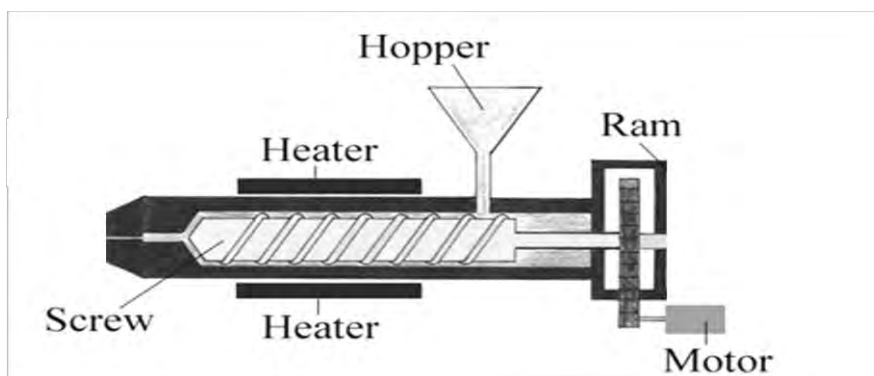


Fig. 4.2.5: Schematic diagram of an extrusion machine.

(i) Extruder Screw

The most important part of the extrusion machine is the extrusion screw. It delivers materials through the barrel. The length of the screw is divided into three zones: feed, compression and metering zones. The purpose of feed zone is to pick up the mixture of raw materials from the feed hopper and to move them into the main length of the extruder. In the compression zone, the loosely packed mixture is compacted and softened to produce a continuous stream of molten composite from the compression zone and feeds it at a controlled rate through the barrel. The final section of the screw is known as metering zone. The function of the metering section is to force the molten polymer through the die at a steady rate and iron out pulsation. The length of the screw used in this machine was 0.09 meter and the diameter of the screw was 0.003 meter.

(ii) Motor

The screw is driven by an a.c. motor and its rpm is also controlled by an a.c. motor. The screw is rotated by the motor at a speed of 80-100 rpm in this extrusion machine.

(iii) Barrel

The barrel surrounds the screw. It is an enclosure in which the feeding material is melt. It resists the pressure generated by the screw, which may be as high as 6000 psi. The whole region of the barrel is electrically heated by band heaters around it.

(iv) Heaters

The extruder has 5 heating zones with blending temperature profiles of 180, 185, 190, 195 and 200°C. The temperature of the heater can be controlled by a controller and can be recorded. The working temperatures of the machine can be set in the range 100-250°C. Heaters surround the barrel and melt the plastic as it travels along the barrel. The granules melt into a liquid which is forced through a die, forming a long 'tube like' shape. The extrusion is then cooled and forms a solid shape as the shape of the tube.

(v) Chopper

A chopper is small part of the extrusion machine. After obtaining the tube or wire (diameter approximately 2-3mm) like extrudate of composite, it was prepared for chopping. Then



Fig. 4.2.6: Photographs of chopper machine and chopped extrudates.

These extrudates were shredded by a chopper machine as shown in Fig. 4.2.6. Each of the samples were chopped and then extruded successively for better mixing. The size of the extrudate wire is approximately $\leq 0.5\text{mm}$ being chopped. The chopped materials were reserved in air tight desiccators.

4.2.4 COMPRESSION MOLDING MACHINE: WEBER-PRESSEN HYDRAULIC PRESS

Weber-pressen hydraulic press is a compression-molding process, model: PW 40H. It is a widely used method for fabrication of articles from polymer materials. Fig.4.2.7 shows a typical mold employed in this study for compression molding. The mold is made of two halves; the upper halves or the male and the lower halves or the female. In most cases, the lower half contains a cavity when the mold is closed. The gap between the projected upper half and the cavity in the lower one gives the shape of the molded article. The mold used in

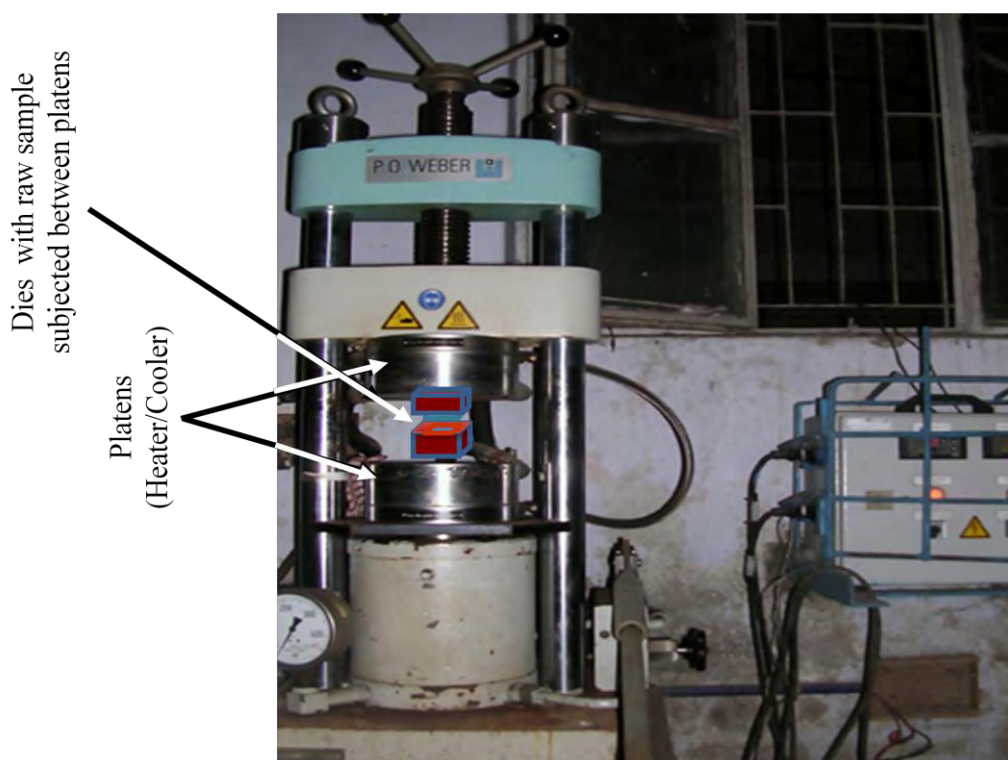
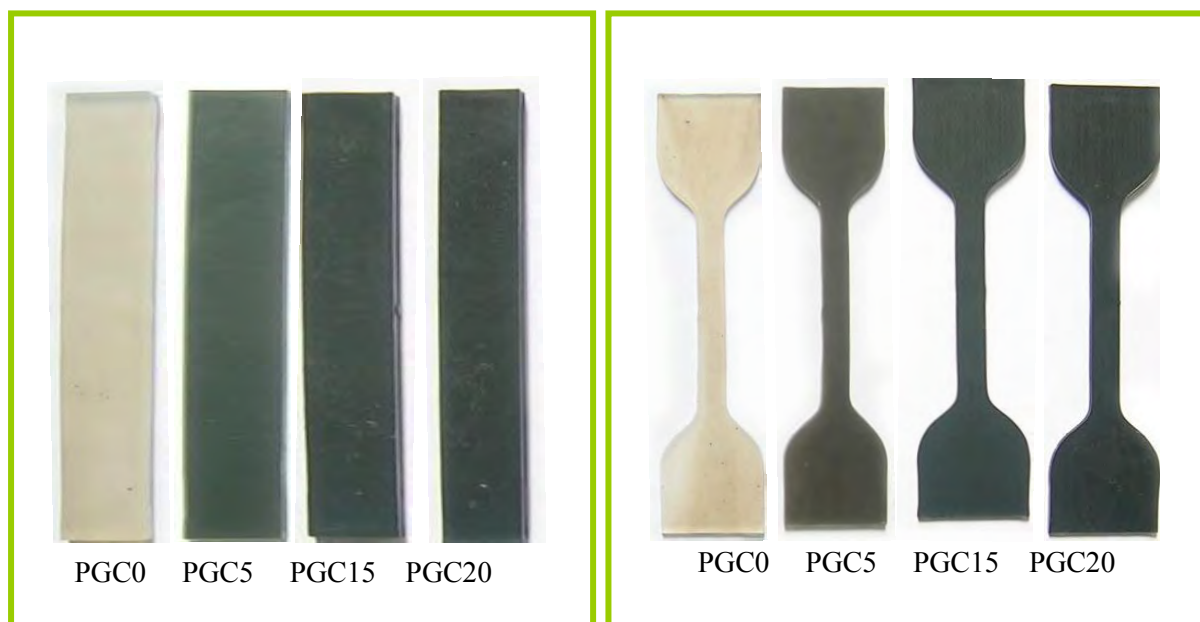


Fig. 4.2.7.: A Weber-pressen hydraulic press.

the research work had both the upper and lower halves but had no cavity in any half of the mold. These two halves are completely plane with smooth surface platens, which also acts as heater and cooler simultaneously. In this molding process, one has to make die for casting with his desired size. A rectangular metal die either with dumbbell-shaped or bar-shaped pattern was used in this study, as discussed in the section 4.2.2. This die with the chopped extrudates is placed in between the platens.

4.3 PREPARATION OF COMPOSITE SAMPLES

The graphite powder was of density, $\rho_f = 2.09 \text{ g/cm}^3$ and was mixed with PLA with appropriate ratios. Separate mixtures of PLA and 0, 5, 10, 15, 20 and 30 wt% graphite content having the aforesaid different sizes were extrudates. The neat PLA is abbreviated as P, and 5 wt% graphite loaded PLA composites with Particles 1, 2, 3, 4 and 5 are hereinafter coded as PGC0, PGC5, PGC10, PGC15, PGC20 and PGC30 respectively. Fig.4.3.1 represents the bar and dumbbell sized samples. The extrudates were shredded by a chopper machine and again molded in both dumbbell and bar-shaped dice at 170°C using a compression molding machine with a load of 100 kN. The solid samples were subjected to measure structural, surface morphological, mechanical and thermal by the following techniques.



(a) Bar shaped samples

(b) Dumbbell shaped samples

Fig. 4.3.1: (a) Bar shaped and (b) Dumbbell shaped samples for particle size 1.

4.4 SURFACE MORPHOLOGY TESTS

Morphology, or "what a sample looks like," is best evaluated using imaging techniques, such as optical microscopy or SEM. These methods can also provide layer thickness and other qualitative information as that shown in Fig. 3.5.1. In this study, SEM, TEM has been done and the descriptions are in the following:

4.4.1 SURFACE MORPHOLOGY TEST BY A SEM

The surface morphologies of non-fractured and fractured samples of the neat PLA sample and the composites with 5, 10, 15, 20 and 30 wt% graphite, were studied by a SEM (JSM-6510 LV, JEOL, Japan) with a maximum operating voltage of 20 kV of the apparatus. Samples were mounted on aluminium stubs with carbon tape and sample-surface was coated with a thin gold layer by a sputtering machine prior to SEM measurements. Each sample was cut with an appropriate size for the study of surface structure. The apparatus used in this study is shown in Fig. 4.4.1.

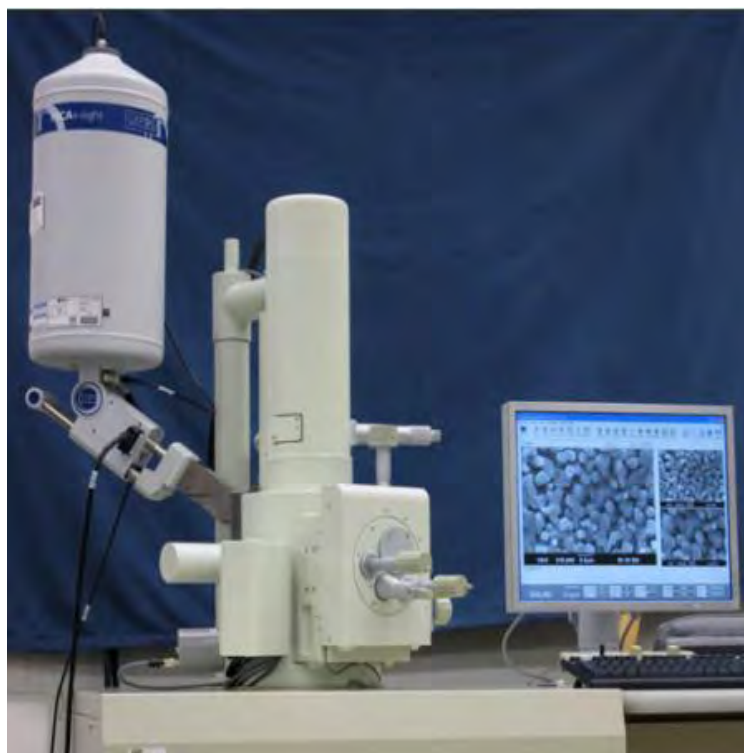


Fig. 4.4.1: Scanning electron microscope

4.4.2 SURFACE MORPHOLOGY TEST BY A TEM

TEM was performed by a Hitachi H-7100 TEM (Japan) with operating voltage of 120 kV to monitor the dispersion of polylactic acid graphite composites. For TEM measurements, a plastic crusher machine was used to crush the composites into powder form, which was

subjected to ultrasonication for 30 minutes with few drops of acetone. After that, drops of powder with mixed liquid were put on a copper grid, dried for a few minutes and then studied by TEM. It is a straight forward technique to determine the size and shape of the nanostructure materials as well as to obtain structural information. In TEM, electrons accelerated to 100 KeV or higher, are projected on to a thin specimen by means of a condenser lens system and they penetrate into the sample [4]. The great advantages that TEM offers the high magnification ranging from 50 to 106 and its ability to provide both image and diffraction information of the same sample. The schematic of a transmission electron microscope is shown in Fig. 4.4.2.



Fig. 4.4.2: A Photograph of a transmission electron microscopy.

4.5 STRUCTURAL MEASUREMENTS

Many of the analytical techniques used to determine the molecular structure of unknown organic compounds are also used in polymer characterization. Spectroscopic techniques such as UV-VIS spectroscopy, IR spectroscopy, RS, NMR spectroscopy, ESR spectroscopy, XRD, and Mass spectrometry are used to identify common functional groups. In this study, FTIR, RS, XRD have been done and the descriptions are in the following:

4.5.1 Fourier Transform Infrared Spectroscopy

FTIR spectra of the samples were recorded at room temperature by using a double beam FTIR spectrophotometer (SHIMADZU, FTIR 8700 spectrophotometer, Japan) in the wave number range of 500-4000 cm^{-1} . For these measurements, the samples were cut into appropriate size and put on a sample holder for recording the FTIR spectrum in the reflectance (%) mode. The schematic of a yopcsortceps derarfni mrofsnart-reiruof is shown in Fig. 4.5.1.



Fig. 4.5.1: A Photograph of an FTIR Spectrometer.

4.5.2 RAMAN SPECTROSCOPY

Raman spectra were obtained using a Raman spectrometer (JASCO, NR-1800, Japan) equipped with a triple polychromator having radiation of wavelength $\lambda=532$ nm from a solid state laser of power 5 mW, and a charged-couple device (CCD) was used to detect the backscattered Raman spectrum. The size of the focused laser spot on the sample was about 5 μm and the resolution of the spectra was 1 cm^{-1} . The exposure time of the sample under the laser beam was 10 s. To determine the effect of laser heating upon the PGC, glass slides containing the samples were placed onto the Raman microscope stage. All the spectra were curve-fitted using Gaussian routines, from which the various band positions and intensities were obtained. The schematic of a Raman spectrometer is shown in Fig. 4.5.2.



Fig.4.5.2: A Photograph of Raman Spectrometer.

4.5.3 X-RAY DIFFRACTOMETRY

XRD can be used as a powerful tool for the study of materials because of its ability to give a broad range of information such as crystal structure, composition and defects. It is a non-destructive technique and does not require any specific sample preparation methods.

In the present study, the structural analysis of material was done for using XRD technique. The bar samples having the same thickness were used for XRD measurements. Wide-angle XRD (WAXD) studies were performed by an X-ray diffractometer (model JDX-8P, JEOL Ltd., Tokyo, Japan) using CuK_α radiation of wavelength, $\lambda = 1.5418 \text{ \AA}$ for the crystallographic analysis, through a step-wise scan over the scattering angle (2θ) from 5 to 50° , with a step of 0.02° . Fig. 4.5.3 shows the photograph of an X-ray diffractometer. The operating voltage and the tube current of the X-ray generator were 30 kV, 200 mA, respectively. Small-angle XRD (SAXD) measurements of the samples were performed using a rotating anode type high-intensity Rotaflex, RU-300 X-ray generator (40 kV \times 200 mA; Rigaku Corporation Tokyo, Japan). The incident X-ray beam, monochromatized by a graphite single crystal, had a wavelength of 1.54 \AA . The X-ray beam was passed through a collimation system with a pinhole of 100 μm in diameter. The camera length for SAXD was 460 mm. The diffraction intensity was recorded by a Rigaku Display System imaging plate (IP) (Rigaku Corporation, Tokyo, Japan). The exposure time was set as 60 min in every X-ray measurements.

The standard JCPDS data cards were used for comparative purpose. The schematic diagram of X-ray diffractometry is shown in the Fig. 4.5.4. X-Ray diffraction is based on the constructive interference of monochromatic X-rays caused by crystalline materials. These X-



Fig. 4.5.3: A Photograph of an X-ray diffractometer.

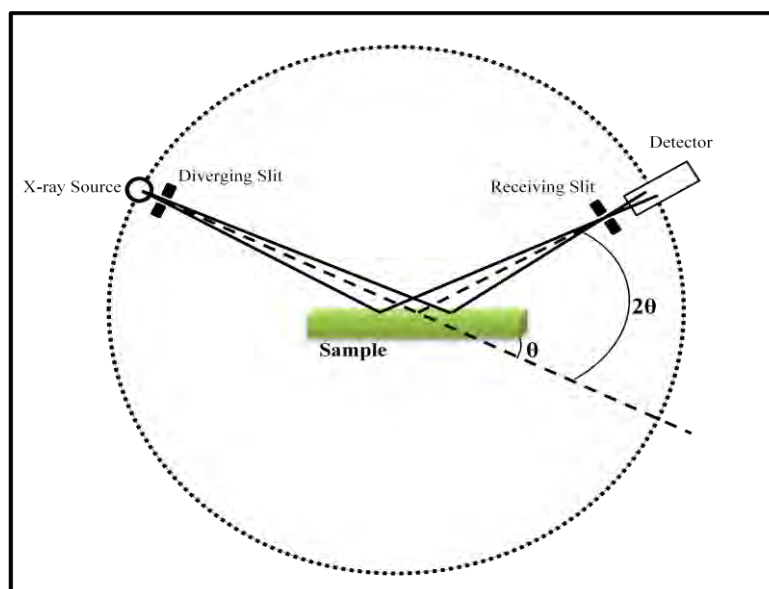


Fig. 4.5.4: Schematic diagram of an X-ray diffractometer.

rays are generated by a cathode ray tube, filtered to produce monochromatic radiation collimated to concentrate and directed towards the sample. The interaction of the incident rays with the sample produces constructive interference when Bragg's law ($n\lambda=2d\sin\theta$) conditions are satisfied. This law relates the wavelength of electromagnetic radiation to the diffraction angle and the lattice spacing in a crystalline sample.

SAXD and WAXD measurements are usually carried out to study the lamellar and crystalline structure of polymers, respectively [5, 6].

4.6 METHODS OF MEASURING MECHANICAL PROPERTIES

The mechanical properties, such as tensile stress, tensile strain, tensile strength and Young's modulus of the prepared samples were evaluated by a universal testing machine (UTM).

4.6.1 Universal Testing Machine

UTM (Hounsfield UTM 10KN; ASTM D-638–98) can be used for measuring the mechanical properties such as, tensile and flexural strength, tensile and flexural strain, and Young's and tangent modulus of the composites. The load range, speed, measuring unit, gauge length etc. can be selected over a wide range. The maximum speed, load range and gauge length to be used in this machine are $0.001 \text{ m}\cdot\text{min}^{-1}$, 500N and 60 mm,

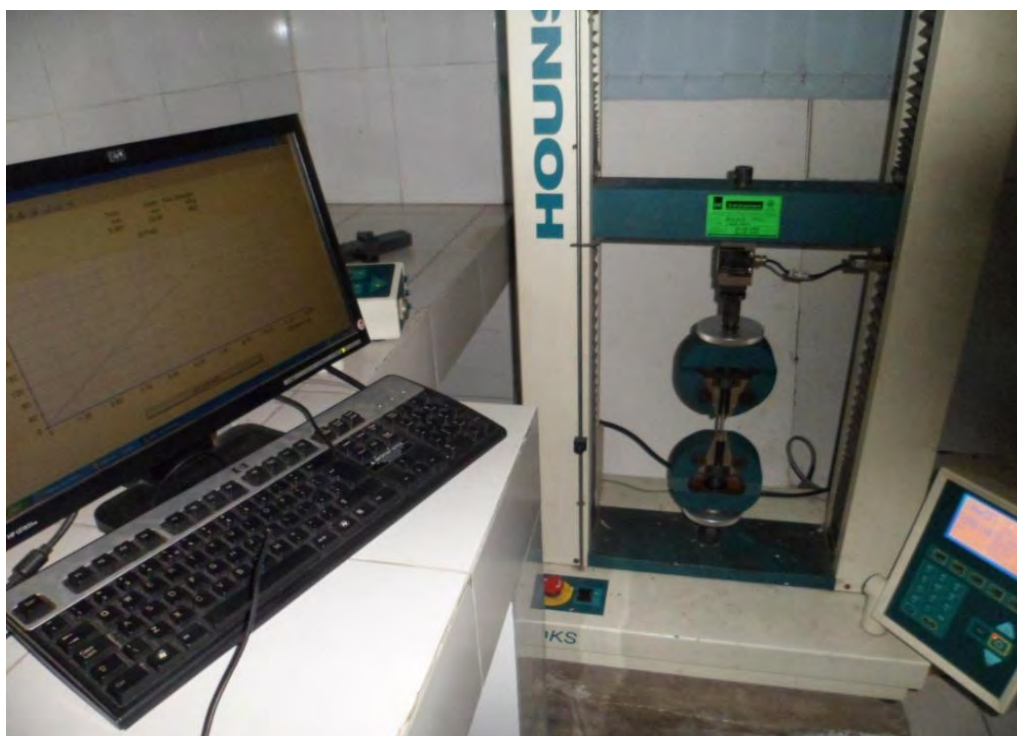


Fig. 4.6.1: A universal testing machine

respectively. A photograph of the Hounsfield UTS 10 KN is shown in Fig. 4.6.1. This machine contains grips to hold a sample, which is stretched by the application of a continuously increasing load to measure the tensile properties. The gap between the grips is maintained according to ISO standard. The maximum load that can be employed in this

machine is 10 kN. The measuring conditions are set by the programmed software. The data acquisition and analyses can be performed by the software.

4.6.2 Measurements by Universal Testing Machine

Tensile strength (TS), tensile strain (ε), tensile stress (σ), percentage of elongation-at-break [$EB(\%)$] and Young's modulus (Y) of the samples were measured by a software controlled universal testing machine [Hounsfield UTM 10KN (H10KS)]. Five samples of each composition were used in the mechanical testing.

4.6.2.1 Measurements of Tensile Properties by UTM

Type M-II specimen for tensile measurement was prepared according to ASTM standard [8]. Schematic diagram of the size and shape of the specimen used in measuring σ , ε , TS , $EB(\%)$ and Y is shown in Fig. 4.2.2(a) and 4.2.2(b). In this measurement, two ends of the sample were tightened by the grips and increasing loads are applied to stretch the sample. Tensile measurements were performed according to ASTM standard (D 638) [7]. Crosshead speed of 5 mm/min and a gauge length 42 mm were maintained. The load is continuously applied to the sample till it is fractured. The loads and corresponding extensions were recorded by the computer. Calculations of tensile properties are described below:

(i) Tensile Stress

Tensile stress was evaluated using the following formula (Section 3.8.1):

$$\sigma = \frac{F}{A} \quad (4.6.1)$$

Where, F = Load applied to the sample

A = Cross sectional area of the test sample

The value of F was obtained from the UTM. The value of A was obtained by a slide calipers by measuring the width and thickness at least three points in the narrow zones of the sample.

(ii) Tensile Strain

Tensile strain was calculated by the relation given below (Section 3.8.1)

$$\varepsilon(\%) = \left(\frac{\Delta L}{L_o} \right) \times 100\% \quad (4.6.2)$$

Where, ΔL = Extension due to applied load

L_o = Gage length or original length of the sample

The value of ΔL was obtained from the UTM.

(iii) Tensile Strength

Tensile strength was estimated by the following formula (Section 3.8.1):

$$TS = \frac{F_{max}}{A} \quad (4.6.3)$$

where, F_{max} = Maximum load applied to the sample

A = Cross sectional area of the sample

(iv) Young Modulus

Young's modulus is an important parameters in characterizing the mechanical properties of solids. The bigger the Young's modulus, the stiffer the material is. For all material it is determined through tensile test. Within elastic limit, the stress-strain variation is linear in a material. Fig 4.6.2 shows a typical stress-strain curve of a polymeric material. The stress increases linearly with the strain upto the yield point. The slope of the linear portion gives the

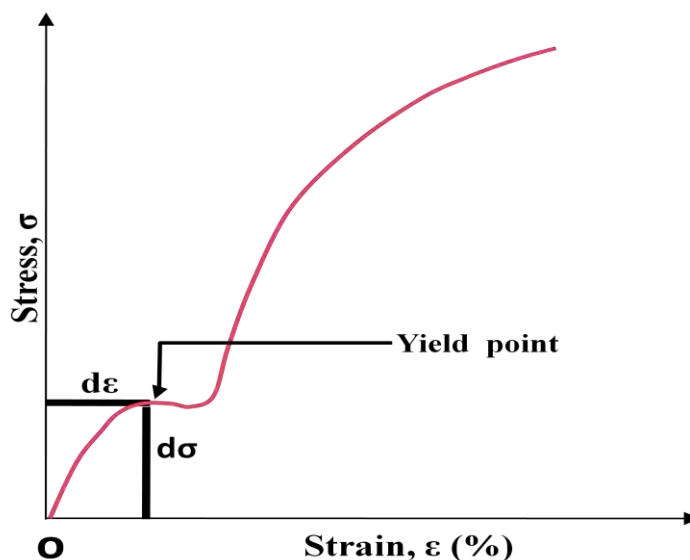


Fig. 4.6.2: A typical stress versus strain curve.

Young's modulus and was determined as (Section 3.8.1):

$$Y = \frac{d\sigma}{d\varepsilon} \quad (4.6.4)$$

Where, $d\sigma$ = Stress at yield point, $d\varepsilon$ = Strain at yield point.

4.6.2.1 Measurements of Flexural Properties by UTM

A bar shaped specimen with a rectangular cross section was prepared for flexural measurement according to ASTM standard [2]. The size of the specimen is shown schematically in Fig. 4.6.3.

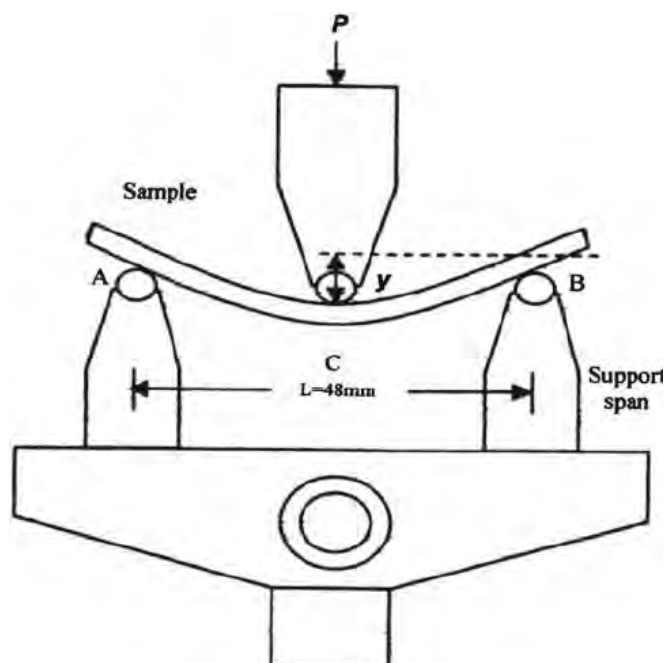


Fig. 4.6.3: 3-point (A,B,C) loading arrangement for flexural measurement.

Flexural measurement were performed according to ASTM standard (D 790) using a three point loading method. A and B are two support spans on which the sample was placed. Continuously increasing load W were applied in the middle of the sample at C. The loads W and corresponding deflections y were recorded by the computer. The loading speed was 1 mm/min and the distance between the support spans was $l=48$ mm. The following flexural measurements were performed on the samples.

(i) Flexural Stress

The load applied on the midspan was taken from the UTM and then the following equation was used to calculate flexural stress of the samples (section: 3.8.2.3)

$$\sigma_f = \frac{3Wl}{2bd^2}$$

Where,

W = load applied on the midspan.

l= Distance between support spans

b= Breadth of the specimen

d= Depth of the specimen

(ii) Flexural Strain

The midspan deflection was taken from the UTM and then the following equation was used to calculate flexural strain of the samples (section: 3.8.2.4)

$$\varepsilon_f(\%) = \frac{6yd'}{l^2} \times 100\%$$

Where,

l= Distance between the support spans

y= Midspan deflection

d'= Depth or thickness of the specimen

(iii) Percentage of Flexural Strain

The midspan deflection at break or at maximum deflection was taken from the UTM and was used in the following equation to calculate maximum flexural strain.

$$FB(\%) = \frac{6y_{\max}d'}{l^2} \times 100\%$$

Where,

l= Distance between the support spans

y_{max}= Midspan deflection at maximum flexural stress

d'= Depth or thickness of the specimen

(iv) Flexural Strength

The maximum load applied on the specimen was taken from the UTM and then the following equation was used to calculate flexural strength of the specimen (section: 3.8.2.3).

$$FS = \frac{3W_{\max}l}{2bd^2}$$

Where,

W_{\max} = Maximum load applied on the midspan

l = Distance between support spans

b = Breadth of the specimen

d = Depth of the specimen

(v) Tangent Modulus

At first the load deflection curve were plotted from the data of UTM. A typical W-y curve is shown in fig. (4.6.4). The slope, $K' = W/y$, of the initial straight line portion of the load deflection curve was estimated and introduced into the following equation to calculate the tangent modulus of the specimen.

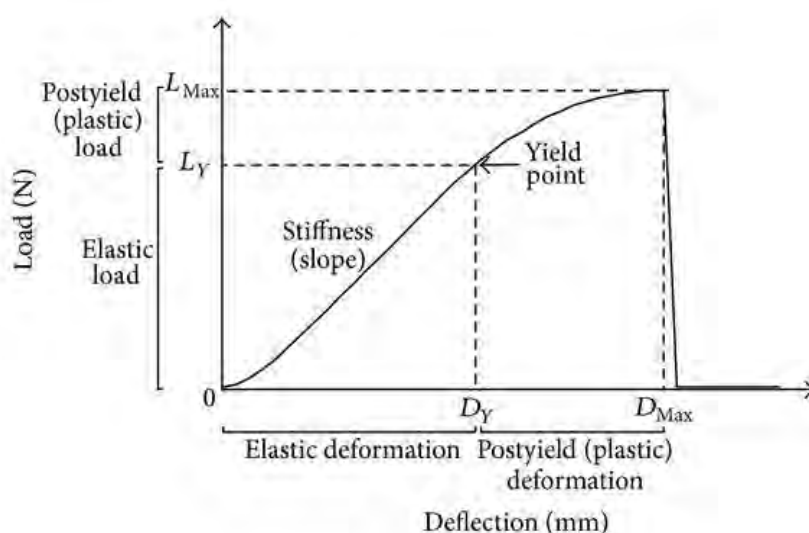


Fig. 4.6.4: A typical load-deflection curve.

$$G = \frac{K'L^3}{4bd^3}$$

Where,

K' = Slope of the initial straight-line portion of the load deflection curve.

L = Distance between support spans.

b = Breadth of the specimen

d = Depth of the specimen

4.7 METHODS OF MEASURING MICROMECHANICAL PROPERTIES

The theory of microhardness is described in section 3.9. A software controlled Vicker's square-based diamond indenter (Shimadzu, Japan) [Fig. 4.7.1(a)] was employed to measure the microhardness (H) from the residual impression on the sample surface after an indentation time of 6sec. The indenter consists of a pyramid-type diamond needle. When the needle is impinged on the surface of a sample for 6sec and removed, an indentation imprint as shown in Fig. 4.7.1(b) is observed. The imprint has two diagonals d_{hor} and d_{per} . In case of amorphous material, $d_{hor} \approx d_{per} \approx d$. The value of d can be measured by a programmed software. Loads of 0.980, 0.245, 0.490 and 0.980N were used to derive a load independent value of H in MPa by the following relation [9, 10]:

$$H = K \frac{P}{d^2} \quad (4.7.1)$$

where, d = The length of indentation diagonal in meter

P = The applied load in Newton

and K = A geometrical factor = 1.854.

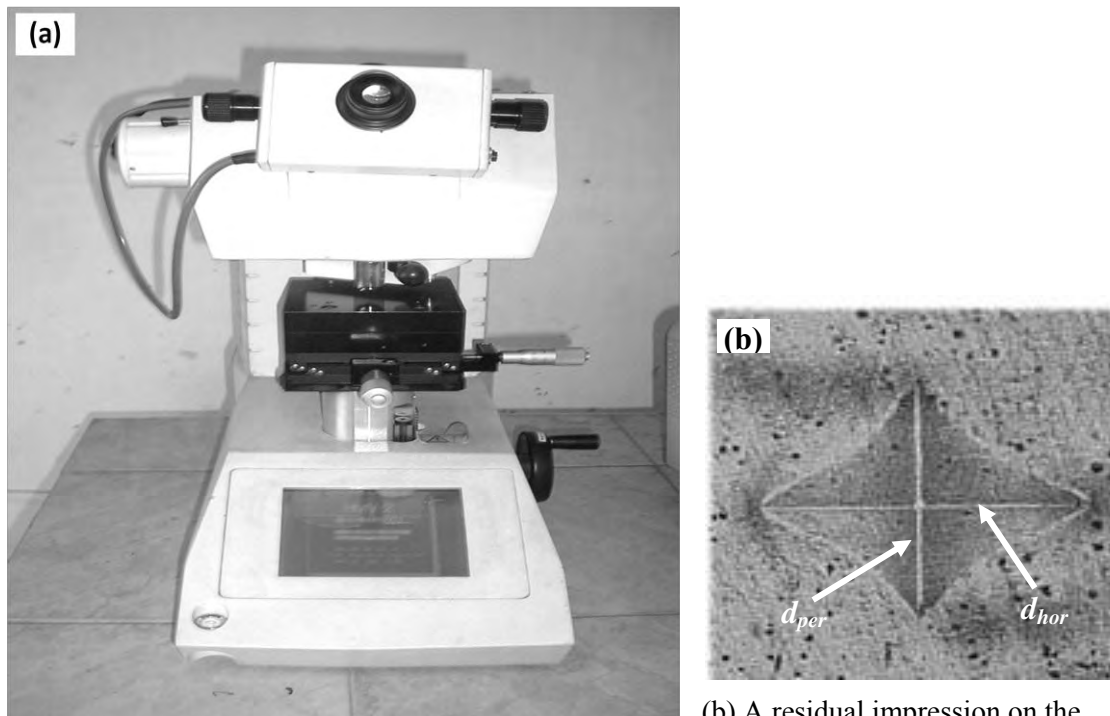


Fig. 4.7.1: (a) Shimadzu microhardness tester

(b) A residual impression on the surface of a polymer.

It is clear from eqn. (4.7.1), if we take several P values, then we get several d values. If P versus d^2 is plotted, a straight line variation can be obtained. Using the slope of this straight

line in eqn. (4.7.1), the H value independent of load can be made. Then H will only depend on graphite concentration. Samples with flat and smooth surface immediately after their preparation were used for this measurement. At least 8 imprints were taken on the surface of each sample for each load and the H was evaluated from the average value of all impressions. For measuring load-independent H value and P versus d^2 was plotted as shown in Fig. 4.7.2. A linear regression line was drawn. The slope of this line gives P/d^2 , which is put in eqn. (4.7.1) to obtain H .

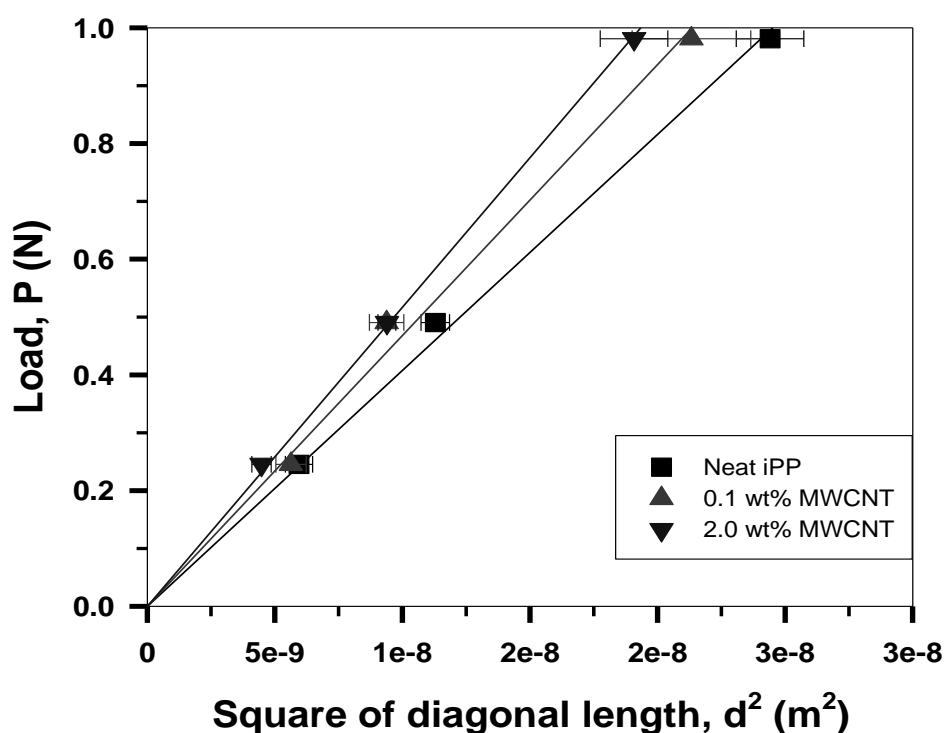


Fig. 4.7.2: Load versus square of diagonal length plot.

4.8 THERMAL MEASUREMENTS

Thermal properties of the samples were monitored by a coupled DTA, TGA. The measurements using DTA and TGA were carried out from 37 to 600°C at a heating rate of 20°C/min under nitrogen gas flow. While the DTA traces give the crystallization, melting and degradation temperatures as determined from the exotherm versus temperature curves, the TGA runs exhibit the weight-loss of the sample with temperature.

4.8.1 Methods of Thermal Measurement

The most important methods used for thermal measurement of polymer sample are discussed in the following:

4.8.1.1 Thermogravimetric Analyses and Differential Thermal Analyses

Fig.4.8.1 illustrates a photograph of a TGA coupled with a DTA [Seiko-Ex-STAR-6300, Japan], which was used in this study. TGA is used primarily for determining thermal stability of polymers [8] and TGA method is based on continuous measurement of weight on a sensitive balance (called thermo balance) as sample temperature is increased in air or in an inert atmosphere. This is referred to as non-isothermal TGA. The studies were conducted in a platinum crucible from room temperature to 600 °C at the heating rate of 20 °C-min⁻¹ under nitrogen gas flow. Data are recorded as thermograms of weight versus temperature. Weight loss may arise from evaporation of residual moisture or solvent at lower temperatures, but at higher temperature it results from polymer decomposition.

Fig. 4.8.2 shows a sample-balance-beam and a reference-balance-beam that are independently supported by a driving coil/pivot. When a weight change occurs at the beam end, the movement is conveyed to the opposite end of the beam via the driving coil/pivot, when optical position sensors detect changes in the position of a slit. The signal from the optical position sensor is sent to the balance circuit. The balance circuit supplies sufficient feedback current to the driving coil so that the slit returns to the balance position. The current running to the driving coil on the reference side is detected and converted into weight signals. The principle of TGA measurements is shown in Fig. 4.8.3.



Fig. 4.8.1: A coupled differential thermal analyzer and thermogravimetric analyzer.

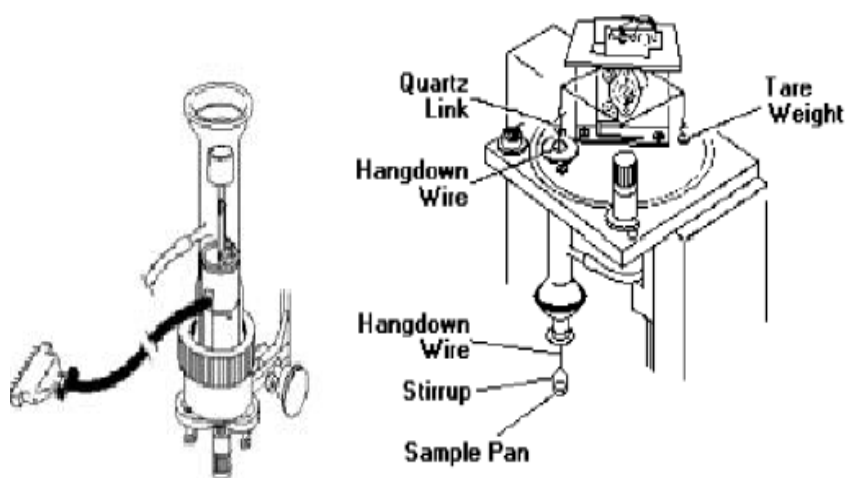


Fig. 4.8.2: Schematic picture of a furnace and a micro balance of a TGA.

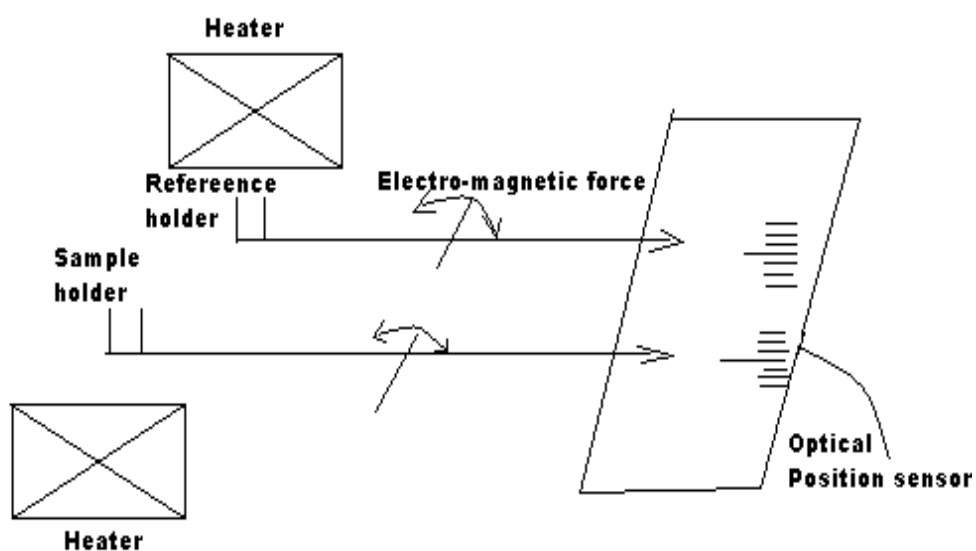


Fig. 4.8.3: Illustrates a scheme of the principle of TGA measurements.

REFERENCES

- [1] ASTM Designation: D 638M-91a, “Standard Test Method for Tensile Properties of Plastics (etric)”, Annual Book of ASTM Standards, Vol. 08.01, 1992.
- [2] ASTM Designation: D 790M-86, “Standard test methods for flexural properties of unreinforced and reinforced plastics and electrical insulating materials (metric)”, Annual Book of ASTM Standards, Vol. 08.01, 1986.
- [3] Chanda M., Roy S.K., “Plastic Technology Handbook”, Third Edition, Marcel Dekker Inc., ISBN 0-8247-0066-X, 1998
- [4] Amelinckx S. (Ed:), “Electron microscopy: principles and fundamentals”, VCH, 1997.
- [5] Asano T., Mina M.F., Fujiwara Y., “A Survey of Polymer Crystallization by X-ray Diffraction”, Chapter 5, SKP Inc. Shizuoka, Japan, 2006.
- [6] Mina M.F., Alam M.M., Akhtar F., Imaizumi K., Yoshida S., Toyana N., Asano T., “Centrifuging effect on the structure and property of natural rubber latex films”, Polym. Plast. Technol. Eng., 42, 503-514, 2003.
- [7] ASTM Designation: D 638M-91a, “Standard Test Method for Tensile Properties of Plastics (etric)”, Annual Book of ASTM Standards, Vol. 08.01, 1992.
- [8] Sjorstrom E., in Wood Chemistry: Fundamentals and Applications, Academic Press, London, 169, 1981.

Chapter Five

RESULTS AND DISCUSSION

5.1 STRUCTURAL ANALYSIS

5.1.1 FOURIER-TRANSFORMS INFRARED SPECTROSCOPY ANALYSIS

Fig. 5.1.1 illustrates the FTIR spectra of all PGCs, recorded as the reflectance (%) versus wavenumber in the range of 4000– 500 cm^{-1} . The principal absorbance peaks obtained for the PLA are: (i) the peak around 3500 cm^{-1} , which may be attributed to the OH stretching, (ii) the strong peaks at 2981 and 1323 cm^{-1} that can be assigned to the asymmetric and symmetric mode of C-H stretching and C-H bending, respectively, (iii) the C=O stretching (from ester linkage) observed at 1700 cm^{-1} , (iv) the C-H deformation appearing at 1386 cm^{-1} , and (v) the O-C asymmetric mode of the ester groups observed at 1083 cm^{-1} [1] .

On the other hand, graphite usually shows the broad, intense band at 3430 cm^{-1} for O-H stretching vibrations, the bands at 2650 cm^{-1} and 2920 cm^{-1} for vibrations of OH in H₂O and dimeric COOH, and 1103 cm^{-1} for C-O stretching vibrations. In addition, there are other band at 1414 cm^{-1} for carboxyl C-O stretching vibrations, 1560 cm^{-1} for skeletal vibrations from unoxidized graphitic domains, and 1726 cm^{-1} for C=O stretching vibrations from carbonyl and carboxylic groups [2] .

However the peak at 1160 cm^{-1} , as indicated by arrows under the spectra, has higher intensity for all PGCs except that for PGC0 and the peak position is shifted to a higher frequency in case of composites. Besides, as can also be seen in the figure, the intensity of C-O stretching decreases with the increase of graphite content. Other peaks of FT-IR spectra of PLA/graphite composite are almost unchanged.

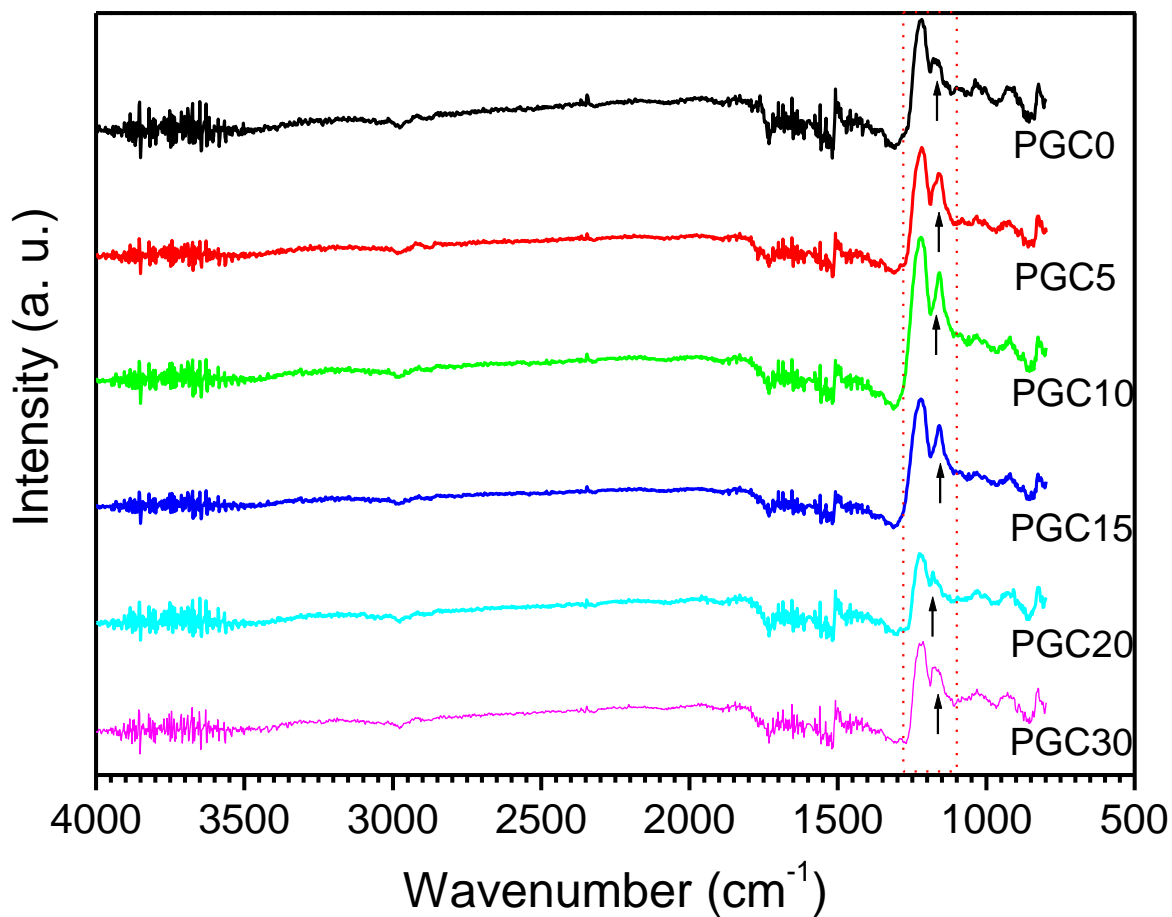


Fig. 5.1.1: FTIR spectra of PGC.

5.1.2 RAMAN SPECTRAL ANALYSES

The Raman spectrum of the pure PGCs is shown in Fig. 5.1.2. The peak at 395 cm^{-1} corresponds to C=O deformation for amorphous PLA fraction [3]. The peak at 411 cm^{-1} arises from C=O deformation from PLA crystalline fraction, to be particularly sensitive to segmental orientation and chain conformation. The peak at 873 cm^{-1} is from C-COO stretching of PLA. The peak at 1128 cm^{-1} represents CH_3 bending of PLA. The peak at 1455 cm^{-1} occurs from CH_3 asymmetric wagging of PLA. The ester C=O stretch appears at 1770 cm^{-1} indicates that the polymer is poorly crystalline. The G-graphite tangential mode appears at 1582 due to the E_{2g} vibration mode of graphite attributed to the vibration of carbons within the polyaromatic structure, and D-mode for graphite appears at 1355 due to a change in the selection rules for the Raman effect. The intensity ratio of D (I_D) to G (I_G) bands have been tabulated (Table 5.1.2). It is well known that the intensity ratio of D (I_D) to G (I_G) band can be used as an indicator of defect quantity [4]. The fewer the defects, the lower the I_D/I_G value. The band frequencies and intensity ratios of D and G bands are evaluated to be 0.855, 0.963, 0.989 and 1.008 corresponding to PGC5, PGC10, PGC20, PGC30, respectively.

Table 5.1.2: Intensity ratio of D (I_D) to G (I_G) band of different samples

Sample	I_D	I_G	I_D/I_G
PGC5	456.202	533.254	0.855
PGC10	644.29	668.67	0.963
PGC20	875.18	884.26	0.989
PGC30	1047	1038	1.008

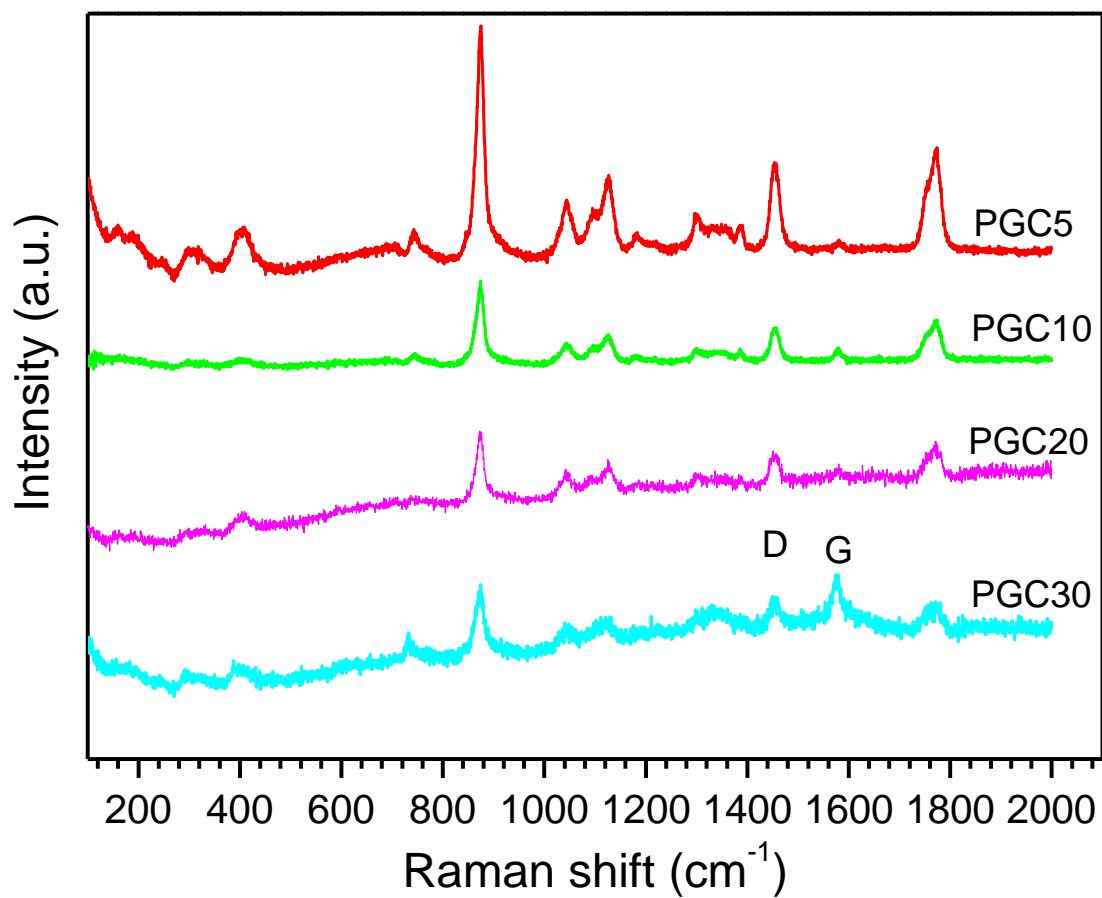


Fig. 5.1.2: Raman Spectra of PGC.

5.1.3 XRD ANALYSIS

Fig. 5.1.3 shows the XRD profiles of PGCs. The important crystalline peak is diffused, appearing on a broad scattering, which is originated from the amorphous region of PLA. The broadly diffused peak suggests that PLA chains are poorly ordered with a low degree of crystallinity due to the rapid cooling of compression molding process. The peak position for PLA is observed close to $2\theta \approx 15.67^\circ$ and 31.91° , as indexed by $(200)_\alpha$ and $(400)_\alpha$, respectively. To analyze these results, we invoked the data of reported crystalline structures of PLA [5,6]. From these data, calculation shows that 200 reflection of the β -phase will appear at $2\theta \approx 17.28^\circ$ and that of the α -phase at $2\theta \approx 16.56^\circ$. This analysis, therefore, dictates to consider the appearance of α -crystal in both the pure PLA and the biocomposites. There is no evolution of new peaks of PLA by increasing content of GP, except the sharp peaks $(002)_{GP}$ and $(004)_{GP}$ appearing from graphite structure. The decrease of X-ray intensity of the $(200)_\alpha$ peak clarifies that increasing amount of GPs degrades the crystallinity in biocomposites. The average lattice spacing estimated from the peak is about 5.81 Å. Increased GP content also decreases the PLA-peak width. This result indicates a change in the average thickness of the PLA crystallites. Moreover, two sharp peaks of which one overlaps $(200)_\alpha$ and the other one slightly at higher angle than $(200)_\alpha$ also appear. The origin of these two peaks is not clearly known. They may arise from graphite structure or from other impurities.

The degree of crystallinity, χ_c , for the samples has been calculated, as shown in Figure 5.1.4. It is seen that the χ_c value decreases with increasing GP content in the composites. This indicates that the GP particles are not suitable nucleating agents for PLA crystallization. The average crystalline thickness, t , estimated for various samples are also shown in Figure 4, indicating a slight decrease in the size of the PLA crystallites.

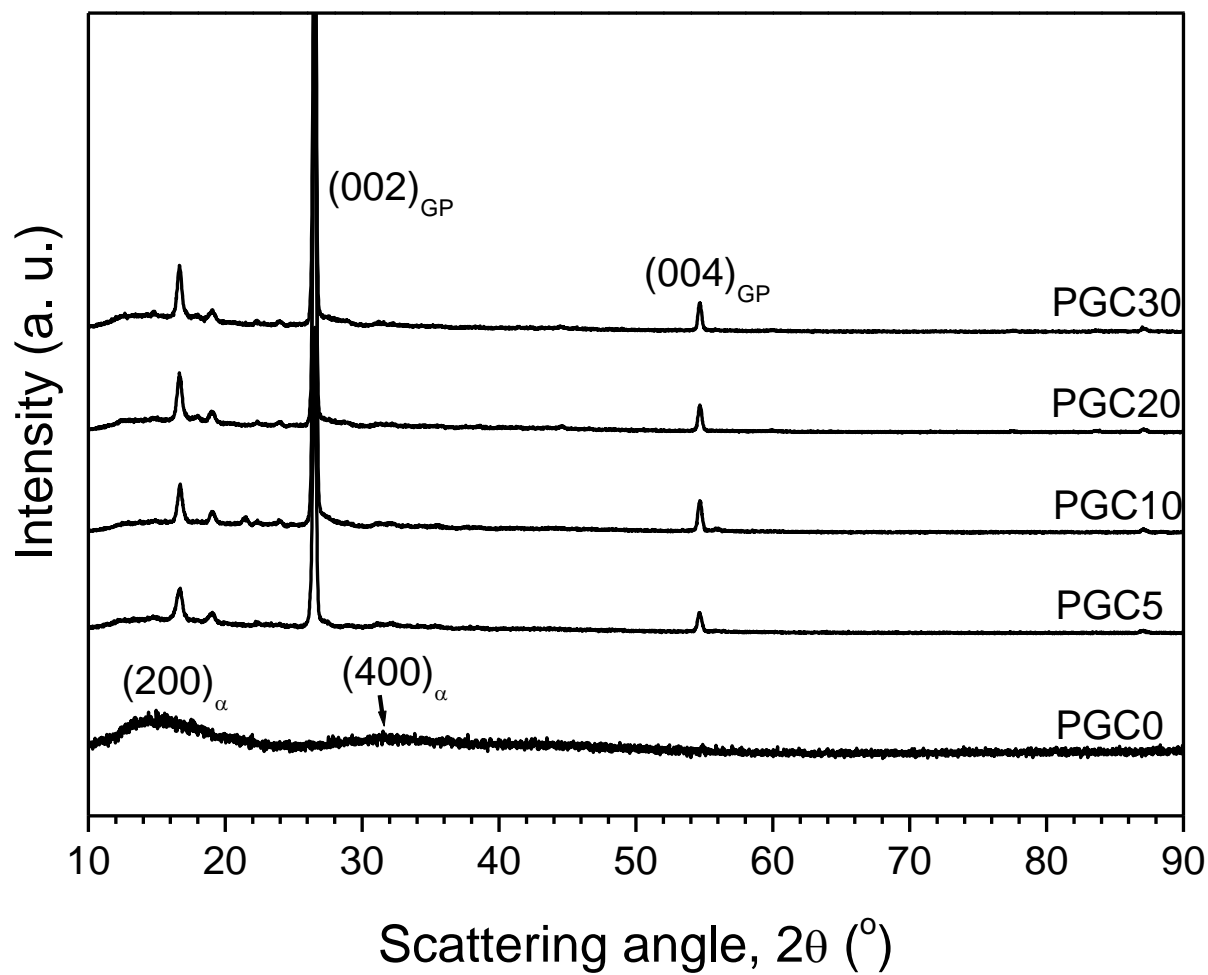


Fig. 5.1.3: XRD pattern of PGC.

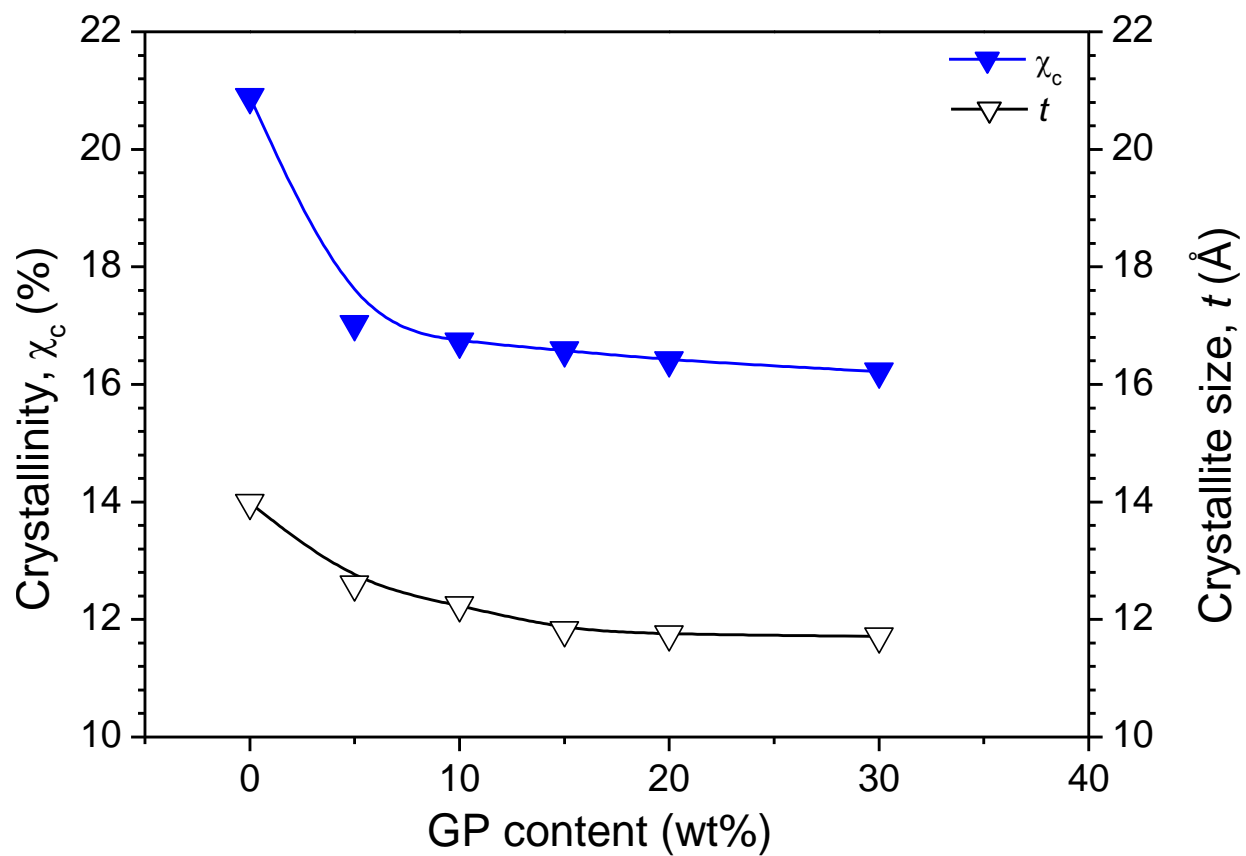


Fig. 5.1.4: Degree of crystallinity of PGC.

5.2 SURFACE MORPHOLOGY

Fig. 5.2.1 represents the SEM micrographs of virgin PLA, and PGC with 5, 10, 15, 20 and 30 wt% GP content. The surface micrographs of PGC0 and PGC5 are almost smooth, whereas roughness on the surface increases with increasing GP contents. The roughest surface is found to be for PGC30. The increase in roughness can decrease in Δh value and hence the value b increases and thus hardness decrease that is consistent with equation (5.4.2).

TEM micrographs of PGC0, PGC10, PGC20 and PGC30 are displayed in Fig. 5.2.2. The PLA shows smooth surface, while small graphite flakes of the order of nanometer to micrometer are embedded with PLA matrix. The surfaces of GP loaded samples are found to be uneven, thereby causing an increase in b parameter of microhardness. The dispersion of GP in the PGC10 samples is apparently good. In contrast, random distribution and clusters of GP are found in the TEM images of PGC20 and PGC30, whose surface structure is found to be relatively rough. It seems that in the images of PGC with higher content of GP (>20 wt %), GP channels or pathways are apparently formed. Clusters or agglomerations are formed due to the particle-particle interactions of GP. Slight voids are also developed at high GP loaded PLA composites. The random distributions of GP in PGC can make physical bonding with PLA. The surface morphology of PGC apparently supports the results of microhardness.

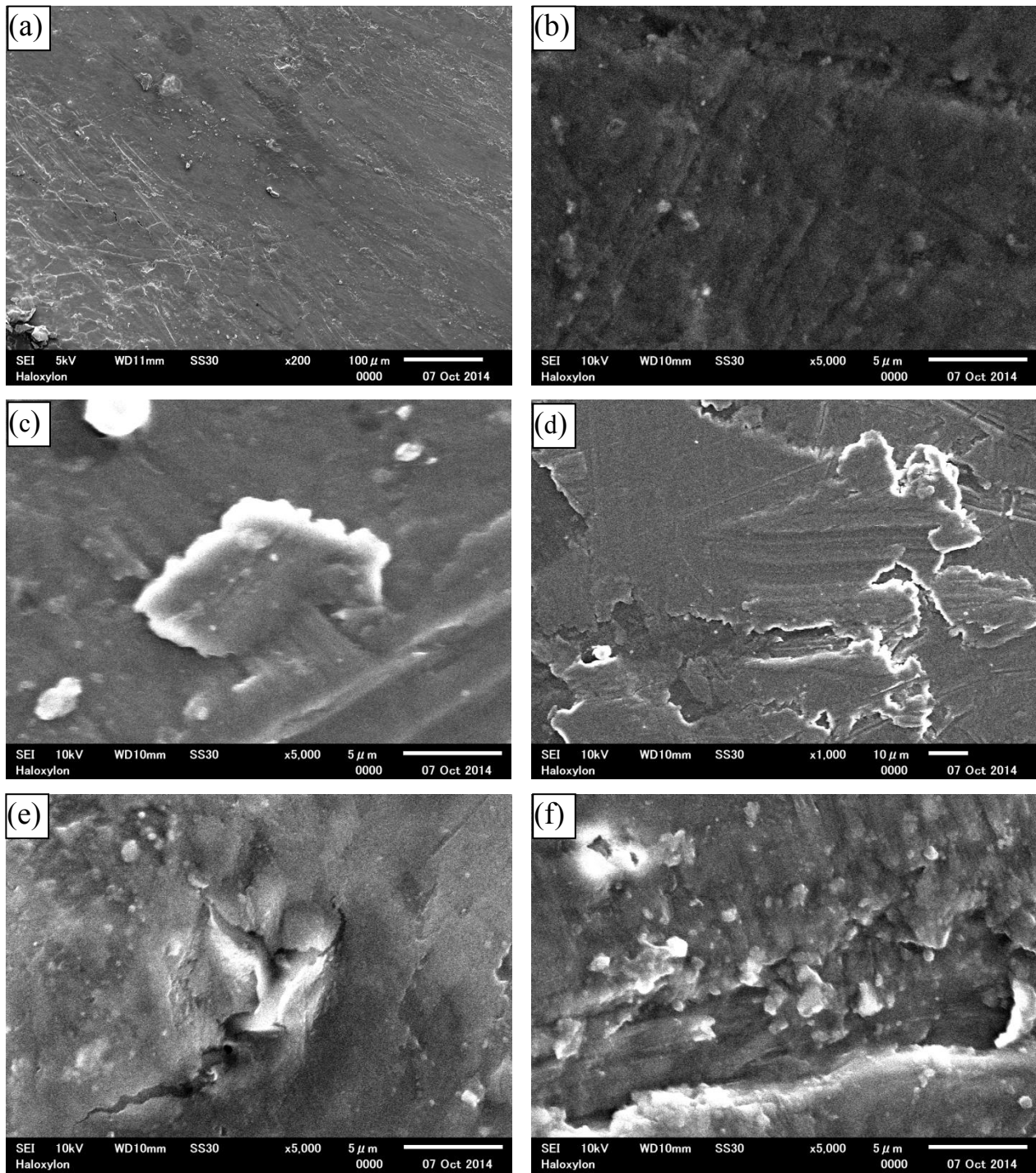


Fig. 5.2.1: Scanning Electron Microscope Micrographs Of PGC.

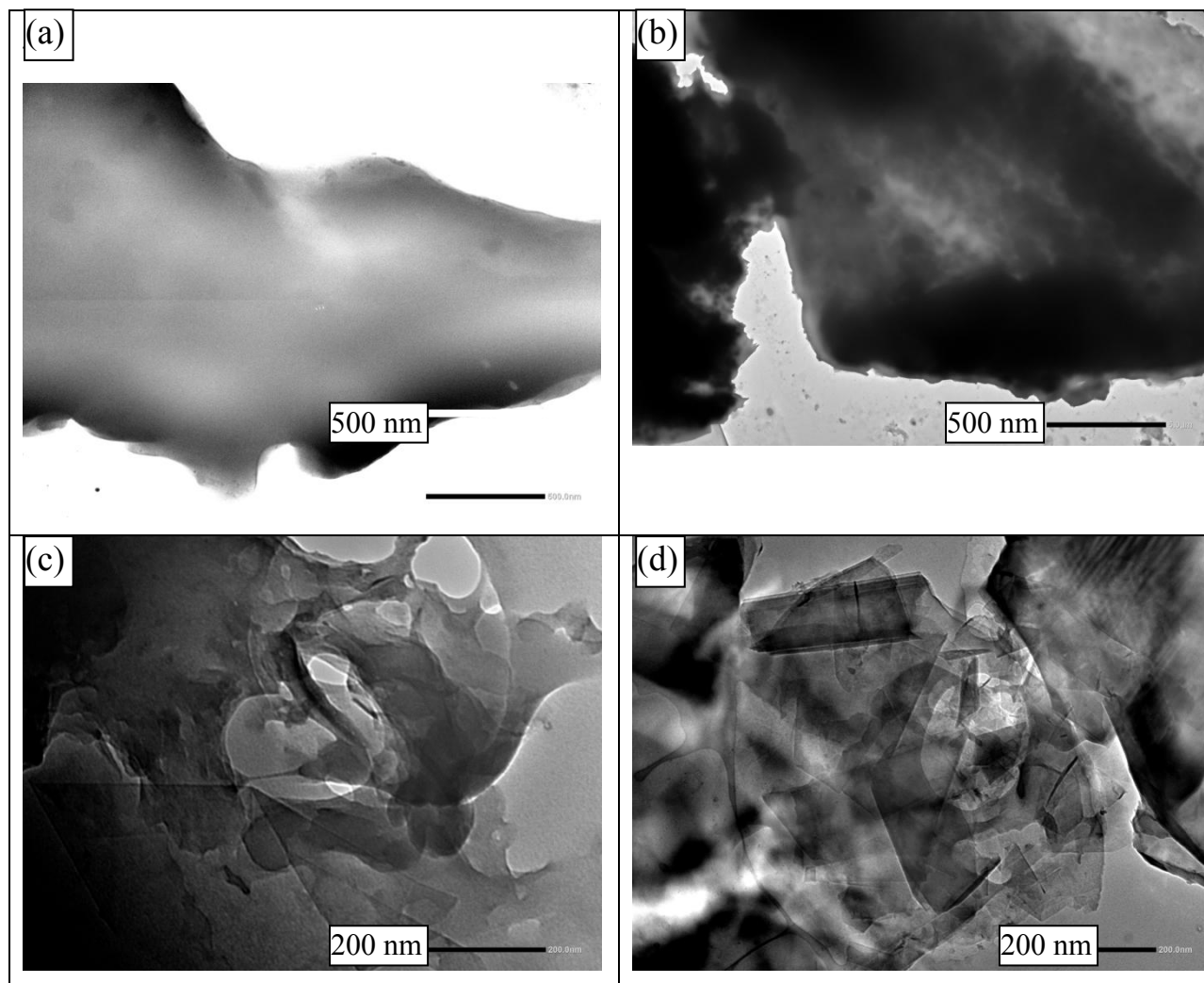


Fig. 5.2.2: Transmission Electron Microscope Micrographs Of PGC.

5.3 MECHANICAL PROPERTIES

The average tensile strength (TS) and Young's modulus (Y_o) evaluated from mechanical tests for various samples are shown in Fig. 5.3.1. The TS value for the pure PLA sample is 55 MPa, while it gradually falls down to a value of 4 MPa for composite with 30 wt% GP content. On the other hand, contrary to the decrease in the TS value, the Y_o is found to increase with the increase of GP contents. The minimum value of Y_o observed for the pure PLA sample is 1.46 GPa and the maximum Y_o value obtained for composite sample with 30 wt% GP is 2.31 GPa. Therefore, the highest increase in the tensile modulus obtained here is 58%.

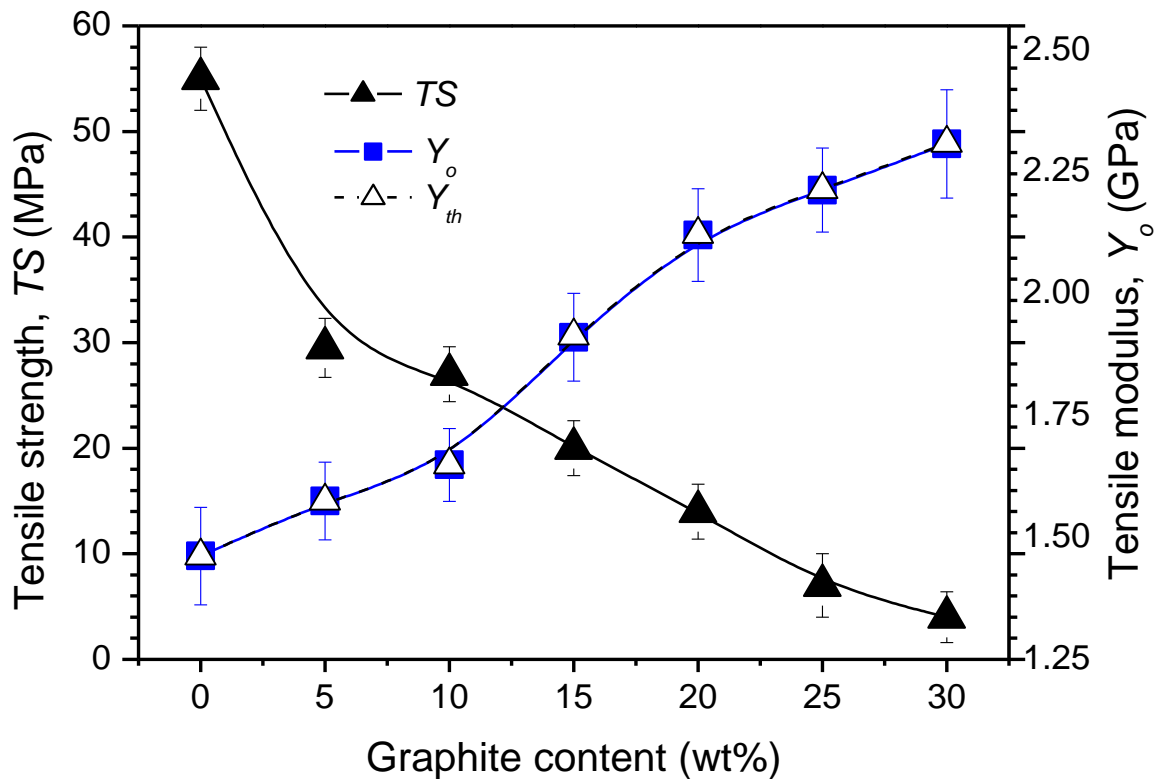


Fig. 5.3.1: Tensile Strength and Young Modulus of PGC.

The lower tensile strength of the composites at increasing volume fraction could be due to a number of reasons, such as weak interfacial bonding at GP and PLA matrix interfaces, agglomeration of carbon black particles, process-related defects such as porosity and so on. It is noteworthy that the tensile strength of a material is the maximum stress exhibited by it under deformation. During the deformation processes, the position and movement of GP aggregates, PLA molecules and developed pores during fabrication inside the material may affect on the resulting interaction among PLA-PLA molecules, GP-GP aggregates and PLA-GP molecules. This lessening of interaction is assumed to reduce the TS values of the composites with increasing GP content. Moreover, the adsorption of the carbon filler limited wet ability in the polyester matrix phase may result in poor interface adhesion of graphite particles to the PLA matrix and inefficient stress transfer between the particle-matrix interface as long as the load is applied.

A number of researchers have documented TS variations with changing filler contents in various polymers, where they have reported that TS decreases with the increase of filler content. Some of them explained this fact using the following Nielson model [7]:

$$\frac{TS_C}{TS_p} = (1 - \phi^{\frac{2}{3}})A_0 \quad (5.3.1)$$

where, TS_C and TS_p denote the tensile strength of the composite and the polymer matrix, respectively; ϕ represents the weight fraction of the filler and A_0 accounts for the adhesion quality between polymer-filler interface. According to the above formula, if a discontinuity in stress transfer to polymer-filler interface occurs, then the value of A_0 decreases. Hence, a

decrease in the tensile strength of the composites with the addition of filler content is reasonable, because the TS_C value decreases as according to equation (5.3.1). Thus, the Neilson model is better suitable to explain well the observed TS decrease with the increase of filler content.

On the other hand, if the gradual increment in Y_o with the increase of GP content is supposed to take place by the increased interactions between PLA-PLA, PLA-GP and GP-GP molecules, a contradiction on the TS -decrease due to weak interactions, as mentioned above, can be severely raised. To surmount this apparent anomaly of Y_o -increase and TS -decrease with the increase of filler content, it is necessary to differentiate the two physical parameters Y_o and TS and how they are measured. The Y_o is principally associated to the interactions among the molecules, whereas TS is associated to both the interactions among the molecules and the deformation processes involved in the material. As mentioned above that there exists three categories of molecule-molecule interactions of which at least one is predominant for the gradual increase in Y_o . Since Y_o increases due to the increase in GP content, it is, therefore, not illogical to consider that the Y_o gradually increases probably because of the increase of filler-filler or GP-GP interactions. Besides, the change in Y_o also relies on the dispersion of GP in PLA matrix. Usually, due to its large surface area, GPs have a greater contact either with PLA or with themselves. If the GP particles find a good dispersion in the PLA matrix, the well dispersed particles may get larger surface contacts, which essentially play roles to increase the tensile modulus of the material. A theoretical model has been given by Guth-Smallwood to predict the theoretical modulus (Y_{th}) by a widely used equation in polymer-filler composites [8]:

$$Y_{th} = Y_o(1 + 2.5V_{GP} + 14.2V_{GP}^2) \quad (5.3.2)$$

where V_{GP} is the volume of GP as determined from the relation: $V_{GP} = [M_{GP} / (100 - M_{GP})] / \rho_{GP}$, where M_{GP} and ρ_{GP} are mass and density of GP, respectively. The calculated Y_{th} values for PGCs plotted in Figure (5.3.1) (dotted line overlapped with original line of Y_o), showing a reasonable good fit. Thus, the volume fraction or the surface contact shows a greater influence on increasing the Y_o value of the composites. Thus, it is notable that GP particles influence largely on the Y_o value since they make physical bonding both with PLA molecules and themselves.

Fig. 5.3.2 shows the flexural strength (FS) and tangent modulus (TM) verses Graphite content (wt%). The trends of TM -increase and FS -decrease are similar to those of Y_m and TS respectively. Thus, similar arguments as that set for Y_m and TS changes can also be given for the changes of TM and FS with increase in filler contents. The TM values for PGC30 are 6.98 GPa and for PGC0 is 3.98 GPa. Therefore, the increase of TM for PGC30 from PGC0 is about 77%.

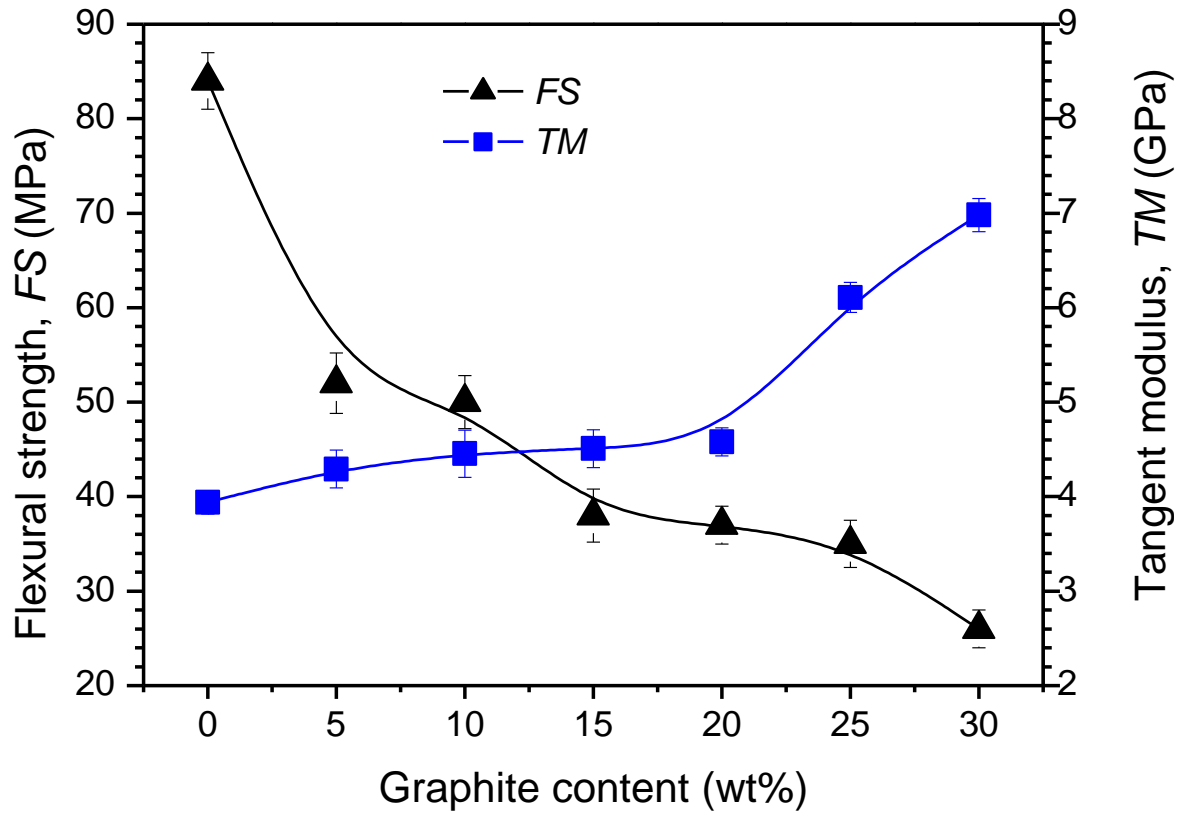


Fig. 5.3.2: Flexural strength and Tangent Modulus Of PGC.

5.4 MICROMECHANICAL PROPERTIES

Fig. 5.4.1 shows the change in microhardness with increasing load, P , for pure PLA and various contents of GP loaded composites.

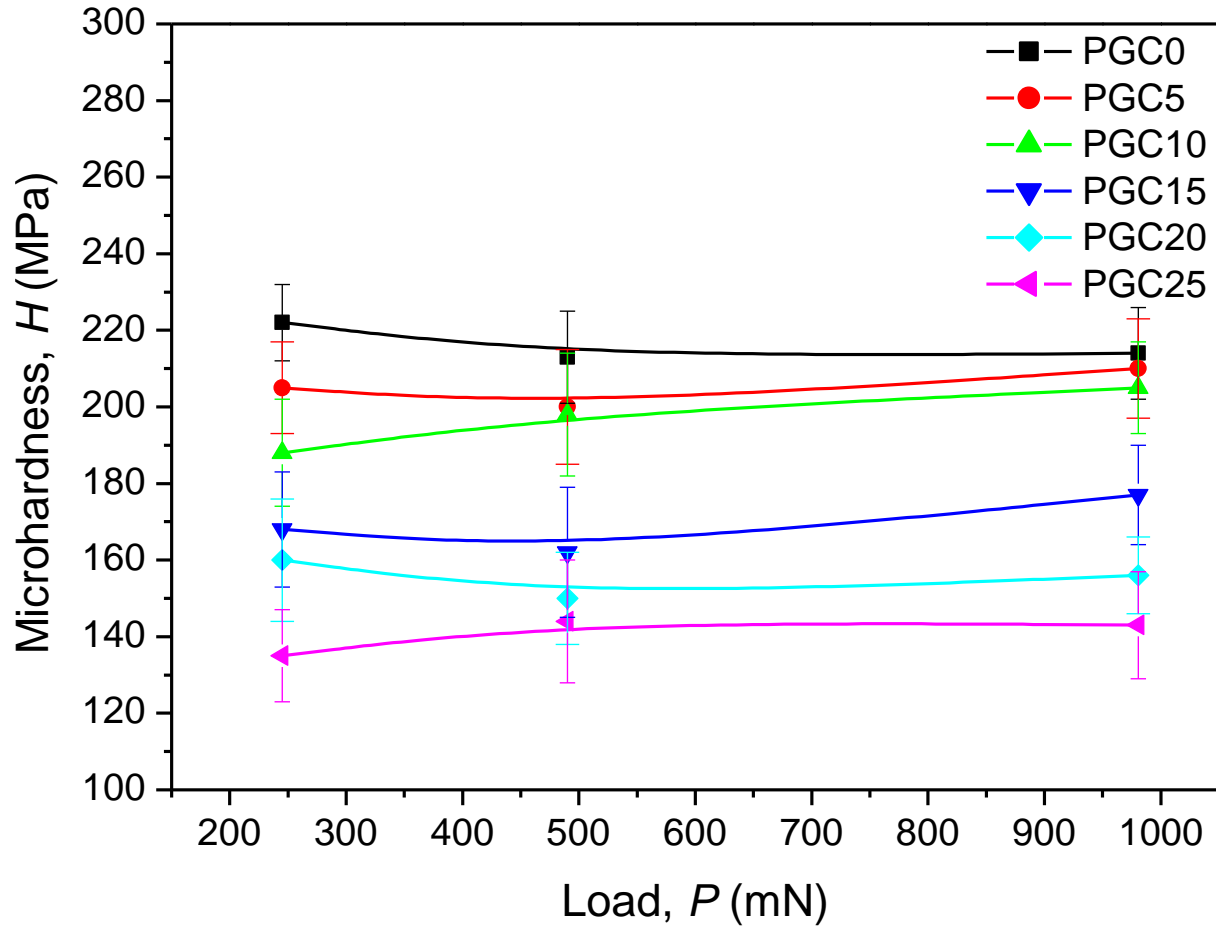


Fig. 5.4.1: Microhardness of PGC.

The microhardness apparently remains unchanged with the increase of the load up to 1000 mN. Nevertheless, a slight variation of hardness with load is observable. To remove this variation or to observe the load independent hardness for different concentrations of GP, d^2 versus P for pure PLA, 5, 10 and 20 wt% of GP loaded PLA composites are shown in the Fig. 5.4.2.

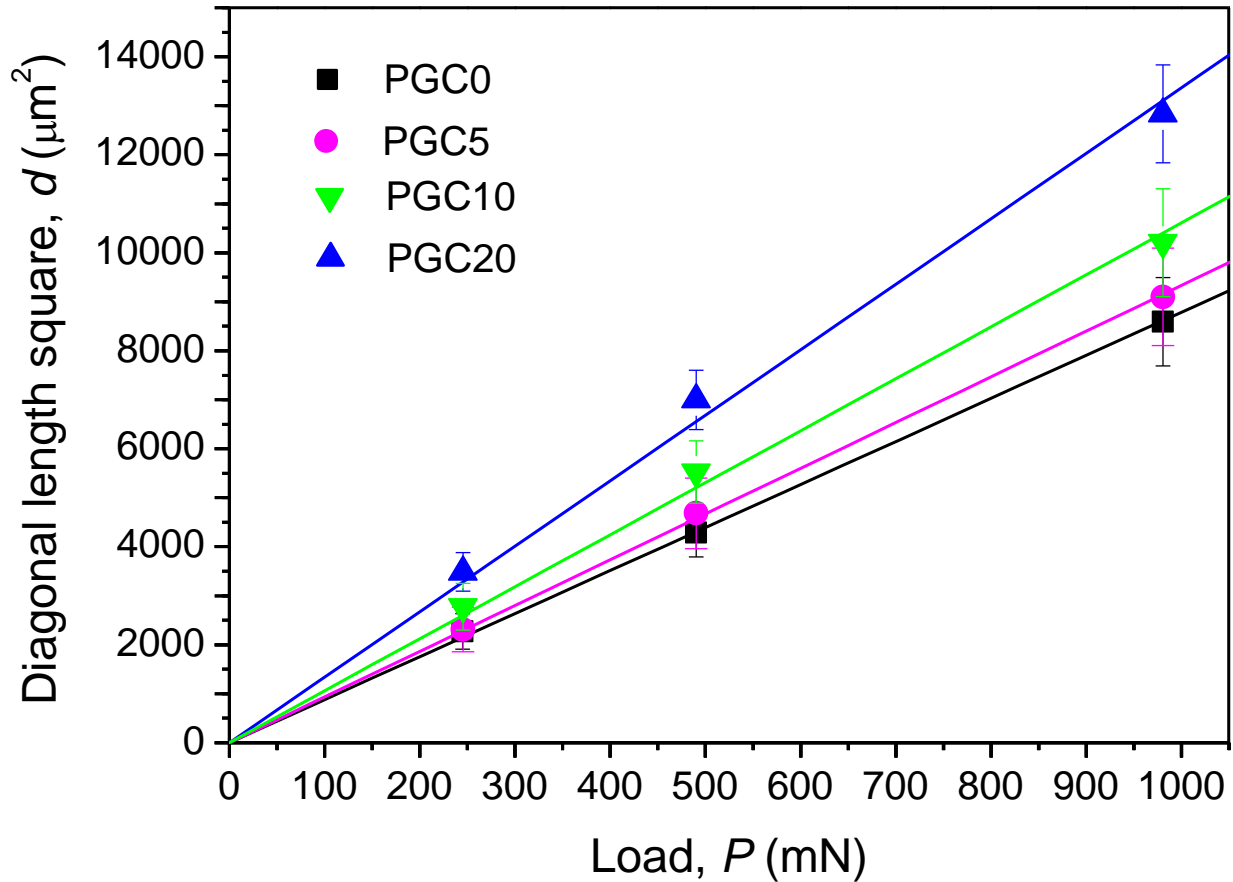


Fig. 5.4.2: Change of diagonal square length with load of PGC.

The microhardness gradually decreases with the increase of GP content and becomes minimum at 30 wt% GP content, as shown in Fig. 5.4.3. The microhardness for pure PLA is 220 MPa and for 30 wt % GP loaded composite is 143 MPa. Therefore, the maximum decrease in H values is 54%. The microhardness provides information of micromechanical properties of a material within a micro region. The observed reduction in H can be attributed to the increased GP content, as also affected by the surface roughness, as well as the decrease in the crystallinity of the resulting material.

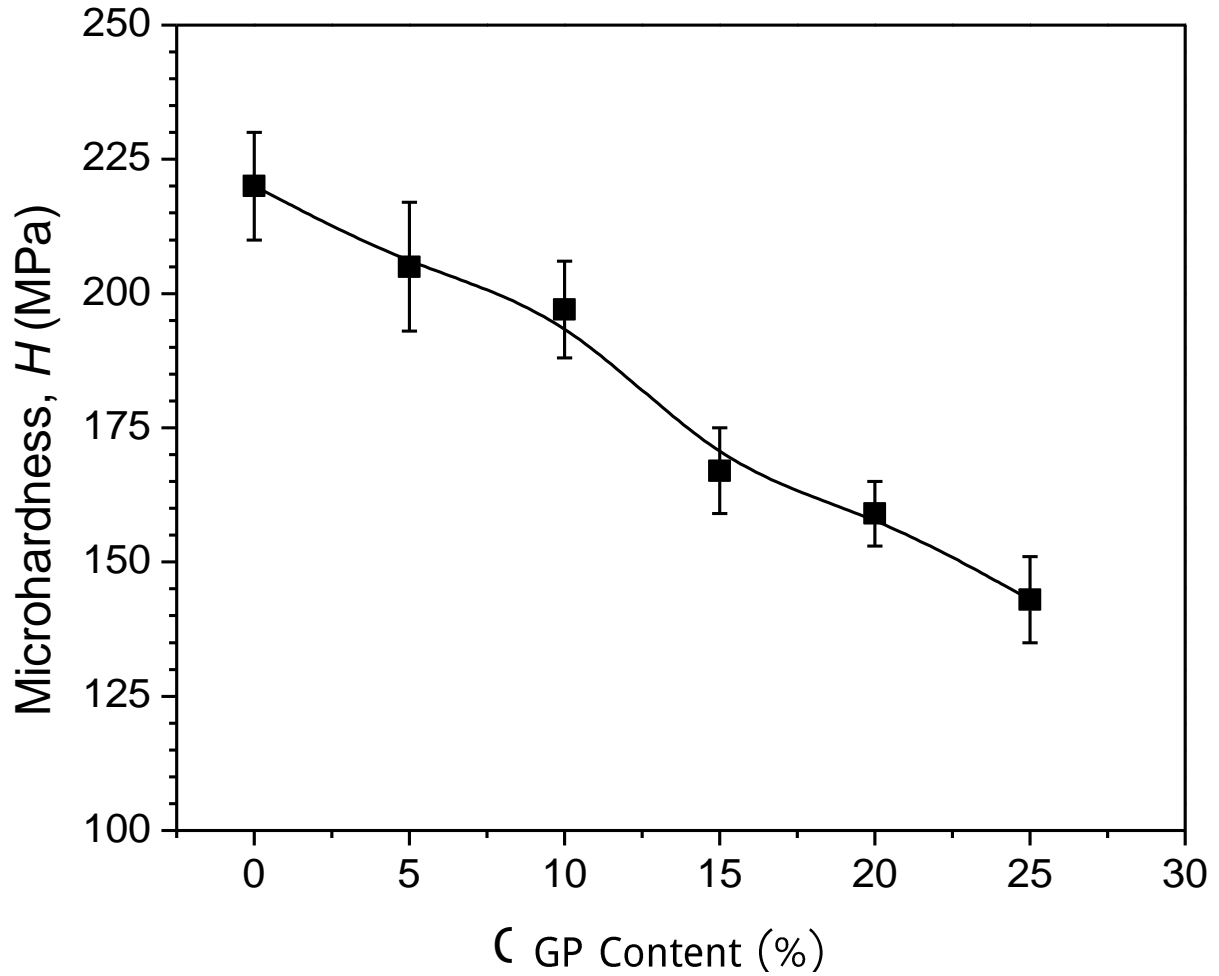


Fig. 5.4.3: Change of microhardness with GP content (wt%).

The hardness of a polymer or polymeric composites can be described in terms of its crystalline hardness H_c , and amorphous hardness H_a , according to the additivity law [9]:

$$H = H_c \chi_c - H_a(1 - \chi_c) \quad (5.4.1)$$

Moreover, the H_c of a polymeric material related to the crystal thickness t and surface energy parameter b through the following expression [10]:

$$H_c = \frac{H_c^\infty}{1 + b/t} \quad (5.4.2)$$

where, H_c^∞ is the hardness of an infinitely thick crystal and $b = 2\sigma_e/\Delta h$, in which σ_e is the free surface energy and Δh is the energy for the plastic deformation of the crystal of a material. Thus, it is clear that σ_e and hence b values influence on the hardness value of a material. In case of PGC, the value of σ_e may decline after blending GP into PLA, because particle incorporation makes the surface of the polymer rougher than that of pure PLA.

On the other hand, a slight decrease in the crystalline thickness or t values is observed from XRD studies. As a result, the term b/t in the denominator increases sufficiently, thereby causing a decrease in hardness as according to equation (5.4.2). Moreover, GP particle is comparatively softer than of PLA. Therefore, the decrease in hardness with the increase in GP particles is also plausible. A detailed review on the strength of particulate–polymer composites has been presented with many phenomenological and semi-empirical models, relying on the parameters of particle size, interface adhesion and particle loading [11], where it is claimed that a few weight per cent particulates with weak interfacial adhesion can largely deteriorate micromechanical properties.

5.5 THERMAL PROPERTIES

DTA curves of the samples are shown in the Fig. 5.5.1. All thermograms indicate a small endothermic peak at around 155°C (dotted line) with similar pattern. This is the melting temperature (T_m) of PLA that does not seem to change at all with particle loading. On the other hand, two broad exothermic peak (dashed line and beyond it) for all samples appear at higher

temperature. These are probably the degradation temperatures (T_d) of PLA, observed by DTA. Clearly, PLA degradation occurs at two stages. For pure PLA, 1st exothermic peak occurs at 370°C and 2nd one occurs at 420°C, whereas for composites, 1st peak occurs at 380°C and 2nd one occurs 458°C.

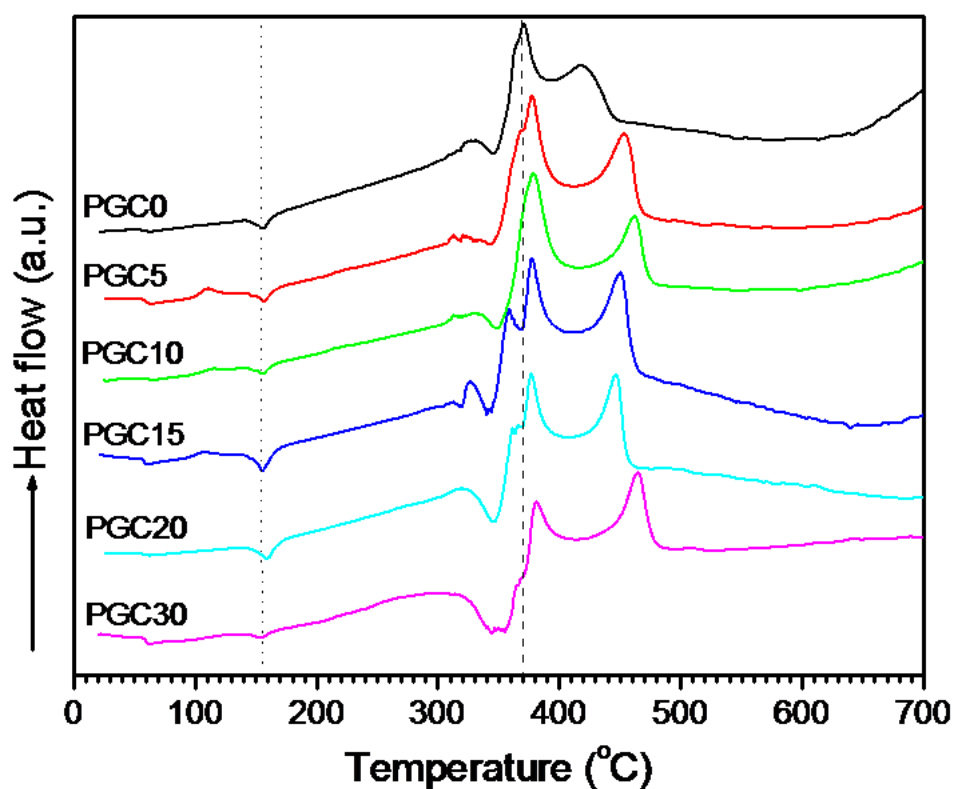


Fig. 5.5.1: DTA curves of PGC.

TGA were performed to measure the amount and rate of changes in the mass of the samples as a function of temperature in a nitrogen atmosphere. Fig. 5.5.2 illustrates the TGA thermograms of various samples. It seems that the weight loss starts to near about 334°C and the loss pattern is

apparently found to be different for different samples. Clearly, the weight loss delays with increasing the temperature with the increase of GP content.

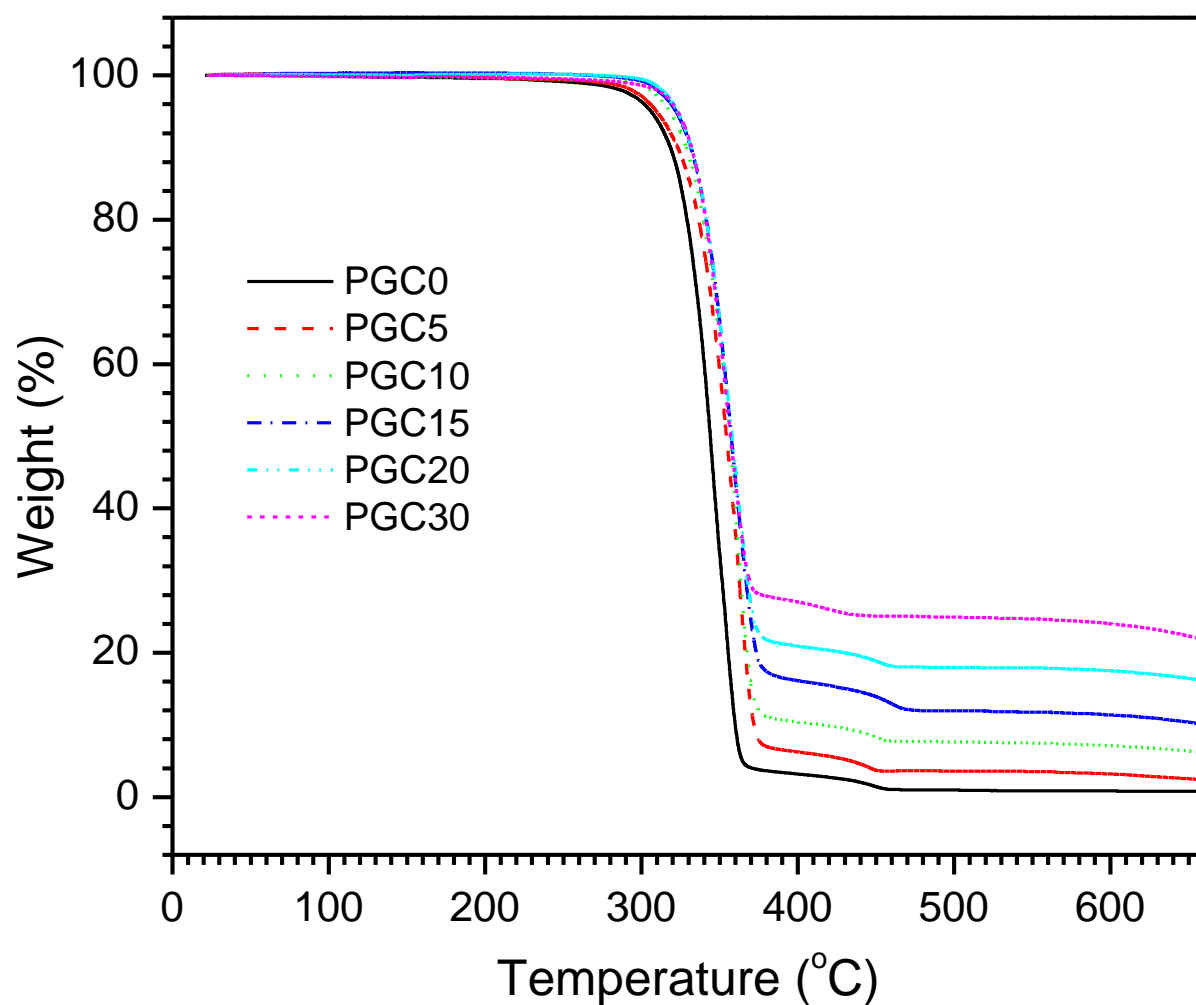


Fig. 5.5.2: TGA curves of PGC.

Three indicators commonly practiced to characterize the onset and structural degradation are the onset temperature (T_o) endset temperature (T_f), decomposition temperature (T_{dec}) and residue

content at T_{dec} (°C) [12]. However, T_o , T_f , T_{dec} and the residue content at T_{dec} °C have been analyzed and tabulated (Table 5.5.1).

Table 5.5.1: The T_o , T_{dec} , T_f and the residue content at T_{dec} °C of different samples.

Sample	T_o (°C)	T_{dec} (°C)	T_f (°C)	Residue content at T_{dec} (°C)
PGC0	334.4	363.48	378.2	1.27
PGC5	346.5	366.12	380.47	4.62
PGC10	351.3	370.65	383.11	5.08
PGC15	356.57	373.3	385.38	7.27
PGC20	358.57	375.56	387.64	13.40
PGC30	360.21	383.11	392.64	18.68

As the GP content is increased, the onset of decomposition is moved to higher temperatures. For instance, the T_o gradually increases from 334 to 360°C from PLA to PGC30. On the other hand, T_{dec} successively increases from 363 to 383°C from PLA to PGC30. Thus, the thermal stability of the composites considerably increases. There are several chemical/physical mechanisms that could affect the stabilization effect of composites due to GP. These mechanisms include the reaction of free radicals coming from the resin matrix with GP, the adsorption of volatile degraded components on GP surface, barrier effect of GP and the reduction of molecular mobility of the resin molecules surroundings GP. The significant increase in T_{dec} under inert atmosphere could be related to the barrier effect of GP which may decrease the diffusion of released oxygen from the resin into composites. Besides, adsorption of volatile components on GP surfaces may retard the degradation process. Therefore, the increase of interfacial area between PLA and graphite content up to 30 wt% enhances the thermal stability of composites considerably. From this TGA measurement, it can be noted that the thermal stability of the PGC

is enhanced with the inclusion of GP content. Moreover, with the increase of the GP content agglomeration of GP particles occurs for which each resin molecule face large surface area of GP particles that encounter the segmental mobility of resin molecules. On the other hand, the residue content (wt%) at T_{dec} °C is increasing with the increase of the GP content. This is due to the fact that for the high degradation temperature of graphite much greater than T_{dec} °C, the GP virtually remains as residue and not degraded at all.

The DTG of the samples are shown in Fig. 5.5.3. The pure PLA shows the DTG peak at around 350°C and other peak position shows a slight variation of temperatures.

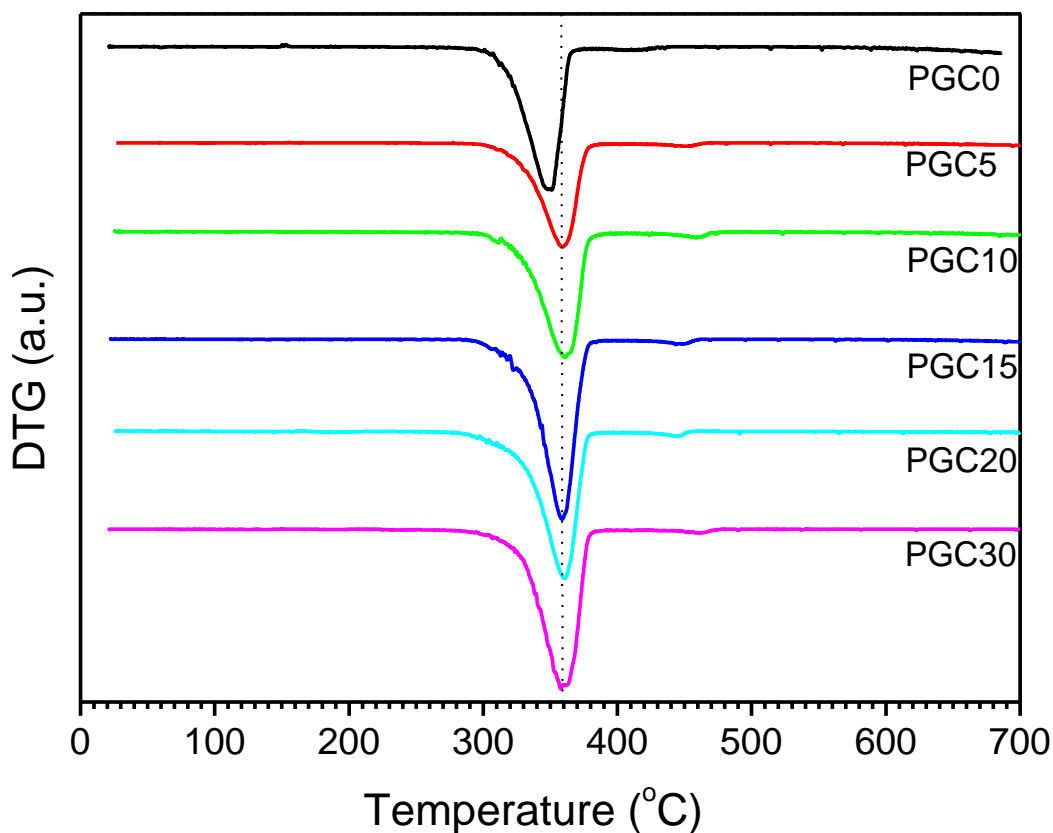


Fig. 5.5.3: DTG curves of PGC.

REFERENCES

- [1] A. K. M. M. Alam, M. D. H. Beg, D. M. R. Prasad, M. R. Khan and M. F. Mina, Structures and Performances of Simultaneous Ultrasound and Alkali Treated Oil Palm Empty Fruit Bunch Fiber Reinforced Poly(Lactic Acid) Composites, *Composites Part A: Appl Sci Manufac*, Vol. 43, pp. 1921-1929, 2012.
- [2] S. Jin, L. S. Xie , Y. L. Ma, J. J. Han, Z. Xia, G. X. Zhang, S. M. Dong, Y. Y. Wang, Low-temperature expanded graphite for preparation of graphene sheets by liquid-phase method, 8th China International Nanoscience and Technology Symposium (CINSTS09), IOP Publishing, *Journal of Physics: Conference Series* 188, 012040, 2009.
- [3] A. Weselucha-Birczyńska, A. Fraczek-Szczytba, E. Długonb, K. Paciorea, A. Bajowskab, A. Koscielnab, M. Błazewicz, Application of Raman spectroscopy to study of the polymer foams modified in the volume and on the surface by carbon nanotubes, *Vib. Spectrosc.*, Vol. 72, pp. 50–56, 2014.
- [4] X. Li, Y. Xiao, A. Bergeret, M. Longerey, J. Che, Preparation of Polylactide/Graphene Composites From Liquid-Phase Exfoliated Graphite Sheets, *Polym. Compos.*, Vol. 35, pp. 396–403, 2014.
- [5] P. De Santis and A. Kovacs, Molecular conformation of poly(S-lactic acid), *Biopolymers* Vol. 6(3), pp. 299-306, 1968.
- [6] W. Hoogsteen, A. R. Postema, A. J. Pennings and G. T. Brinke, Crystal structure, conformation and morphology of solution-spun poly(L-lactide) fibers, *Macromolecules*, Vol. 23(2), pp. 634-642, 1990.
- [7] R. Nielson, *Mechanical Properties of Polymers and Composites*, Marcel Dekker: New York, 1974.
- [8] Z. Zhao, W. Wu, E. He and Z. Chen, “The conduction mechanism of carbon black-filled poly (vinylidene fluoride) composite”, *Mater. Lett.*, Vol. 57, pp. 3082–3088, 2003.
- [9] A. Flores, F. Ania and F.J. Balta Calleja. From the glassy state to ordered polymer structures: A microhardness study, *Polymer*, Vol. 50, pp. 729–746, 2009.
- [10] F. J. Balta Calleja, S. Fakirov “Microhardness of Polymers”, Cambridge University Press, 2000.

- [11] S.Y. Fu, X.Q. Feng, B. Lauke, Y.W. Mai. Effects of particle size, particle/matrix interface adhesion and particle loading on mechanical properties of particulate–polymer composites, *Compos. Part B: Eng.*, Vol. 39, pp. 933–961, 2008.
- [12] M. F. Mina, S. Seema, R. Matin, M. J. Rahman, R. B. Sarker, M. A. Gafur, M. A. H. Bhuiyan, Improved performance of isotactic polypropylene/titanium dioxide composites: Effect of processing conditions and filler, *Polym. Degrad. Stab.*, Vol. 94, pp. 183-188, 2009.

6.1 CONCLUSION

GP powders have been mechanically mixed in PLA with 0, 5, 10, 15, 20, 25 and 30 wt% GP content by extrusion molding followed by compression molding technique. FTIR spectra demonstrate the formation of physical bonds (Vander Waals) between GP and PLA. Raman spectroscopy distinguishes amorphous and crystalline phases in PLA as well as defect structure due to the presence of GP. Inclusion of GP shows a decrease in crystallinity and crystallite size in PLA. This indicates that the GP particles are not suitable nucleating agents for PLA crystallization. SEM exhibits an increase in surface roughness at higher loading of GP particles and TEM reveals a good dispersion of GP particles in PLA matrix at lower loading and inhomogeneous dispersion at higher loading. The tensile and flexural strengths of the composite decrease with the increase of fillers, and this decrease is explained on the basis of Nielson model. A significant increase in Young's and tangent moduli of about 58 and 77% is observed, respectively. A remarkable decrease in microhardness for increasing GP content up to 30 wt% is observed. This change in micromechanical properties is due to the decrease of crystallinity in PLA and more especially due to the inclusion of paracrystalline GP particles. TGA shows an increased thermal stability of the samples, as the GP content is increased, the onset of decomposition is moved to higher temperatures. For instance, the T_o gradually increases from 334 to 356°C from PLA to PGC30. On the other hand, T_{dec} successively increases from 363 to 383°C from PLA to PGC30. Thus, the thermal stability of the composites considerably increases. The observed properties of the resulting composites can be useable in any suitable applications like indoor and outdoor panels, structures, furniture and commodities.

6.2 SUGGESTIONS FOR FUTURE WORK

The investigated outcomes can predict the application of composites in various fields. The variation of filler lengths, diameters, contents and synthesis techniques may vary the properties substantially. So, the following suggestions are given for unveiling more information of the behavior of the composites:

- (i) This study was carried out for filler etihparg loading 0, 5,30 dna 25 ,20 ,10 wt% in the PLA matrix.
- (ii) Electrical properties of the composites can be measured to find out its suitability in electrical applications.
- (iii) Graphene oxide or graphene can be added to PLA to change the physico-mechanical properties.
- (iv) Differential scanning calorimetry (DSC) can be done to -50°C to measure the glass transition behavior of the composites.
- (v) Temperature dependent AC electrical measurement may be carried out to find specific dielectric applications of the composites. Temperature dependent DC electrical properties can be investigated to know the temperature dependent conduction mechanism.
- (vi) AFM and FESEM spectral studies can be performed to examine the nature of bonding between fillers and PLA
- (vii) Optical properties such as optical absorption and transmission of the nanocomposites can be revealed by carrying out UV-Visible spectroscopic study.
- (viii) Besides, graphite can be replaced by other nano fillers like, metals or nano particles, which can provide new information of the new composites.